2017

Development of Epilepsy-on-a-chip System for High-throughput Antiepileptogenic Drug Discovery

Jing Liu
Lehigh University

Development of Epilepsy-on-a-chip System for High-throughput Antiepileptogenic Drug Discovery

by

Jing Liu

A Dissertation

Presented to the Graduate and Research Committee

of Lehigh University

in Candidacy for the Degree of

Doctor of Philosophy

in

Electrical Engineering

Lehigh University

August 2017

Approved and recommended for acceptance as a dissertation in partial fulfillment of the requirements for the degree of Doctor of Philosophy.

"Development of epilepsy-on-a-chip system for high-throughput antiepileptogenic drug discovery"

_____ _____

Jing Liu Date

_____

Accepted Date

_____

Yevgeny Berdichevsky, Ph.D., Dissertation Advisor

_____

Svetlana Tatic-Lucic, Ph.D., Committee Member

_____

James Hwang, Ph.D., Committee Member

_____

R. Michael Burger, Ph.D., Committee Member

_____

Chao Zhou, Ph.D., Committee Member

Acknowledgements

I would like to extend my sincerest gratitude to the people who have shaped both my academic and personal life for the past five years at Lehigh.

First and foremost, I would like to thank my advisor, Dr. Yevgeny Berdichevsky, who has supported me throughout my thesis with his patience and knowledge. It has been an honor to be his first Ph.D. student. I appreciate all his contributions of time, ideas, and funding to make my Ph.D. experience productive and stimulating. More importantly, he taught me how to think and approach research problems intelligently and effectively while allowing me to act independently as a scientist. For that, I have the utmost respect and gratitude for Dr. Berdichevsky.

I would also like to thank my thesis committee: Dr. Svetlana Tatic-Lucic, Dr. James Hwang, Dr. Chao Zhou, and Dr. R. Michael Burger for their encouragement and insightful comments which incented me to widen my research from various perspectives. A special thanks to Dr. Xuanhong Cheng and Dr. Anand Jagota, who generously allowed me to work in their lab. The field potential modeling discussed in this dissertation would not have been possible without Dr. Cheng's collaboration. Furthermore, I would like to thank Dr. Tianyi Zhou and university staff: Raymond Filozof and Tony Jeffers for their unfailing support and assistance in my microfabrication work.

I have been blessed with a friendly and cheerful group of fellow students: Yu Song, Chris Dussourd, Shabnam Ghiasvand, and Md Fayad Hasan, as well as the undergraduates who

have joined the Berdichevsky's lab, especially, Anna Sternberg who provided the biochemistry assay data in Chapter 3. I would like to thank them for their feedback, cooperation, and friendship.

Moreover, I am grateful to my friends: Chien-wen (Anna) Chen, Dr. Pin-Chuan (Daniel) Su, Sheng-Hsiu (Sunny) Lin, Yun-wen (Irene) Chen, and Rui (Rita) Chen for their listening, understanding, inspiring, and for all the adventures we had together. Finally, I would like to thank my family: my parents and my sister for their unceasing love, encouragement, and support in all my pursuits.

Jing Liu

Lehigh University

July 2017

Table of Contents

List of Tables

List of Figures

Abstract

Epilepsy is one of the most common neurological disorders and affects millions of people in the United States. Currently available antiepileptic drugs require continuous administration for suppression of seizures and have not been shown to prevent the development of epilepsy (epileptogenesis). The discovery of antiepileptogenic drug is complicated by the long time course of epileptogenesis in animal models of epilepsy and the requirement of continuous monitoring of epileptiform activity in vivo for the assessment of drug efficacy. In recent years, organotypic hippocampal cultures have been increasingly used as an in vitro model of post-traumatic epilepsy in both basic and translational research. Epileptogenesis in this in vitro model has a compressed time scale and can be monitored by detection of electrographic and biochemical markers of seizure-like activity. However, the lack of a scalable chronic electrical recording platform is a significant bottleneck in high-throughput antiepileptogenic drug discovery using organotypic cultures.

In an effort to circumvent the throughput limitations of in vitro antiepileptogenic drug discovery, a hybrid microfluidic-multiple electrode array (μflow-MEA) technology was developed for scalable chronic electrical assay of epileptogenesis in vitro. Specifically, the microfluidic perfusion technique was utilized to miniature the culture platform, which enabled the long-term maintenance of an organotypic culture array on a single device. The integration of the microfluidic perfusion system with a customized planar MEA allowed

for parallel continuous recordings. As a proof-of-concept demonstration, a pilot screen of receptor tyrosine kinase (RTK) inhibitor library was performed on μflow-MEA based electrical assay platform. The screen results revealed significant antiepileptogenic effect of cFMS RTK inhibitor.

This thesis also provides further validation of the organotypic hippocampal culture model of epilepsy by investigating the influence of culture medium composition on epileptogenesis. We found that epileptogenesis occurred in any culture medium that was capable of supporting neural survival, indicating that culture medium composition has limited influence on epileptogenesis in organotypic hippocampal cultures.

It is hoped that the techniques presented in this thesis will accelerate the antiepileptogenic drug discovery and contribute to the development of new therapeutics to treat individuals at risk of epileptogenesis.

Chapter 1

Introduction

1.1 In vitro model of epileptogenesis and drug discovery

Epilepsy affects around 50 million people worldwide, making it one of the most common neurological disorders [1]. Diverse acquired brain insults, including traumatic brain injury, stroke, infections, and tumors [2,3], can introduce epileptogenesis, a process by which normal brain is transformed into epileptic brain generating spontaneous recurrent seizures. Epileptogenesis includes (1) a latent period between brain insults and the onset of seizure, and (2) the progression of epilepsy after it is established [4] (Figure 1.1). The latent period may vary from months to years in patients [5–7], presenting a window of opportunity for therapies that aim to prevent or delay the development of epilepsy [8]. Alternatively, treatments may be administered after the seizure onset to modify the progression of epilepsy, by reducing or eliminating seizures permanently. These therapies are defined as having an effect of antiepileptogensis [4]. Currently available antiepileptic drugs (AEDs) are anticonvulsants that require continuous administration for suppression of seizures, and they have not been shown to prevent epileptogenesis [9–11]. Furthermore, approximately 30% of patients are drug refractory [12]. At present, epileptogenesis is not a treatment

indication, and there is no therapy available in clinic to treat individuals at risk of epileptogenesis. Therefore, discovery of antiepileptogenic interventions that prevent, interrupt or reverse epileptogenesis has been identified as an epilepsy research benchmark [13,14].

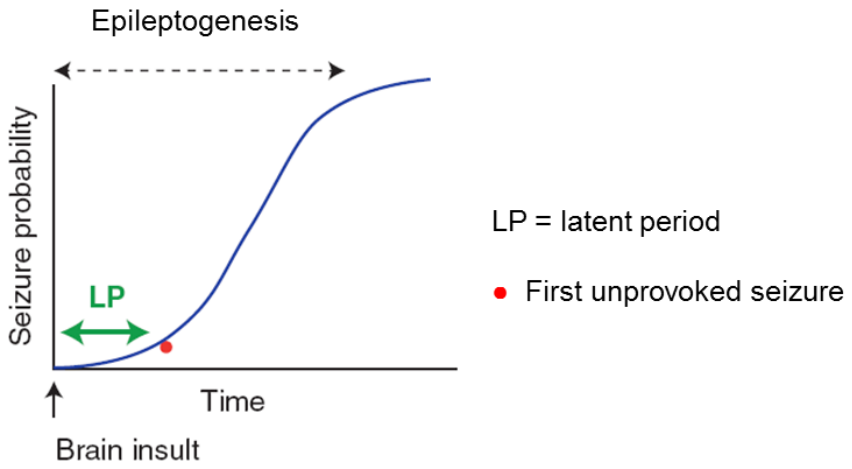

Figure 1.1 Definition of epileptogenesis. Epileptogenesis includes the latent period, which is defined as the time between brain insults and the occurrence of the first unprovoked seizure, and extends beyond the latent period, when seizure frequency and severity progressively increase over time. Reproduced with permission from [4].

Development of antiepileptogenic drugs is complicated by the long latent period which varies from weeks to months in epileptic animal models [15–17]. Antiepileptogenic effects, including (1) delays in seizure onset, alterations in seizure probability versus time after injury, and (2) reductions in seizure frequency, intensity, and duration, can occur over timescales of days to weeks after compounds application. Thus, continuous electroencephalogram (EEG) monitoring of electrographic seizures is necessary for sensitive and quantitative assessment of drug efficacy [2,3], which requires time-consuming and expensive surgical procedures for electrode implantation in animals models. Difficulty and high-cost of long-term continuous recording result in a low experimental

throughput, presenting a practical challenge for antiepileptogenic drug development. Limited throughput is also a major factor that prevents the use of small molecule panels in a target-independent approach for antiepileptogenic drug discovery. One promising option to circumvent these problems is to use in vitro preparations of epileptogenesis [18].

As an in vitro alternative to animal models, brain slices are extensively used for toxicological and pharmacological profiling, or carrying out candidate compound screens to discover new drugs against neurological diseases [19–24]. Especially, hippocampal slices are increasingly used as an in vitro model of traumatic brain injury-induced epilepsy, or post traumatic epilepsy [25–28]. Organotypic brain slice cultures were developed to maintain slice viability for weeks and months [29]. Since the cultures maintain the cytoarchitecture of the originating brain regions, they are termed organotypic slice cultures (Figure 1.2A), and these cultures are often used as models for studies on long term neurological processes, such as neurogenesis [30], synaptic plasticity [31], and epileptogenesis [25,28,32]. The time scale of epileptogenesis in organotypic hippocampal slice cultures (1-2 weeks) is much faster than in animal models, and more amenable to high-throughput analysis (Figure 1.2B). This model captures critical features of epileptogenesis, including the latent period between trauma and the appearance of spontaneous epileptiform activity, seizure-dependent cell death, and responses to anticonvulsants [28,33] (Figure 1.2C). Epileptogenesis in this model can be monitored with chronic imaging, electrical recording, or by detecting biochemical markers of seizures [28,33,34]. Organotypic cultures thus provide an easy-to-access in vitro model for antiepileptic drug discovery [33–38]. The organotypic hippocampal culture based "epilepsy-in-a-dish" model was first developed in 2010, when Dyhrfjeld-Johnsen et al.

provided detailed characterizations of the development and evolution of epileptiform activity within this in vitro model of chronic epilepsy [32]. In 2012, Berdichevsky et al. further characterized the features of this model, like activity-dependent cell death, response to anticonvulsants, and emergence of anticonvulsant resistance [28]. After that, the organotypic hippocampal slice culture was proposed as an in vitro disease model for screening of anticonvulsants and antiepileptogenic therapies, which identified the cyclooxygenase inhibitor, Celecoxib, as a novel anticonvulsant and mTOR as an effective target of epileptogenesis [33,38].

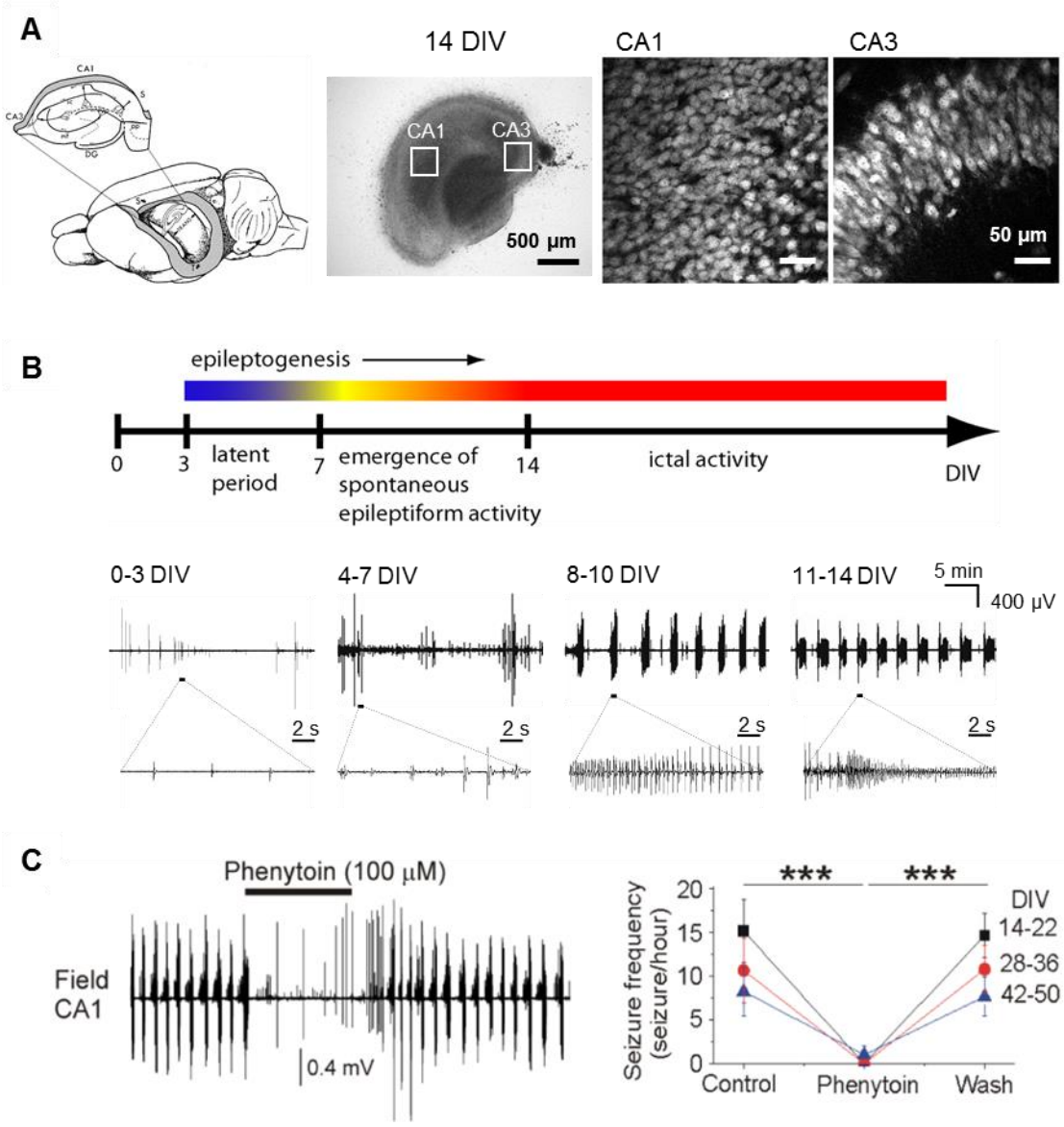

Figure 1.2 Post traumatic epilepsy is modeled in organotypic hippocampal cultures. (A) Left, hippocampus anatomy in rodent brain. Middle, brightfield image of organotypic hippocampal culture after 14 days in vitro (DIV). Scale bar, 500 µm. Right, confocal imaging of NeuN staining in CA1 and CA3 regions show densely packed neurons. Scale bars, 50 µm. (B) Representative recordings on different DIV, revealing the time course of epileptogenesis in organotypic hippocampal cultures. (C) Electrographic responses to known anticonvulsant. Left, electrical recording reveals that seizures stopped during phenytoin application. Right, these results were typical (n = 6, each group). Reproduced with permission from [28].

High-throughput drug screens based on the organotypic hippocampal culture model will require massively parallel recordings for over two weeks for the observation of epileptogenesis. However, traditional methods of maintaining organotypic cultures, interface methods [29] and roller-tube methods [39], are not directly compatible with electrophysiology platforms for chronic recording or scalable to support high-throughput electrical assays [40] (Figure 1.3A, B). The lack of a scalable chronic electrical recording system is a significant bottleneck for antiepileptogenic drug discovery using organotypic cultures.

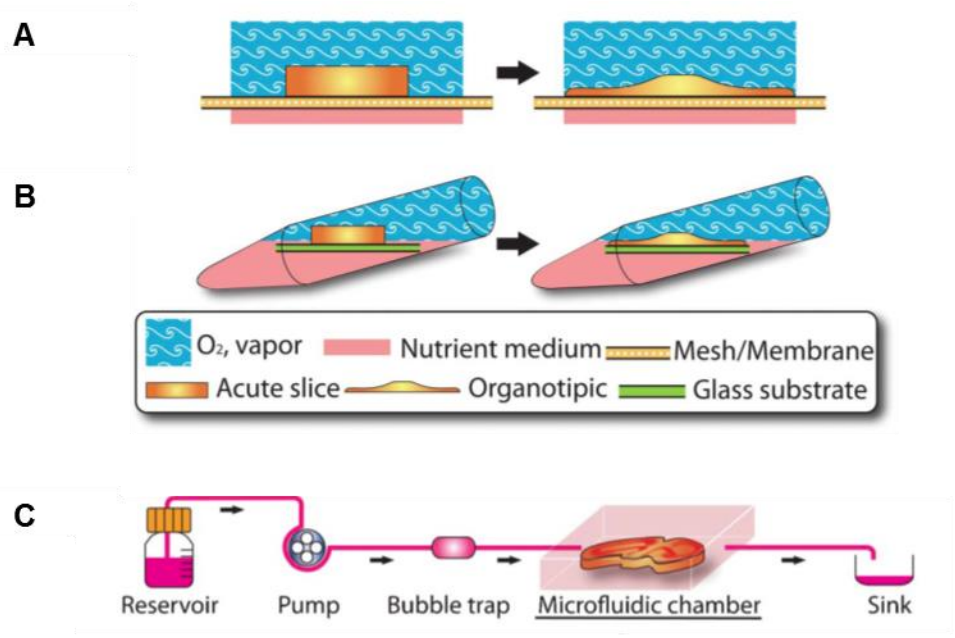

Figure 1.3 Conventional and microfluidic perfusion methods to maintain brain slices. Interface methods (A) and roller-tube methods (B) to maintain organotypic brain slice cultures. (C) Microfluidic perfusion system for brain slice that can highly miniaturize the culture platform and provide versatile designs. Reproduced with permission from [40].

The rapid progress of technologies for microfluidics and biological microelectromechanical systems (BioMEMS) over the past decade has enabled the

development of simplified, microengineered platforms that are highly amenable to miniaturization, high-throughput experimentations, and real-time analysis for in vitro neurobiological studies [40,41], providing an avenue to address the throughput limitations in organotypic culture based drug discovery.

1.2 Microfluidic-MEA technology for brain slice based study

Neural activity within a volume of brain tissue gives rise to transmembrane currents, including synaptic activity, action potentials, Ca^{2+} spikes, and intrinsic currents and resonances [42]. All ionic processes superimpose in space to yield field potentials (FPs) that can be measured in the extracellular medium. Synaptic transmembrane currents are the major contributors to FPs [42]. When neuron receives a synaptic input, the generated transmembrane current gives rise to a current sink, where currents flow from the extracellular into the intracellular space, and a current source, where currents flow from the intracellular to the extracellular space, along the neuron. Depending on the locations of sink and source, a current dipole or higher order n-pole is formed, giving rise to the FPs (Figure 1.4A). Unlike intracellular recording techniques that use sharp or patch microelectrodes to detect activity of individual neurons, extracellular recording of FPs with metal microelectrodes is able to detect both single and multiple neuron activity, and it is therefore more applicable to network level analysis of population activity in neuronal networks, like sharp wave-ripples and epilepsy [43] (Figure 1.4B).

Multiple microelectrodes can be integrated on a planar surface to create multiple electrode arrays (MEAs), a technique adopted from the microelectronics industry [44,45]. When

fabricating an MEA chip, the selection of materials depends on the type of experiment that will be conducted: dissociated neuron, acute brain slices, or organotypic cultures. Some factors to be considered are: biocompatibility, optical transparency, and insulation durability. The most commonly used material for the substrate is glass, which can be easily interfaced with optical microscopy. Gold, platinum, titanium nitride, and indium-tin oxide are used for conductor patterns, including electrodes, track, and contact pads. In the case of gold and platinum, an additional metal layer such as titanium or chromium is required to promote the adhesion between the glass substrate and metal. The standard fabrication process includes conductor patterning, insulator coating and electrode opening (Figure 1.4C). The conductor layer is deposited onto the substrate using sputtering, thermal evaporation or e-beam evaporation. The desired pattern is defined by photolithography followed by a wet or dry etching process. To prevent signal crosstalk and dissipation, an insulation layer is required to passivate conductor tracks. Normally used isolation types are: Silicon dioxide, silicon nitride, SU-8, polyimide, and Polydimethylsiloxane (PDMS). Following the insulation, the layout of electrodes and contact pads are exposed by photolithography and etching (depending on the material). Dozens of microelectrodes on MEA chip enable multiple-sites recordings with high spatial resolution, which is crucial for studies of network activities, like signal processing and neurotransmission. Importantly, a planar MEA provides a noninvasive neural-electrode interface that allows for long-term recording and stimulation.

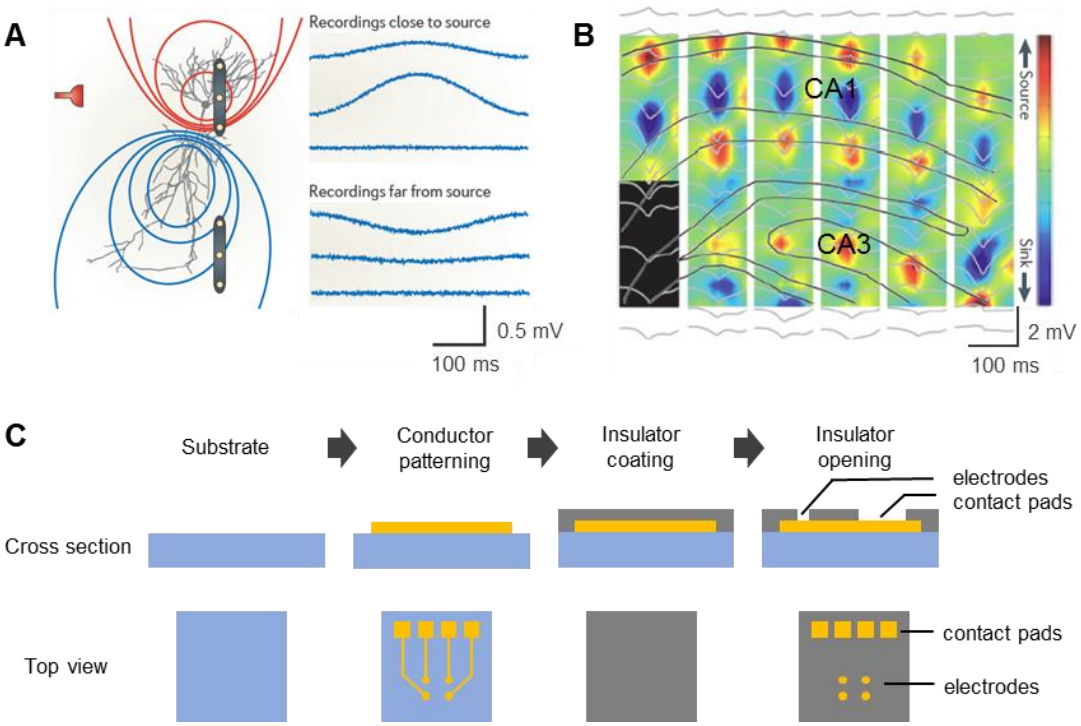

Figure 1.4 Multiple electrode array (MEA) for extracellular electrophysiology. (A-B) The origin of extracellular field potentials (FPs). Reproduced with permission from [42]. (A) A current sink-source dipole is induced by inhibitory synaptic input at the perisomatic region (red symbol). Lines represent isopotentials (red, positive; blue, negative). FPs are recorded from 6 sites at vicinity of the neuron. Electrodes are shown in yellow. (B) FPs recorded from different sites in hippocampus during synchronized sharp wave activity (traces shown in grey). Current sink-source distribution is shown in color map. (C) Standard MEA fabrication process.

Using MEAs to record epileptiform activity in brain slices gives rise to novel epilepsy-on-a-chip systems [46–49]. Hill et al. used MEAs to record burst activities in an acute hippocampal slice model of status epilepticus. Multiple-sites recordings were used to assess burst propagation speed and frequency as novel parameters for anticonvulsants screening [46]. To investigate the modulatory effect of thalamic inputs on seizures generated in anterior cingulate cortex (ACC), Chang et al. used MEA recordings to study spatiotemporal properties of epileptiform activity in acute thalamic-ACC slice [47]. Hsiao et al. reported MEA recordings from different subregions of human epileptic hippocampal

slice to study epilepsy generation and propagation in hippocampal circuitry [48]. Ferrea et al. developed a large-scale array recording simultaneously from 4096 electrodes to study propagating epileptiform activity in acute murine cortico-hippocampal brain slices, and topologically localized and quantified the effects of antiepileptic drugs in local neuronal microcircuits [49].

It is important to note that planar MEA chips are compatible with organotypic culture methods and have been used to chronically record spontaneous activity in cortical and hippocampal cultures over several weeks [50–57]. To study the formation and stabilization of axonal projections, Hofmann et al. kept organotypic co-culture of entorhinal cortex (EC) and dentate gyrus (DG) slice on an MEA chip for up to 6 weeks (Figure 1.5A). The progress of neurite outgrowth and the establishment of functional connections were evaluated by analyzing the correlation of evoked signals in EC and DG after electrical stimulation in EC [54]. Gong et al. developed a high-density MEA to record electrical activity of individual neurons at a high spatial resolution, while monitoring neuronal network activity simultaneously in an organotypic hippocampal slice for 4 weeks [55]. A recently developed integrated device combined interstitial perfusion and perforated MEA to optimize nutrient and oxygen diffusion and enable long-term maintenance of organotypic cultures [56]. MEAs can provide immensely parallel recording for high-throughput electrical assay of epileptogenesis in vitro. However, currently available MEA chips, for example Multichannel Systems, MED64, and Qwane Biosciences, are designed to support only one slice culture. The primary factor limiting the number of cultures that can be placed on a MEA chip is that traditional culture methods consume large areas of MEA real estate, thus preventing high-throughput on-chip experimentations.

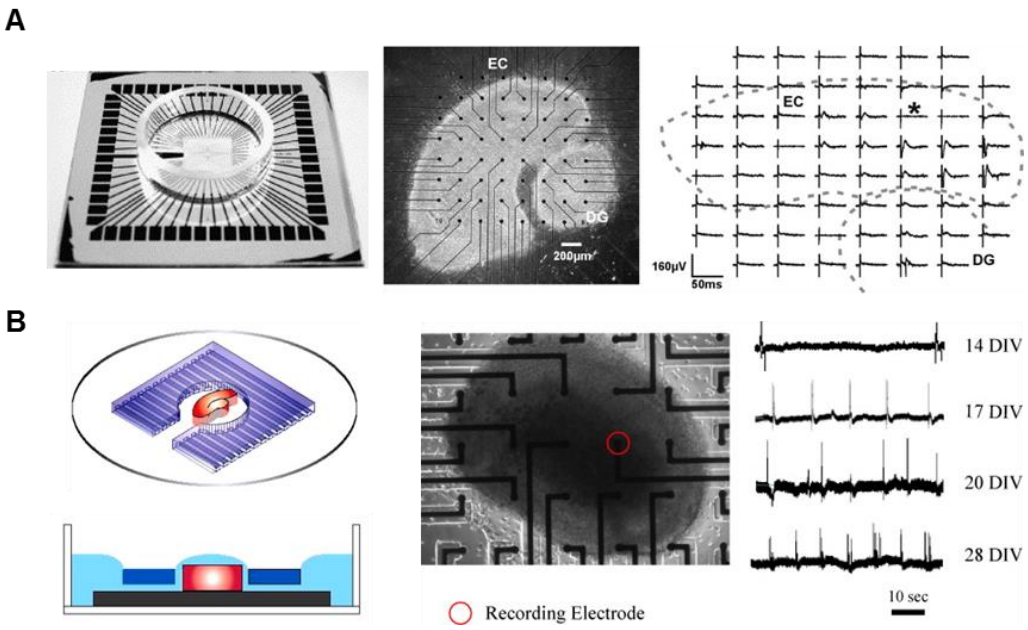

Figure 1.5 MEA device supports long-term recordings in organotypic culture. (A) Organotypic co-culture of entorhinal cortex (EC) and dentate gyrus (DG) maintained on MEA chip and evoked signals recorded by MEA electrodes. Reproduced with permission from [54]. (B) Microfluidic compartment integrated MEA device supports organotypic hippocampal culture and electrophysiology for 4 weeks. Reproduced with permission from [58].

Microfluidics has been previously used to pattern dissociated-neuron based model systems [59–62] and to perfuse brain slices [40]. Several groups have reported successful integration of microchannel patterns and MEAs with precise alignment between fluidic and electronic device components for neural-electrical interfaces [63,64,58,65]. Kanagasabapathi et al. bonded compartmented neuron co-culture system to MEAs to study the propagation of neural activities between cortical and thalamic neurons [63]. Dworak et al. integrated MEAs with PDMS microtunnels to study in vitro neuronal communication. In this device, axons extended through the narrow microchannels, and highly selective recordings of axonal signals were acquired by MEAs underneath [64]. To investigate the information processing in neural networks, Scott et al. developed a microfluidic MEA

device with the capability to allow simultaneous multi-sites extracellular recording, and focal chemical stimuli delivered by microfluidic network [65]. Berdichevsky et al. used a PDMS mini-well to maintain organotypic hippocampal slice cultures on MEA surface for 4 weeks, and microchannels were incorporated into the mini-well to guide the axons sprouting [58] (Figure 1.5B). Microfluidic perfusion can be introduced to miniaturize the brain slice culture platform, by removing medium storage off-device and provide versatile designs [40] (Figure 1.3C). Furthermore, perfused brain slices may more closely resemble their in situ counterparts that are highly perfused by vascular networks in vivo [66–68]. However, most microfluidic perfusion systems are used in acute brain slice based studies, and relatively little attention has been paid to using microfluidic technology to improve the throughput of organotypic culture based experiments.

A novel MEA chip that is integrated with scalable microfluidic perfusion system, which enables long-term parallel recordings from multiple organotypic cultures in a single device, will make it possible for high-throughput electrical assay for antiepileptogenic drug discovery in vitro.

1.3 Cell signaling pathways in epilepsy

Some of the characteristics of the epileptic brain include axon sprouting, synaptic reorganization, inflammation, and hyperexcitability [2,3,8]. These processes are regulated by kinase signaling pathways [8,69–76]. Furthermore, the human genome includes over 500 kinase genes [77], and many of them play important roles in cellular processes in the nervous system [78]. It is highly possible that they are involved in epileptogenesis. Small

molecular inhibitors have been synthesized for many of these kinases and are used extensively in cancer research. Inhibition of these pathways has the potential to prevent formation of epileptic circuitry and thus prevent epileptogenesis after brain injury, or even disrupt existing epileptic circuits and cure epilepsy. Some kinase signaling pathways, including the PI3k-Akt-mTOR, JAK-STAT, and BDNF-TrkB pathways, have been implicated in animal and in vitro models of acquired chronic epilepsies [33,75,79–84]. However, only a small percentage of the total kinome have been explored as potential targets for antiepileptogenic drugs. For example, many receptor tyrosine kinases (RTKs) are expressed in the brain and have been reported to respond to brain injury [85–94], but only a few of them have been investigated for inhibition of epileptogenesis. Interestingly, the TrkB receptor and the Insulin-like Growth Factor-I Receptor (two types of RTKs) have been implicated in epileptogenesis [82–84,95,96]. Other pathways, including JAK-STAT and Wnt signaling, which have strong cross-talk with RTK, have also been found to play a role in epilepsy [97–99]. This evidence suggests that the RTK signaling network plays a prominent role in epileptogenesis and may provide potential targets for antiepileptogenic drugs. However, the RTK signaling network is highly complex. There are over 20 RTKs expressed in the hippocampus and cortex at significant levels (based on Allen Brain Atlas mouse data), and the downstream signaling have cross-talk with multiple other pathways [100], which makes the matrix of experiments very large.

This thesis will focus on the development of an organotypic hippocampal culture based screen platform for systematic investigation of the role of cell signaling pathways in epileptogenesis, which may have a transformative impact on the search for better therapies

for epilepsy. A pilot screen of RTK inhibitor library will be described as a demonstration of how this platform provides rapid dissection of signaling pathways in epilepsy.

1.4 Goals of this thesis

The general aim of the work described in this thesis is to develop a hybrid microfluidic-MEA (μflow-MEA) technology for scalable chronic electrical assay of epileptogenesis in vitro and to demonstrate how μflow-MEA facilitates antiepileptogenic drug discovery. The specific objectives are:

1. To develop a scalable microfluidic perfusion system for long-term maintenance of organotypic hippocampal cultures (Chapter 2) [101].

2. To integrate microfluidic perfusion system with MEAs for scalable chronic electrical assay of epileptogenesis and carry out a pilot screen of a small-molecule kinase (RTK) inhibitor library (Chapter 3).

3. To validate the organotypic hippocampal culture model of epilepsy by studying the influence of culture medium composition on epileptogenesis (Chapter 4) [102].

Finally, future work of this research is discussed (Chapter 5).

1.5 References

1. WHO | Epilepsy. In: WHO [Internet]. [cited 19 Jun 2017]. Available: http://www.who.int/mediacentre/factsheets/fs999/en/

2. Loscher W, Brandt C. Prevention or Modification of Epileptogenesis after Brain Insults: Experimental Approaches and Translational Research. Pharmacol Rev. 2010;62: 668–700. doi:10.1124/pr.110.003046

3. Pitkänen A, Lukasiuk K. Mechanisms of epileptogenesis and potential treatment targets. Lancet Neurol. 2011;10: 173–186. doi:10.1016/s1474-4422(10)70310-0

4. Pitkänen A, Lukasiuk K, Dudek FE, Staley KJ. Epileptogenesis. Cold Spring Harb Perspect Med. 2015;5: a022822. doi:10.1101/cshperspect.a022822

5. Salazar AM, Jabbari B, Vance SC, Grafman J, Amin D, Dillon JD. Epilepsy after penetrating head injury. I. Clinical correlates: a report of the Vietnam Head Injury Study. Neurology. 1985;35: 1406–14.

6. Annegers JF, Hauser WA, Coan SP, Rocca WA. A population-based study of seizures after traumatic brain injuries. N Engl J Med. 1998;338: 20–24.

7. Raymont V, Salazar A, Lipsky R, Goldman D, Tasick G, Grafman J. Correlates of posttraumatic epilepsy 35 years following combat brain injury. Neurology. 2010;75: 224–229.

8. Goldberg EM, Coulter DA. Mechanisms of epileptogenesis: a convergence on neural circuit dysfunction. Nat Rev Neurosci. 2013;14: 337–349.

9. Temkin NR. Antiepileptogenesis and Seizure Prevention Trials with Antiepileptic Drugs: Meta-Analysis of Controlled Trials. Epilepsia. 2001;42: 515–524. doi:10.1046/j.1528-1157.2001.28900.x

10. Temkin NR. Preventing and treating posttraumatic seizures: the human experience. Epilepsia. 2009;50 Suppl 2: 10–13. doi:10.1111/j.1528-1167.2008.02005.x

11. Thompson K, Pohlmann-Eden B, Campbell LA, Abel H. Pharmacological treatments for preventing epilepsy following traumatic head injury. Cochrane Database of Systematic Reviews. John Wiley & Sons, Ltd; 2015. doi:10.1002/14651858.CD009900.pub2

12. Schmidt D, Löscher W. New Developments in Antiepileptic Drug Resistance: An Integrative View. Epilepsy Curr. 2009;9: 47–52. doi:10.1111/j.1535-7511.2008.01289.x

13. Kelley MS, Jacobs MP, Lowenstein DH. The NINDS epilepsy research benchmarks. Epilepsia. 2009;50: 579–582.

14. 2014 NINDS Benchmarks for Epilepsy Research | National Institute of Neurological Disorders and Stroke [Internet]. [cited 19 Jun 2017]. Available: https://www.ninds.nih.gov/About-NINDS/Strategic-Plans-Evaluations/Strategic-Plans/2014-NINDS-Benchmarks-Epilepsy-Research

15. Curia G, Longo D, Biagini G, Jones RS, Avoli M. The pilocarpine model of temporal lobe epilepsy. J Neurosci Methods. 2008;172: 143–157.

16. Morimoto K, Fahnestock M, Racine RJ. Kindling and status epilepticus models of epilepsy: rewiring the brain. Prog Neurobiol. 2004;73: 1–60.

17. Williams PA, White AM, Clark S, Ferraro DJ, Swiercz W, Staley KJ, et al. Development of spontaneous recurrent seizures after kainate-induced status epilepticus. J Neurosci. 2009;29: 2103–12. doi:10.1523/jneurosci.0980-08.2009

18. Simonato M, Löscher W, Cole AJ, Dudek FE, Engel J, Kaminski RM, et al. Finding a better drug for epilepsy: Preclinical screening strategies and experimental trial design. Epilepsia. 2012;53: 1860–1867. doi:10.1111/j.1528-1167.2012.03541.x

19. Fountain S, Ting Y-L, Teyler T. The in vitro hippocampal slice preparation as a screen for neurotoxicity. Toxicol In Vitro. 1992;6: 77–87.

20. Stopps M, Allen N, Barrett R, Choudhury H, Jarolimek W, Johnson M, et al. Design and application of a novel brain slice system that permits independent electrophysiological recordings from multiple slices. J Neurosci Methods. 2004;132: 137–148.

21. Cho S, Wood A, Bowlby MR. Brain slices as models for neurodegenerative disease and screening platforms to identify novel therapeutics. Curr Neuropharmacol. 2007;5: 19.

22. Kroker KS, Rosenbrock H, Rast G. A multi-slice recording system for stable late phase hippocampal long-term potentiation experiments. J Neurosci Methods. 2011;194: 394–401.

23. Graef JD, Wei H, Lippiello PM, Bencherif M, Fedorov N. Slice XVIvo^{TM}: A novel electrophysiology system with the capability for 16 independent brain slice recordings. J Neurosci Methods. 2013;212: 228–233.

24. Heinemann U, Staley KJ. What is the clinical relevance of in vitro epileptiform activity? Issues in Clinical Epileptology: A View from the Bench. Springer; 2014. pp. 25–41.

25. Coulter D, Rafiq A, Shumate M, Gong Q, DeLorenzo R, Lyeth B. Brain injury-induced enhanced limbic epileptogenesis: anatomical and physiological parallels to an animal model of temporal lobe epilepsy. Epilepsy Res. 1996;26: 81–91.

26. Santhakumar V, Ratzliff AD, Jeng J, Toth Z, Soltesz I. Long-term hyperexcitability in the hippocampus after experimental head trauma. Ann Neurol. 2001;50: 708–717.

27. Kharatishvili I, Nissinen J, McIntosh T, Pitkänen A. A model of posttraumatic epilepsy induced by lateral fluid-percussion brain injury in rats. Neuroscience. 2006;140: 685–697.

28. Berdichevsky Y, Dzhala V, Mail M, Staley KJ. Interictal spikes, seizures and ictal cell death are not necessary for post-traumatic epileptogenesis in vitro. Neurobiol Dis. 2012;45: 774–785.

29. Stoppini L, Buchs P-A, Muller D. A simple method for organotypic cultures of nervous tissue. J Neurosci Methods. 1991;37: 173–182.

30. Raineteau O, Rietschin L, Gradwohl G, Guillemot F, Gähwiler BH. Neurogenesis in hippocampal slice cultures. Mol Cell Neurosci. 2004;26: 241–250.

31. Muller D, Buchs P-A, Stoppini L. Time course of synaptic development in hippocampal organotypic cultures. Dev Brain Res. 1993;71: 93–100.

32. Dyhrfjeld-Johnsen J, Berdichevsky Y, Swiercz W, Sabolek H, Staley K. Interictal spikes precede ictal discharges in an organotypic hippocampal slice culture model of epileptogenesis. J Clin Neurophysiol. 2010;27: 418–424.

33. Berdichevsky Y, Dryer AM, Saponjian Y, Mahoney MM, Pimentel CA, Lucini CA, et al. PI3K-Akt signaling activates mTOR-mediated epileptogenesis in organotypic hippocampal culture model of post-traumatic epilepsy. J Neurosci. 2013;33: 9056–9067.

34. Lillis KP, Wang Z, Mail M, Zhao GQ, Berdichevsky Y, Bacskai B, et al. Evolution of network synchronization during early epileptogenesis parallels synaptic circuit alterations. J Neurosci. 2015;35: 9920–9934.

35. Park K-I, Dzhala V, Saponjian Y, Staley KJ. What elements of the inflammatory system are necessary for epileptogenesis in vitro? eneuro. 2015;2: ENEURO. 0027-14.2015.

36. Gutiérrez R, Heinemann U. Synaptic reorganization in explanted cultures of rat hippocampus. Brain Res. 1999;815: 304–316.

37. Dzhala V, Staley KJ. Acute and Chronic Efficacy of Bumetanide in an in vitro Model of Posttraumatic Epileptogenesis. CNS Neurosci Ther. 2015;21: 173–180.

38. Berdichevsky Y, Saponjian Y, Park K-I, Roach B, Pouliot W, Lu K, et al. Staged anticonvulsant screening for chronic epilepsy. Ann Clin Transl Neurol. 2016;3: 908–923. doi:10.1002/acn3.364

39. Gahwiler B TS McKinney A, Debanne D, Robertson R. Organotypic Slice Cultures of Neural Tissue. In: Culturing Nerve Cells. 2nd ed. Massachusetts Institute of Technology; 1998.

40. Huang Y, Williams JC, Johnson SM. Brain slice on a chip: opportunities and challenges of applying microfluidic technology to intact tissues. Lab Chip. 2012;12: 2103. doi:10.1039/c2lc21142d

41. Yi Y, Park J, Lim J, Lee CJ, Lee S-H. Central Nervous System and its Disease Models on a Chip. Trends Biotechnol. 12;33: 762–776. doi:10.1016/j.tibtech.2015.09.007

42. Buzsáki G, Anastassiou CA, Koch C. The origin of extracellular fields and currents—EEG, ECoG, LFP and spikes. Nat Rev Neurosci. 2012;13: 407–420.

43. Buzsáki G. Hippocampal sharp wave-ripple: A cognitive biomarker for episodic memory and planning. Hippocampus. 2015;25: 1073–1188. doi:10.1002/hipo.22488

44. Morin FO, Takamura Y, Tamiya E. Investigating neuronal activity with planar microelectrode arrays: achievements and new perspectives. J Biosci Bioeng. 2005;100: 131–143. doi:10.1263/jbb.100.131

45. Jones IL, Livi P, Lewandowska MK, Fiscella M, Roscic B, Hierlemann A. The potential of microelectrode arrays and microelectronics for biomedical research and

diagnostics. Anal Bioanal Chem. 2010;399: 2313–2329. doi:10.1007/s00216-010-3968-1

46. Hill AJ, Jones NA, Williams CM, Stephens GJ, Whalley BJ. Development of multi-electrode array screening for anticonvulsants in acute rat brain slices. J Neurosci Methods. 1;185: 246–256. doi:10.1016/j.jneumeth.2009.10.007

47. Chang W-P, Wu J-S, Lee C-M, Vogt BA, Shyu B-C. Spatiotemporal organization and thalamic modulation of seizures in the mouse medial thalamic-anterior cingulate slice. Epilepsia. 2011;52: 2344–2355. doi:10.1111/j.1528-1167.2011.03312.x

48. Hsiao M-C, Yu P-N, Song D, Liu CY, Heck CN, Millett D, et al. An in vitro seizure model from human hippocampal slices using multi-electrode arrays. J Neurosci Methods. 4;244: 154–163. doi:10.1016/j.jneumeth.2014.09.010

49. Ferrea E, Maccione A, Medrihan L, Nieus T, Ghezzi D, Baldelli P, et al. Large-scale, high-resolution electrophysiological imaging of field potentials in brain slices with microelectronic multielectrode arrays. Front Neural Circuits. 2012;6. doi:10.3389/fncir.2012.00080

50. Egert U, Schlosshauer B, Fennrich S, Nisch W, Fejtl M, Knott T, et al. A novel organotypic long-term culture of the rat hippocampus on substrate-integrated multielectrode arrays. Brain Res Protoc. 1998;2: 229–242.

51. Corner M, Van Pelt J, Wolters P, Baker R, Nuytinck R. Physiological effects of sustained blockade of excitatory synaptic transmission on spontaneously active developing neuronal networks—an inquiry into the reciprocal linkage between

intrinsic biorhythms and neuroplasticity in early ontogeny. Neurosci Biobehav Rev. 2002;26: 127–185.

52. Beggs JM. Neuronal Avalanches Are Diverse and Precise Activity Patterns That Are Stable for Many Hours in Cortical Slice Cultures. J Neurosci. 2004;24: 5216–5229. doi:10.1523/jneurosci.0540-04.2004

53. Johnson HA, Buonomano DV. Development and Plasticity of Spontaneous Activity and Up States in Cortical Organotypic Slices. J Neurosci. 2007;27: 5915–5925. doi:10.1523/jneurosci.0447-07.2007

54. Hofmann F, Guenther E, Hämmerle H, Leibrock C, Berezin V, Bock E, et al. Functional re-establishment of the perforant pathway in organotypic co-cultures on microelectrode arrays. Brain Res. 8;1017: 184–196. doi:10.1016/j.brainres.2004.05.044

55. Gong W, Sencar J, D J, x00E, ckel, J M, et al. Long-term, high-spatiotemporal resolution recording from cultured organotypic slices with high-density microelectrode arrays. 2015. pp. 1037–1040. doi:10.1109/TRANSDUCERS.2015.7181103

56. Killian NJ, Vernekar VN, Potter SM, Vukasinovic J. A Device for Long-Term Perfusion, Imaging, and Electrical Interfacing of Brain Tissue In vitro. Front Neurosci. 2016;10: 135. doi:10.3389/fnins.2016.00135

57. Hofmann F, Bading H. Long term recordings with microelectrode arrays: Studies of transcription-dependent neuronal plasticity and axonal regeneration. J Physiol-Paris. 3;99: 125–132. doi:10.1016/j.jphysparis.2005.12.005

58. Berdichevsky Y, Sabolek H, Levine JB, Staley KJ, Yarmush ML. Microfluidics and multielectrode array-compatible organotypic slice culture method. J Neurosci Methods. 2009;178: 59–64. doi:10.1016/j.jneumeth.2008.11.016

59. Taylor A, Jeon NL. Microfluidic and compartmentalized platforms for neurobiological research. Crit Rev Biomed Eng. 2011;39.

60. Taylor AM, Blurton-Jones M, Rhee SW, Cribbs DH, Cotman CW, Jeon NL. A microfluidic culture platform for CNS axonal injury, regeneration and transport. Nat Methods. 2005;2: 599–605.

61. Peyrin J-M, Deleglise B, Saias L, Vignes M, Gougis P, Magnifico S, et al. Axon diodes for the reconstruction of oriented neuronal networks in microfluidic chambers. Lab Chip. 2011;11: 3663. doi:10.1039/c1lc20014c

62. Neto E, Leitão L, Sousa DM, Alves CJ, Alencastre IS, Aguiar P, et al. Compartmentalized Microfluidic Platforms: The Unrivaled Breakthrough of *In Vitro* Tools for Neurobiological Research. J Neurosci. 2016;36: 11573–11584. doi:10.1523/JNEUROSCI.1748-16.2016

63. Kanagasabapathi TT, Franco M, Barone RA, Martinoia S, Wadman WJ, Decré MMJ. Selective pharmacological manipulation of cortical–thalamic co-cultures in a dual compartment device. J Neurosci Methods. 3;214: 1–8. doi:10.1016/j.jneumeth.2012.12.019

64. Dworak BJ, Wheeler BC. Novel MEA platform with PDMS microtunnels enables the detection of action potential propagation from isolated axons in culture. Lab Chip. 2009;9: 404–410. doi:10.1039/B806689B

65. Scott A, Weir K, Easton C, Huynh W, Moody WJ, Folch A. A microfluidic microelectrode array for simultaneous electrophysiology, chemical stimulation, and imaging of brain slices. Lab Chip. 2013;13: 527–535. doi:10.1039/C2LC40826K

66. Passeraub PA, Almeida A, Thakor N. Design, microfabrication and analysis of a microfluidic chamber for the perfusion of brain tissue slices. Biomed Microdevices. 2003;5: 147–155.

67. Choi Y, McClain MA, LaPlaca MC, Frazier AB, Allen MG. Three dimensional MEMS microfluidic perfusion system for thick brain slice cultures. Biomed Microdevices. 2007;9: 7–13.

68. Rambani K, Vukasinovic J, Glezer A, Potter SM. Culturing thick brain slices: an interstitial 3D microperfusion system for enhanced viability. J Neurosci Methods. 2009;180: 243–254.

69. Pitkänen A, Lukasiuk K. Molecular and cellular basis of epileptogenesis in symptomatic epilepsy. Epilepsy Behav. 2009;14: 16–25.

70. Amato S, Liu X, Zheng B, Cantley L, Rakic P, Man H-Y. AMP-activated protein kinase regulates neuronal polarization by interfering with PI 3-kinase localization. Science. 2011;332: 247–251.

71. Chan CB, Liu X, Pradoldej S, Hao C, An J, Yepes M, et al. Phosphoinositide 3-kinase enhancer regulates neuronal dendritogenesis and survival in neocortex. J Neurosci. 2011;31: 8083–8092.

72. Cuesto G, Enriquez-Barreto L, Caramés C, Cantarero M, Gasull X, Sandi C, et al. Phosphoinositide-3-kinase activation controls synaptogenesis and spinogenesis in hippocampal neurons. J Neurosci. 2011;31: 2721–2733.

73. Howlett E, Lin CC-J, Lavery W, Stern M. A PI3-Kinase–Mediated Negative Feedback Regulates Neuronal Excitability. PLoS Genet. 2008;4: e1000277.

74. Oliva AA, Atkins CM, Copenagle L, Banker GA. Activated c-Jun N-terminal kinase is required for axon formation. J Neurosci. 2006;26: 9462–9470.

75. Grabenstatter HL, Russek SJ, Brooks-Kayal AR. Molecular pathways controlling inhibitory receptor expression. Epilepsia. 2012;53: 71–78.

76. Yoshii A, Constantine-Paton M. Postsynaptic BDNF-TrkB signaling in synapse maturation, plasticity, and disease. Dev Neurobiol. 2010;70: 304–322.

77. Manning G, Whyte DB, Martinez R, Hunter T, Sudarsanam S. The protein kinase complement of the human genome. Science. 2002;298: 1912–1934.

78. Martin KJ, Arthur JSC. Selective kinase inhibitors as tools for neuroscience research. Neuropharmacology. 2012;63: 1227–1237.

79. Buckmaster PS, Ingram EA, Wen X. Inhibition of the mammalian target of rapamycin signaling pathway suppresses dentate granule cell axon sprouting in a rodent model of temporal lobe epilepsy. J Neurosci. 2009;29: 8259–8269.

80. Zeng L-H, Rensing NR, Wong M. The mammalian target of rapamycin signaling pathway mediates epileptogenesis in a model of temporal lobe epilepsy. J Neurosci. 2009;29: 6964–6972.

81. Scharfman HE. Brain-derived Neurotrophic Factor and Epilepsy—A Missing Link? Epilepsy Curr. 2005;5: 83–88. doi:10.1111/j.1535-7511.2005.05312.x

82. Aungst S, England PM, Thompson SM. Critical role of trkB receptors in reactive axonal sprouting and hyperexcitability after axonal injury. J Neurophysiol. 2013;109: 813–824.

83. Dinocourt C, Gallagher SE, Thompson SM. Injury-induced axonal sprouting in the hippocampus is initiated by activation of trkB receptors. Eur J Neurosci. 2006;24: 1857–1866.

84. Liu G, Gu B, He X-P, Joshi RB, Wackerle HD, Rodriguiz RM, et al. Transient inhibition of TrkB kinase after status epilepticus prevents development of temporal lobe epilepsy. Neuron. 2013;79: 31–38.

85. Liu B, Chen H, Johns TG, Neufeld AH. Epidermal Growth Factor Receptor Activation: An Upstream Signal for Transition of Quiescent Astrocytes into Reactive Astrocytes after Neural Injury. J Neurosci. 2006;26: 7532–7540. doi:10.1523/JNEUROSCI.1004-06.2006

86. Leadbeater WE, Gonzalez A-M, Logaras N, Berry M, Turnbull JE, Logan A. Intracellular trafficking in neurones and glia of fibroblast growth factor-2, fibroblast growth factor receptor 1 and heparan sulphate proteoglycans in the injured adult rat cerebral cortex. J Neurochem. 2006;96: 1189–1200. doi:10.1111/j.1471-4159.2005.03632.x

87. Nagayama T, Nagayama M, Kohara S, Kamiguchi H, Shibuya M, Katoh Y, et al. Post-ischemic delayed expression of hepatocyte growth factor and c-Met in mouse brain following focal cerebral ischemia. Brain Res. 2004;999: 155–166. doi:10.1016/j.brainres.2003.11.052

88. Schäbitz W-R, Krüger C, Pitzer C, Weber D, Laage R, Gassler N, et al. A Neuroprotective Function for the Hematopoietic Protein Granulocyte-Macrophage Colony Stimulating Factor (GM-CSF). J Cereb Blood Flow Metab. 2008;28: 29–43. doi:10.1038/sj.jcbfm.9600496

89. Tokita Y, Keino H, Matsui F, Aono S, Ishiguro H, Higashiyama S, et al. Regulation of Neuregulin Expression in the Injured Rat Brain and Cultured Astrocytes. J Neurosci. 2001;21: 1257–1264.

90. Sköld MK, Gertten CV, Sandbergnordqvist A-C, Mathiesen T, Holmin S. VEGF and VEGF Receptor Expression after Experimental Brain Contusion in Rat. J Neurotrauma. 2005;22: 353–367. doi:10.1089/neu.2005.22.353

91. Helmy A, Carpenter KL, Menon DK, Pickard JD, Hutchinson PJ. The Cytokine Response to Human Traumatic Brain Injury: Temporal Profiles and Evidence for

Cerebral Parenchymal Production. J Cereb Blood Flow Metab. 2011;31: 658–670. doi:10.1038/jcbfm.2010.142

92. Sandberg Nordqvist AC, von Holst H, Holmin S, Sara VR, Bellander BM, Schalling M. Increase of insulin-like growth factor (IGF)-1, IGF binding protein-2 and -4 mRNAs following cerebral contusion. Brain Res Mol Brain Res. 1996;38: 285–293.

93. Madathil SK, Evans HN, Saatman KE. Temporal and regional changes in IGF-1/IGF-1R signaling in the mouse brain after traumatic brain injury. J Neurotrauma. 2010;27: 95–107. doi:10.1089/neu.2009.1002

94. Rubovitch V, Edut S, Sarfstein R, Werner H, Pick CG. The intricate involvement of the Insulin-like growth factor receptor signaling in mild traumatic brain injury in mice. Neurobiol Dis. 2010;38: 299–303. doi:10.1016/j.nbd.2010.01.021

95. Scharfman HE. Brain-derived Neurotrophic Factor and Epilepsy—A Missing Link? Epilepsy Curr. 2005;5: 83–88.

96. Song Y, Pimentel C, Walters K, Boller L, Ghiasvand S, Liu J, et al. Neuroprotective levels of IGF-1 exacerbate epileptogenesis after brain injury. Sci Rep. 2016;6. doi:10.1038/srep32095

97. Grabenstatter H, Del Angel YC, Carlsen J, Wempe M, White A, Cogswell M, et al. The effect of STAT3 inhibition on status epilepticus and subsequent spontaneous seizures in the pilocarpine model of acquired epilepsy. Neurobiol Dis. 2014;62: 73–85.

98. Lund IV, Hu Y, Raol YH, Benham RS, Faris R, Russek SJ, et al. BDNF Selectively Regulates GABAA Receptor Transcription by Activation of the JAK/STAT Pathway. Sci Signal. 2008;1: ra9. doi:10.1126/scisignal.1162396

99. Theilhaber J, Rakhade SN, Sudhalter J, Kothari N, Klein P, Pollard J, et al. Gene expression profiling of a hypoxic seizure model of epilepsy suggests a role for mTOR and Wnt signaling in epileptogenesis. PloS One. 2013;8: e74428. doi:10.1371/journal.pone.0074428

100. Volinsky N, Kholodenko BN. Complexity of Receptor Tyrosine Kinase Signal Processing. Cold Spring Harb Perspect Biol. 2013;5. doi:10.1101/cshperspect.a009043

101. Liu J, Pan L, Cheng X, Berdichevsky Y. Perfused drop microfluidic device for brain slice culture-based drug discovery. Biomed Microdevices. 2016;18: 46. doi:10.1007/s10544-016-0073-z

102. Liu J, Saponjian Y, Mahoney MM, Staley KJ, Berdichevsky Y. Epileptogenesis in organotypic hippocampal cultures has limited dependence on culture medium composition. PLOS ONE. 2017;12: e0172677. doi:10.1371/journal.pone.0172677

Chapter 2

Development of microfluidic perfusion culture platform

The work described in this section has been published in "Perfused drop microfluidic device for brain slice culture-based drug discovery" by Liu J, Pan L, Cheng X, Berdichevsky Y, Biomed Microdevices. 2016;18: 46.

2.1 Motivation

Both perfusion and electrophysiology are highly amenable to miniaturization, and a number of groups reported microfluidic perfusion devices and multiple electrode array chips (MEAs) designed specifically for brain slices. Major goals of microfluidic device development were to precisely control slice microenvironment [1], enhance nutrient and oxygen supply [2–4], or improve experimental access to the slice [5] (see [6] for a comprehensive review). MEA development focused on capturing spatiotemporal patterns of neural activity by increasing the number of electrodes per slice [7,8], recording from neurons deep within the slice [9], or improving viability of the slice on electrode array chip [10]. These efforts may be summarized as applications of microtechnology to improve the fidelity of brain slice experiments.

On the other hand, relatively little attention has been paid to using microtechnology to improve the throughput of brain slice experiments, especially the long-term experiments

that require electrical recordings of organotypic cultures for multiple days or weeks. Brain slice based drug screens typically rely on simple interface or submerged-type perfusion and only one or two electrodes per slice for stimulation or recording. However, a screen of a compound library may require hundreds or thousands of well-controlled experiments with replicates. Multi-slice systems have been developed to allow simultaneous, independent electrophysiological recordings from multiple brain slices [11–13]. However, these systems require the use of multiple perfusion systems, machined slice chambers and discrete micromanipulator-mounted electrodes, imposing practical limitations on the number of parallel experiments. Slice survival in these multiple-slice systems is limited to only 7 hours, precluding long-term experiments on organotypic cultures [12].

We set out to apply microtechnology to increase the throughput of organotypic hippocampal culture based antiepileptogenic drug screening. Techniques for maintaining organotypic brain slice cultures for multiple weeks have been developed over 20 years ago (methods and applications of brain slice cultures are reviewed in [14]). In an interface method, the slice is placed on a porous membrane, and culture medium is added so that the slice is located at an air-medium interface [15]. In a roller-tube method, the slice is attached to a glass cover slip with a blood clot or collagen gel. The slip is then placed into a tube with culture medium that is rotated on a roller drum at a slow speed, bringing the slice in and out of medium [16]. Both methods ensure that the slice is directly exposed to atmospheric oxygen (100% of the time with the interface method, and approximately 50% of the time with the roller-tube method) to ensure viability in vitro for multiple weeks. Since slices maintain the cytoarchitecture of the originating brain regions, they are termed organotypic slice cultures. However, neither interface nor roller-tube methods of producing

organotypic cultures are directly compatible with microfluidics. A more recently developed method is based on maintaining a slice in a culture medium-filled well cut in a polydimethylsiloxane (PDMS) film [17]. The well is connected with a larger medium reservoir via channels in PDMS film. Glass culture substrate can be easily substituted for a glass-based MEA to enable continuous electrical recording of neural activity in the slice. A disadvantage of this method is the requirement for a large medium reservoir that takes up valuable MEA area and limits the number of cultures that can be placed on a single MEA chip. Another limitation is the lack of a perfusion system for applying drugs or other compounds to slices.

In this work we developed a novel perfused drop technique to enable the placement of multiple organotypic cultures on a single microfluidic device. This scalable culture platform is compatible with MEA and capable of significantly increasing the throughput of organotypic culture experiments on chip. In our design, hippocampal slice are maintained in individual drops confined by PDMS wells. The drops are continuously perfused with fresh culture medium through microchannels. PDMS microfluidic network can be easily integrated with a planar MEA chip for chronic recordings. The device requires only 3 cm^2 area per culture, potentially enabling experiments with up to 6 cultures per single 2"x 2" MEA chip. A single integrated device may potentially replace an entire system for parallel electrophysiology in multiple organotypic hippocampal cultures, enabling scalable electrical assay of epileptogenesis in vitro.

2.2 Device design and theory

In our design, slice culture is maintained on a glass substrate in a PDMS culture well with lithographically defined microchannel as the medium flow inlet and an open channel as the outlet (Figure 2.1). The microchannel is connected to a feeding syringe tube placed at a specific height to provide proper medium flow rate. The outlet is connected to a reservoir where waste medium is removed by a vacuum needle. Culture well is open for optimal oxygen diffusion to the cultures (similar to interface method for organotypic cultures) and to provide culture medium surface tension to push the slices against culture substrate for better tissue attachment.

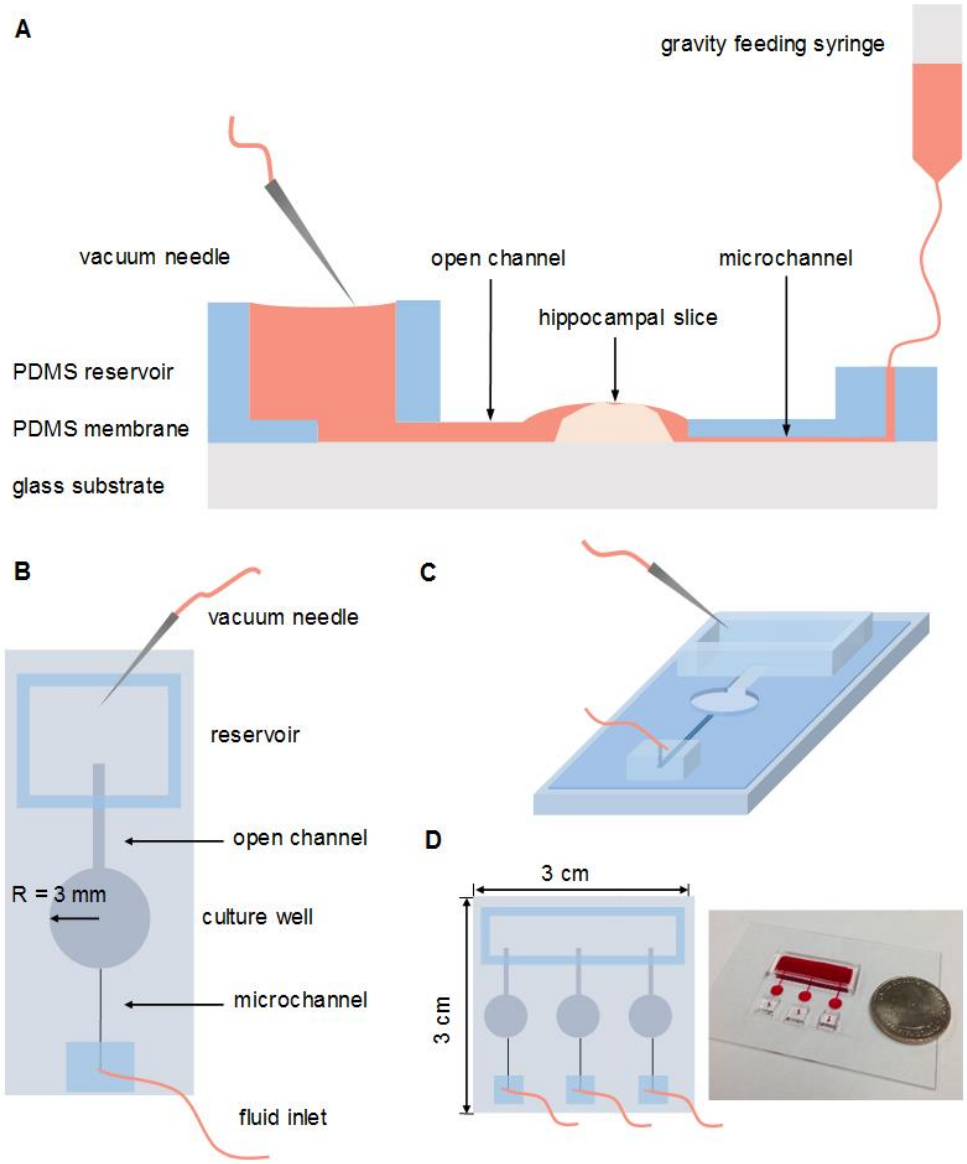

Figure 2.1 Perfused drop organotypic slice culture platform. (A) Schematic of the system setup. PDMS device consists of a membrane (110 µm thick) with an inlet microchannel (20 µm high, 50 µm wide), an open outlet channel (0.5 mm wide) and a culture well (3 mm radius), as well as a PDMS tubing stand and reservoir (2 mm thick). Gravity provides the input culture medium flow through microchannel. Output flow goes to reservoir through open channel and is collected by a vacuum needle. Top view (B) and 3D view (C) of a single device layout. (D) Schematic and photograph of a triple slice device filled with dye solution. Overall device size is 3 cm × 3 cm.

In the absence of flow, size of the drop in the culture well and fluid level in the reservoir are balanced by surface tension and gravity. Adjustment of fluid height in the reservoir H_1

changes the drop size in the culture well (Figure 2.2). Since drop in the culture well is not strictly symmetrical due to the presence of an open outlet channel, we describe it by left contact angle β_l (closest to reservoir) and the right contact angle β_r (closest to inlet), and their average β. We built a simple static model consisting of several force components. In the reservoir, there is pressure due to gravity P_1, and pressure due to capillary force P_2; in culture well, there is also pressure due to gravity P_3, and pressure due to surface tension P_4. In the absence of flow,

$$P_2 - P_1 = P_4 - P_3 \quad (1)$$

$$P_1 = \rho g H_1 \quad (2) \quad P_2 = 2\gamma cos\alpha \left(\frac{1}{w} + \frac{1}{h}\right) \quad (3) \quad P_3 = \rho g H_2 \quad (4) \quad P_4 = \frac{2\gamma cos\beta}{R} \quad (5)$$

where ρ is the density of fluid, g is gravity acceleration, γ is surface tension of fluid, α is the contact angle in the reservoir, w is the width of the reservoir, h is the length of the reservoir, H_1 is fluid height in the reservoir, H_2 is fluid height in the culture well, R is the radius of the culture well, z_1 is the height of the reservoir, and z_2 is the height of the culture well. H_2 can be described in terms of contact angle β:

$$H_2 = z_2 - \frac{R}{cos\beta}(1 - sin\beta) \quad (6)$$

$cos\alpha$ can be described in terms of H_1:

$$cos\alpha = -\frac{w(H_1 - z_1)}{\left(\frac{w}{2}\right)^2 + (H_1 - z_1)^2} \quad (7)$$

We can then express the average contact angle β of the culture drop in terms of fluid height H_1 in the reservoir:

$$\frac{2\gamma cos\beta}{R} - \rho g\left(z_2 - \frac{R}{cos\beta}(1 - sin\beta)\right) = -\frac{2\gamma w(H_1 - z_1)}{(\frac{w}{2})^2 + (H_1 - z_1)^2}\left(\frac{1}{w} + \frac{1}{h}\right) - \rho g H_1 \quad (8)$$

Solving Navier-Stokes equation gives the velocity profile for a pressure-driven, steady-state flow in a microchannel of rectangular cross section. The flow rate Q can be found by integrating flow velocity in the inlet channel of width W and height H. For a channel with aspect ratio $a < 1$ ($a = H/W$), flow rate can be approximated by [18]:

$$Q \approx \frac{H^4 \Delta p}{12\eta L a}(1 - 0.63a) \quad (9)$$

where η is the viscosity of fluid, L is the length of microchannel, and Δp is the pressure difference between two ends of the microchannel, in this case, the gravity pressure due to feeding syringe:

$$\Delta p = \rho g Z \quad (10)$$

Z is the height difference between the fluid level in the feeding syringe and the device.

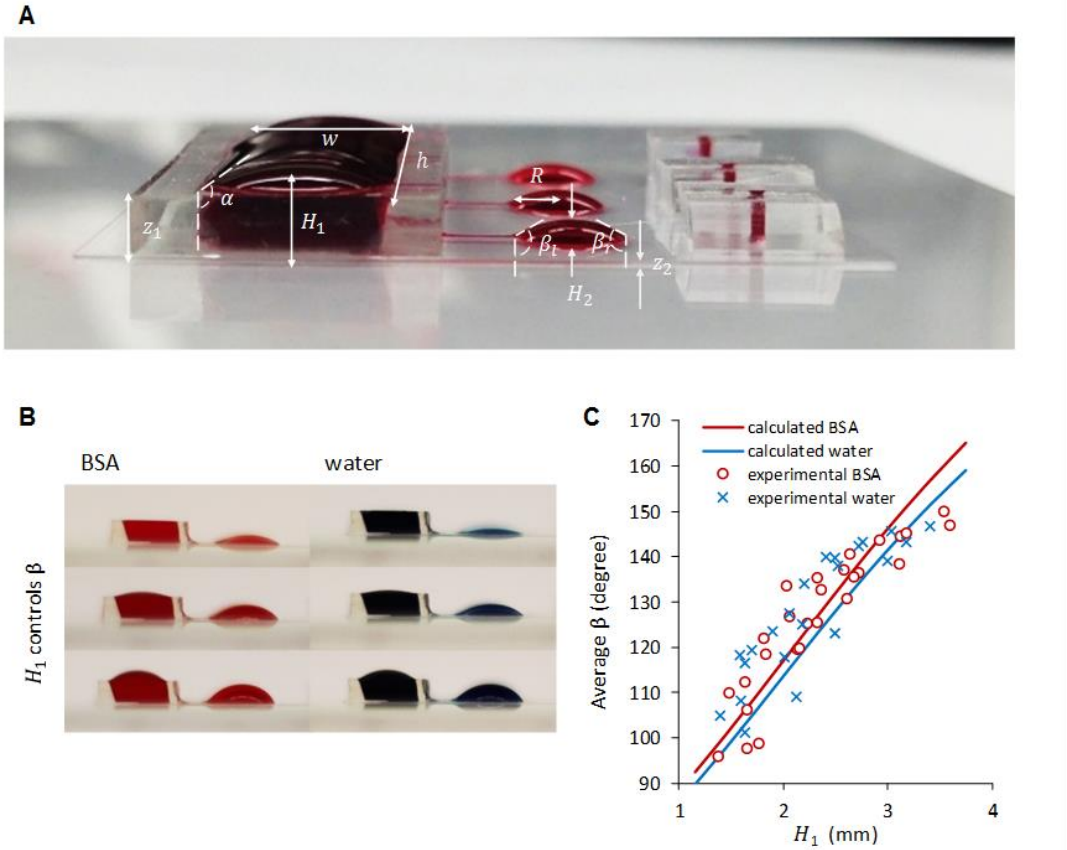

Figure 2.2 Device in the absence of flow. (A) Photograph of the dye-filled device with no input flow. (B) Different levels of fluid in the reservoir control the shape of the culture well drop. BSA solution contains red dye, while water is colored with blue dye. (C) Experimental measurements and analytical solution of β versus H_1 for BSA solution (2.5 g/L) and water. Correlation coefficient R^2 is 0.78 for water and 0.83 for BSA solution; p <0.001 for both fluids.

2.3 Experimental methods

2.3.1 Device fabrication

Culture compartments were fabricated from PDMS. Silicon mold masters were prepared by defining a microchannel pattern *via* SU-8 (Microchem) photolithography on a 3" silicon wafer. A pattern of 20 µm height and 50 µm width was fabricated. Liquid PDMS was spin-

coated onto the silicon master at 600 rpm for 1 min, and cured at 75 °C for at least 4 h. The resulting 110 µm PDMS film with imprinted microchannels was removed from the silicon wafer. Culture wells of 6 mm diameter and the open channels of 0.5 mm × 8 mm were cut in the PDMS membrane. Fluid inlets of 0.025 mm diameter were created by puncturing the PDMS membrane with a syringe needle. The length of inlet microchannel *L* (edge to edge distance between fluid input to the device and culture well) is 6 mm (Figure 2.1). PDMS compartments were attached to glass substrate through oxygen plasma bonding. Then 2 mm thick PDMS reservoir (5 mm × 25 mm inner area) and input tubing stand (5 mm × 5 mm) were bonded to PDMS membrane. Tubing stand through-hole (0.1 mm diameter) was centered on the punctured fluid inlet. The edge to edge distance between reservoir and culture well is 4 mm. Devices were autoclaved for sterilization. Then each device was placed in a 100 mm petri dish, and incubated in humidified atmosphere at 37 °C overnight, with culture wells coated with poly-D-lysine (PDL, Sigma). Devices were then washed in three changes of sterile distilled water, and incubated for at least 3 hours with culture wells covered with NeurobasalA/B27 medium (Invitrogen) before culturing.

2.3.2 Velocity modeling

Flow in the culture well was simulated using COMSOL-Multiphysics. Geometry of the simulated chamber mimicked the ones used for the experiments. A plug flow of 0.01 m/s was applied at the inlet of the microchannel leading to the slice chamber. The velocity was calculated as the preset flow rate of 1 mL/day divide by the cross section area of the microchannel (20 µm x 50 µm). The fluid surface exposed to air was set as an open boundary and the air phase was neglected, considering the low viscosity of air compared to water. All the other boundaries were set as no-slip boundaries. Brain tissue in the culture

well was represented by a solid cylindroid located at the center with a semi-major axis of 1.2 mm, semi-minor axis of 1 mm and height of 0.2 mm. Fluid parameters corresponding to water were used in the simulation.

2.3.3 Organotypic cultures

Hippocampi were dissected from postnatal day 7-8 Sprague-Dawley rat pups (Charles River Laboratories), cut into 350 µm slices on a McIlwain tissue chopper (Mickle Laboratory Eng. Co., Surrey, United Kingdom). Slices were placed in the culture wells of the microfluidic devices, and controls were placed onto PDL coated 6-well tissue culture plates. All cultures were maintained in serum-free NeurobasalA/B27 medium containing 0.5 mM glutaMAX (Invitrogen) and 30 mg/L gentamicin (Invitrogen) and incubated at 37 °C in 5% CO_2. Control slices placed in 6-well culture plate were placed on a rocking platform. Medium was changed twice a week. Slices within microfluidic perfusion devices were gravity-fed from a syringe tube with a loose-fitting cap, and the flow rate was set to approximately 1 ml/day per culture by placing the feeding syringe at a height of 20 cm. Fluid was split by a 1 to 6 mini-manifold (Warner Instruments) to supply 2 triple microfluidic perfusion devices. The fluid level in the feeding syringe was checked daily and replenished every day to maintain same height *Z*. The feeding tubing was 0.030" ID, 0.065" OD ultra-purity white silicone tubing (Mcmaster-Carr). Polyethylene tubing with 0.023" ID, 0.038" OD (Warner Instruments) was used as the interconnector of feeding tubing to mini-manifold, and feeding tubing to PDMS tubing stand. Manifolds and tubing were sterilized by autoclaving, except for polyethylene tubing which was sterilized by ethanol. All animal use protocols were approved by the Institution Animal Care and Use Committee (IACUC) at Lehigh University and were conducted in accordance with the

United States Public Health Service Policy on Humane Care and Use of Laboratory Animals.

2.3.4 Immunohistochemistry

NeuN antibody is a marker for neurons that specifically recognizes DNA-binding, neuron-specific protein NeuN, which is present in most CNS and PNS neuronal cell types. Cultures were washed in phosphate-buffered saline (PBS), and fixed for 2 h in 4% paraformaldehyde. Cultures were then transferred to 48-well petri dish, and permeabilized in 0.3% Triton X-100 (Sigma-Aldrich) in PBS for 2 h, then blocked with 10% goat serum in PBS for 1 h, followed by incubation for 24 h in 1% NeuN at +4 ℃ on a shaker. Slices were then washed and mounted for confocal microscopy. Z-stack images were collected on confocal microscope (Zeiss LSM 510 META, Germany) with 5x and 40x objectives. Z-stack layers were separated by 2 µm, and depth ranged from 40 µm-60 µm. Images were then processed in Fiji [19]. Neuron numbers were quantified per single field of view of high-magnification images, in the optical slice with maximum number of neurons in CA1 and CA3 areas of control and perfused-drop cultures.

2.4 Results and discussion

2.4.1 Static analysis

Devices were evaluated under static (no flow) conditions with bovine serum albumin (BSA) solution (2.5 g/L), which mimics the surface tension of culture medium, and distilled water. We increased the fluid volume in the reservoir to increase the fluid level in the culture well (Figure 2.2B). Averages of 3 separate measurements of H_1, β_l and β_r for each fluid volume were calculated for three different devices and plotted in Figure 2.2C. Results were compared to formula (8), evaluated with average dimensions of 3 different devices: z_1 = 1.7 mm, w = 5.8 mm, h = 25.8 mm, R = 3 mm, and z_2 = 110 μm, ρ = 10^3 kg/m^3. Surface tension values of distilled water and BSA solution (2.5g/L) at 37 °C were 70 mN/m and 54 mN/m, respectively [20,21]. Analytical solutions of β dependence on H_1 for BSA-containing solution and water were plotted in Figure 2.2C. A good fit with the experimental data for water and BSA solution was observed. Correlation coefficients between experimental and theoretical values were R^2 = 0.78 for water, and R^2 = 0.83 for BSA solution; p <0.001 for both fluids.

In the static model (Figure 2.2), we only consider the operation range of 1 mm < H_1 < 4 mm because values of H_1 less than 1mm reduce β below 90 degrees. This may lead to cultures drying out. Fluid confinement by hydrophobic PDMS surface fails for H_1 > 4mm, imposing an upper limit to the range of H_1. The open channel connecting culture well and reservoir may also contribute to fluid balance. However, considering that its area is less than 10% of the culture well area, its surface tension may be ignored. In Figure 2.2C, theoretical curves of water and BSA solution are close to each other signifying that

difference in surface tensions between these two fluids does not strongly affect operation of our device. This is also supported by lack of difference between experimental data for water and BSA.

2.4.2 Dynamic analysis

Z was set to 20 cm in subsequent culture experiments. β_l and β_r were measured while the drop in culture well was perfused with BSA solution, and compared to static values obtained from the same device without perfusion (Figure 2.3A, B). The introduction of flow had no significant influence on the geometry of drop in culture well (for β_l, p = 0.911; for β_r, p = 0.760; n=3, paired t test). While fluid flow introduces pressure changes inside the culture well, the highest pressure change is at the fluid inlet (approximately 0.01 Pa, from COMSOL simulation), was less than 0.015% of the pressure in no-flow condition ($P_3 - P_4$ is approximately 70 Pa). Therefore, the shape of the drop in culture well is largely determined by static forces.

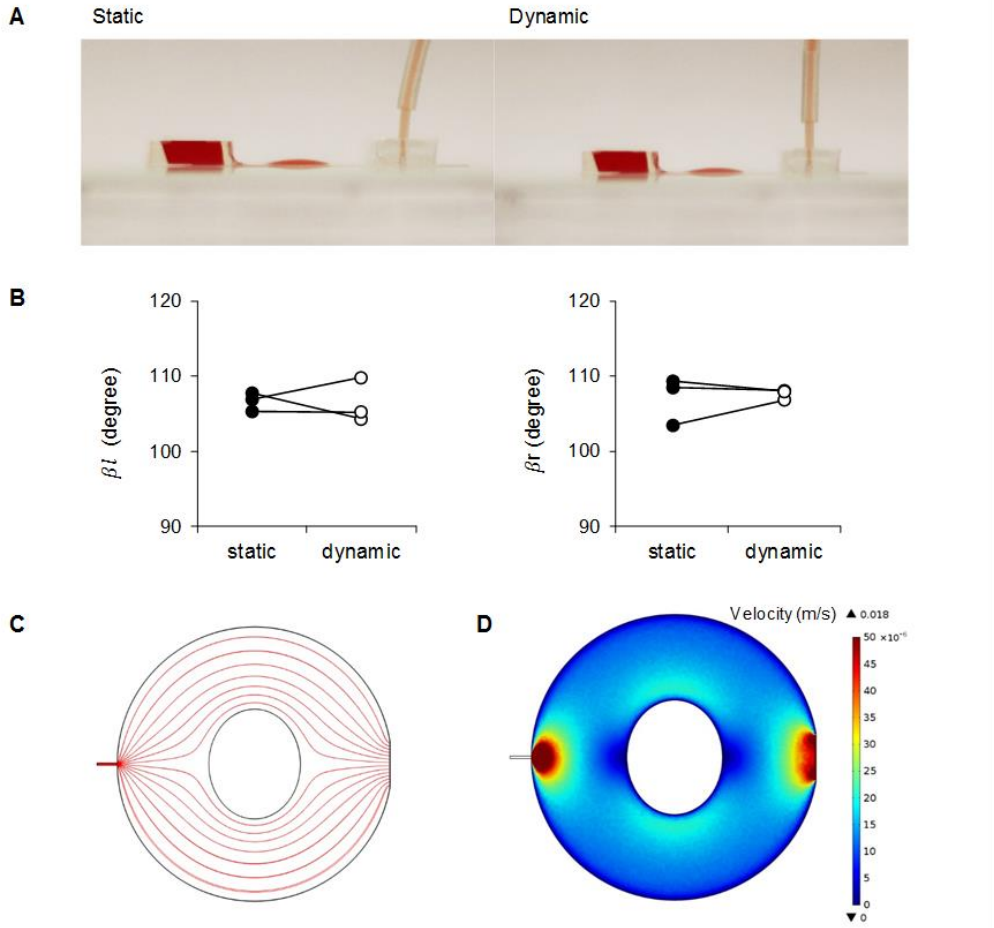

Figure 2.3 Dynamic modeling of streamline and velocity profile in the perfused drop device. (A) Photograph of the device under static condition (left, flow was stopped by switch) and dynamic condition (right, there is continuous input flow). H_1, β_l and β_r were measured in these two conditions on 3 devices. (B) Comparison of β_l and β_r under static condition and dynamic conditions. ● represents no flow, and ○ represents continuous flow. (C) Streamlines of the velocity field. Circle in the center of the culture well represents brain slice. Flow enters the culture well from the microchannel on the left, flows around the culture and then leaves through the open channel on the right. (D) Velocity magnitude distribution inside the culture well. High velocity appears at the inlet and outlet but decreases quickly closer to the brain slice. (The simulation results refer to the horizontal plane at the microchannel midpoint).

We then determined if Eq. (9) accurately models the flow rate in our device. We used the following values: H = 20 µm, a = 0.4, Z = 20 cm, and L = 6 mm. Viscosity of water is η = 0.71×10^{-3} Pa·s at 37 °C [22]. Viscosity of BSA solution is approximately the same since

low concentration of BSA used in culture medium does not significantly alter fluid viscosity [23]. The calculated flow rate Q was 42 µl/h, which is approximately 1 ml/day per slice. In culturing experiments approximately 1 ml/day of culture medium was used per slice, which matches with the calculated flow rate.

Increase of flow rate improves the oxygen/nutrient delivery [24]. However, the correspondingly increased fluid velocity can cause larger shear forces that have the potential to damage tissues [25]. In our platform, the flow rate is set at 1 ml/day. For slices cultured in standard 6-well plate, the medium consumption rate is about 0.3 ml/day [26]. Thus, our perfused drop device is characterized by a comparatively high perfusate exchange rate which may lead to improved culture viability. COMSOL simulation of the streamline and velocity profile 10 µm above the substrate (microchannel midpoint) are shown in Figure 2.3C, D. A relatively high velocity above 0.01 m/s only occur near the inlet and outlet. The maximum velocity of 0.018 m/s occurs at the outlet of the microchannel, and decreases rapidly after entering the culture well. As demonstrated in Figure 2.3D, velocity is in the range of 5-20 × 10^{-6} m/s in the vicinity of cultured slice, indicating that slice experiences relatively little shear stress.

2.4.3 Culture viability

H_1 was set to 1.5 mm to make β approximately 100 degrees. This was found to be the optimum drop shape for culture viability, since drops with larger β caused slices to detach, while drops with smaller β caused slices to dry out. The culture viability was evaluated at 5 DIV and 9 DIV by brightfield microscope imaging and confocal imaging of NeuN stained organotypic hippocampal cultures (Figure 2.4). Compared with control cultures, perfused

drop cultures showed similar well maintained cytoarchitecture with clearly defined neural layers. Neuron counts on 9 DIV were not different between control and perfusion slices in CA1 ($p = 0.599$, student *t* test, $n = 3$ each condition), but perfusion cultures had significantly higher number of neurons than control cultures in CA3 ($p = 0.036$, student *t* test, $n = 3$ each condition) (Figure 2.4C).The results showed that viable cultures could be maintained in microfluidic perfusion system for at least 9 DIV with no reduction in the number of neurons in the hippocampal pyramidal layers.

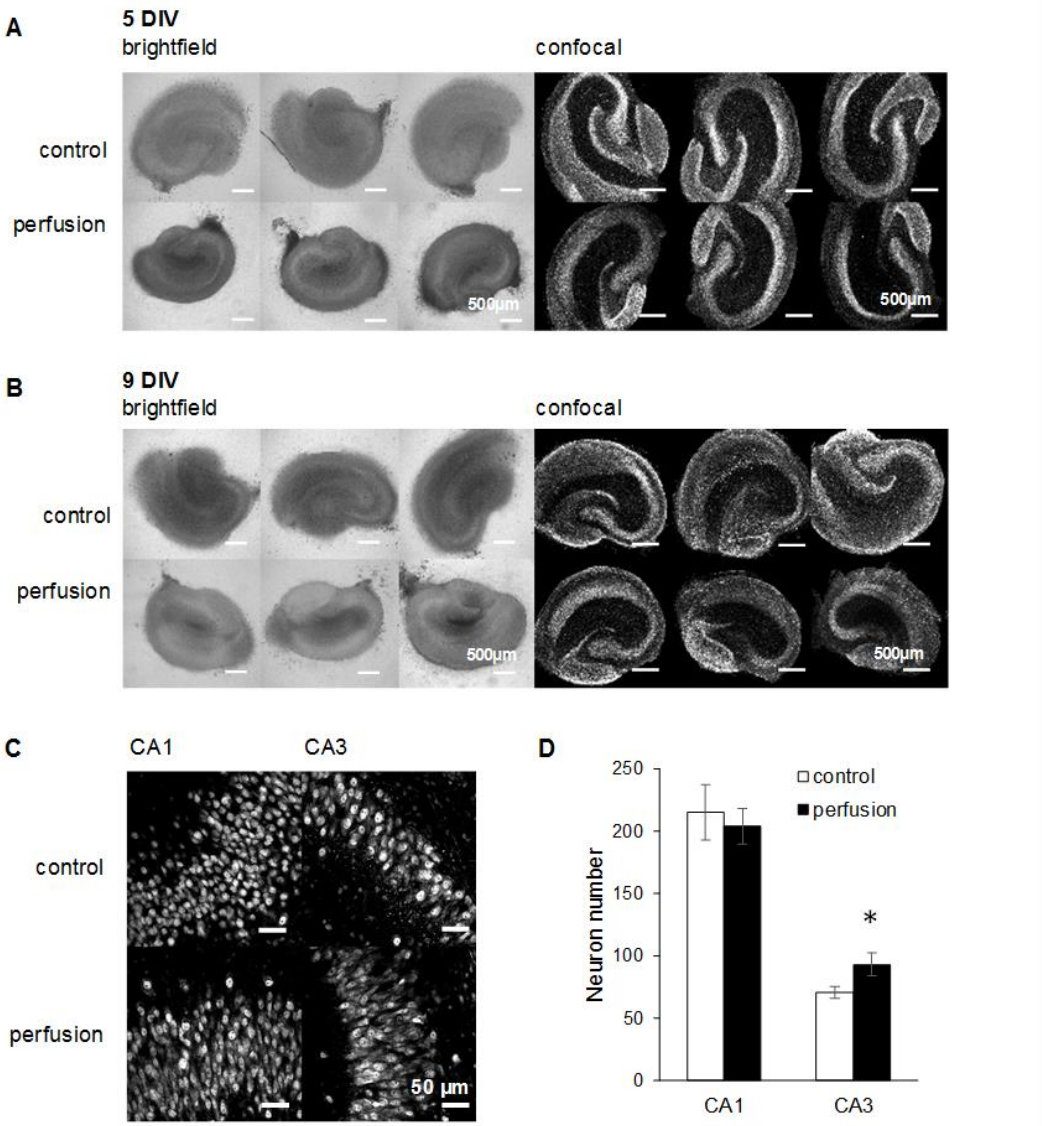

Figure 2.4 Morphology of organotypic hippocampal cultures maintained in the perfused drops. Morphology of control (interface method) cultures and perfused drop cultures were compared on 5 DIV (A) and 9 DIV (B) by brightfield and confocal imaging. Cultures were stained with NeuN for confocal imaging. Scale bars, 500 µm. (C) Higher magnification micrographs of NeuN staining in CA1 and CA3 regions show that similar numbers of neurons survived in control and perfused drop cultures. Scale bars, 50 µm. (D) Neuron counts in CA1 and CA3. n = 3 each condition. Error bars indicate SD, * $p < 0.05$.

Our morphological findings show that perfused drop method enables organotypic cultures that are as viable as cultures maintained with roller-tube or interface methods. Perfused drop method enables integration of organotypic cultures with MEA fabricated on any

PDMS-bondable substrate such as glass, without the need for specialty perforated MEA [10], thus potentially reducing the costs of organotypic culture-based drug discovery. Traditional methods of maintaining organotypic cultures require large area of culture substrate to hold the culture medium. In a 6 well plate, each slice takes up to ~10 cm^2, while actual area of a hippocampal slice is only ~ 0.07 cm^2. In our triple device (Figure 2.1D), each slice takes up only 3 cm^2 if reservoir area is taken into account. The reduction in required area is achieved by moving the medium storage off the device. Since more than three culture wells can share one reservoir, the amount of area required per cultured slice will become smaller with more slices per device. More cultures can be added by simply patterning more wells and microchannels in the PDMS film without an increase in the cost of the device. Thus, our perfused drop culture method is inherently scalable, and may replace entire systems [11–13] with a single integrated microfluidic-MEA chip. Another advantage of this platform is the transparent and planar design that enables convenient optical microscopy.

2.5 Conclusions

In this work, we developed a microfluidics-based method that highly increases the scalability of organotypic culture platform. Our method is compatible with planar MEA technology, and will enable parallel chronic electrical recordings of epileptogenesis in vitro.

2.6 Reference

1. Queval A, Ghattamaneni NR, Perrault CM, Gill R, Mirzaei M, McKinney RA, et al. Chamber and microfluidic probe for microperfusion of organotypic brain slices. Lab Chip. 2010;10: 326–334.

2. Passeraub PA, Almeida A, Thakor N. Design, microfabrication and analysis of a microfluidic chamber for the perfusion of brain tissue slices. Biomed Microdevices. 2003;5: 147–155.

3. Choi Y, McClain MA, LaPlaca MC, Frazier AB, Allen MG. Three dimensional MEMS microfluidic perfusion system for thick brain slice cultures. Biomed Microdevices. 2007;9: 7–13.

4. Rambani K, Vukasinovic J, Glezer A, Potter SM. Culturing thick brain slices: an interstitial 3D microperfusion system for enhanced viability. J Neurosci Methods. 2009;180: 243–254.

5. Blake AJ, Rodgers FC, Bassuener A, Hippensteel JA, Pearce TM, Pearce TR, et al. A microfluidic brain slice perfusion chamber for multisite recording using penetrating electrodes. J Neurosci Methods. 2010;189: 5–13.

6. Huang Y, Williams JC, Johnson SM. Brain slice on a chip: opportunities and challenges of applying microfluidic technology to intact tissues. Lab Chip. 2012;12: 2103. doi:10.1039/c2lc21142d

7. Oka H, Shimono K, Ogawa R, Sugihara H, Taketani M. A new planar multielectrode array for extracellular recording: application to hippocampal acute slice. J Neurosci Methods. 1999;93: 61–67.

8. Egert U, Heck D, Aertsen A. Two-dimensional monitoring of spiking networks in acute brain slices. Exp Brain Res. 2002;142: 268–274.

9. Heuschkel MO, Fejtl M, Raggenbass M, Bertrand D, Renaud P. A three-dimensional multi-electrode array for multi-site stimulation and recording in acute brain slices. J Neurosci Methods. 2002;114: 135–148.

10. Jahnsen H, Kristensen BW, Thiébaud P, Noraberg J, Jakobsen B, Bove M, et al. Coupling of organotypic brain slice cultures to silicon-based arrays of electrodes. Methods. 1999;18: 160–172.

11. Stopps M, Allen N, Barrett R, Choudhury H, Jarolimek W, Johnson M, et al. Design and application of a novel brain slice system that permits independent electrophysiological recordings from multiple slices. J Neurosci Methods. 2004;132: 137–148.

12. Kroker KS, Rosenbrock H, Rast G. A multi-slice recording system for stable late phase hippocampal long-term potentiation experiments. J Neurosci Methods. 2011;194: 394–401.

13. Graef JD, Wei H, Lippiello PM, Bencherif M, Fedorov N. Slice XVIvo^{TM}: A novel electrophysiology system with the capability for 16 independent brain slice recordings. J Neurosci Methods. 2013;212: 228–233.

14. Gähwiler B, Capogna M, Debanne D, McKinney R, Thompson S. Organotypic slice cultures: a technique has come of age. Trends Neurosci. 1997;20: 471–477.

15. Stoppini L, Buchs P-A, Muller D. A simple method for organotypic cultures of nervous tissue. J Neurosci Methods. 1991;37: 173–182.

16. Gahwiler B TS McKinney A, Debanne D, Robertson R. Organotypic Slice Cultures of Neural Tissue. In: Culturing Nerve Cells. 2nd ed. Massachusetts Institute of Technology; 1998.

17. Berdichevsky Y, Sabolek H, Levine JB, Staley KJ, Yarmush ML. Microfluidics and multielectrode array-compatible organotypic slice culture method. J Neurosci Methods. 2009;178: 59–64. doi:10.1016/j.jneumeth.2008.11.016

18. Tanyeri M, Ranka M, Sittipolkul N, Schroeder CM. A microfluidic-based hydrodynamic trap: design and implementation. Lab Chip. 2011;11: 1786–1794.

19. Schindelin J, Arganda-Carreras I, Frise E, Kaynig V, Longair M, Pietzsch T, et al. Fiji: an open-source platform for biological-image analysis. Nat Methods. 2012;9: 676–682.

20. Vargaftik N, Volkov B, Voljak L. International tables of the surface tension of water. J Phys Chem Ref Data. 1983;12: 817–820.

21. Suttiprasit P, Krisdhasima V, McGuire J. The surface activity of α-lactalbumin, β-lactoglobulin, and bovine serum albumin: I. Surface tension measurements with single-component and mixed solutions. J Colloid Interface Sci. 1992;154: 316–326.

22. Korson L, Drost-Hansen W, Millero FJ. Viscosity of water at various temperatures. J Phys Chem. 1969;73: 34–39.

23. Yadav S, Shire SJ, Kalonia DS. Viscosity analysis of high concentration bovine serum albumin aqueous solutions. Pharm Res. 2011;28: 1973–1983.

24. Hájos N, Mody I. Establishing a physiological environment for visualized in vitro brain slice recordings by increasing oxygen supply and modifying aCSF content. J Neurosci Methods. 2009;183: 107–113.

25. Christ KV, Williamson KB, Masters KS, Turner KT. Measurement of single-cell adhesion strength using a microfluidic assay. Biomed Microdevices. 2010;12: 443–455.

26. Opitz-Araya X, Barria A. Organotypic hippocampal slice cultures. J Vis Exp. 2011; doi:10.3791/2462

Chapter 3

µflow-MEA technology for antiepileptogenic drug discovery

3.1 Motivation

High-throughput drug screens based on organotypic culture model of epilepsy require massively parallel recordings for over two weeks for the observation of epileptogenesis. Multiple electrode array (MEA) technology provides the highly parallel recordings and supports chronic recordings in organotypic brain slice cultures over several weeks [1–8]. However, typical MEA devices are deigned to support only one brain slice culture, due to the low scalability of organotypic culture chamber. Here we describe a hybrid microfluidic-MEA (µflow-MEA) technology that incorporates perfused drop technique [9] described in Chapter 2 and MEA based parallel electrophysiology into a miniaturized device for scalable electrical assays of epileptogenesis.

In standard MEA designs, an insulation layer is required to confine the active area of electrodes in order to prevent signal dissipation and increase detection sensitivity. The most used isolation types are: Silicon dioxide, silicon nitride, and SU-8 [10–13]. Silicon dioxide and silicon nitride require chemical vapor deposition (CVD) and etching process for electrode opening. SU-8 layer is spin coated to the device, and then electrodes are exposed

by photolithography. This chapter will describe a simplification in the MEA design to detect electrographic seizures which are characterized by synchronized population activity. Computational simulation of field potential was conducted to verify the capability of this simplified MEA to achieve good detection of seizure-like activity.

To demonstrate how this μflow-MEA technology can facilitate antiepileptogenic drug discovery, we conducted a pilot screen of small molecular inhibitors. In this work, we focus on the investigation of receptor tyrosine kinases (RTKs), a class of kinases that act as cell surface receptors. Many of RTKs are expressed in the hippocampus, and have been reported to respond to brain injury [14–20], the most common known cause of acquired epilepsy [21,22]. Therefore there is a significant likelihood that RTKs may play a role in epileptogenesis. Lactate and Lactate dehydrogenase (LDH) measurements have been used to evaluate antiepileptic drug efficacy in organotypic cultures [23–25], since their concentrations in the spent culture medium were found to be correlated with seizure-like activity and seizure-dependent cell death, respectively. Lactate and LDH productions can be measured by commercial assay kits, enabling rapid analysis of drug effects on epileptogenesis. Lactate level also depends on the number of surviving neurons in the culture since neurons produce physiological lactate even when there is no seizure. Thus, analysis of cell death via LDH assay is necessary to interpret lactate level as a marker of seizure-like activity. However, LDH assay cannot reflect the cell death when apoptotic cells degrade without releasing LDH into culture supernatant [26]. Candidate drugs might have unpredictable effects on cell survival, which would complicate the interpretation of lactate and LDH data. Furthermore, spent culture medium are sampled at twice-weekly medium changes for lactate and LDH assays. So that the lactate and LDH levels reflect the

overall seizure load in the 3-4 days period between medium changes, providing a measurement of seizure activity with low temporal resolution. In contrast, continuous electrical recordings provide direct measurement of electrographic seizures at high-resolution. Therefore, for accurate assessment of drug efficacy, it is important to use chronic electrical assay to verify the lactate and LDH data, or even replace the lactate and LDH assays when high-throughput can be achieved. In this work, we present a two-stage screening platform based on organotypic hippocampal cultures model of epilepsy. The first stage was for biochemistry assays, where epileptogenesis was evaluated by measurements of lactate and LDH levels during chronic inhibitor application. The second stage was for µflow-MEA technology based chronic electrical assay to verify the results obtained in stage I.

3.2 Experimental methods

3.2.1 Device design and fabrication

The µflow-MEA device was the integration of customized MEA chip with PDMS microfluidic perfusion compartments we developed in our previous work [9] described in Chapter 2. The device has 8 metal microelectrodes (30 µm × 3 mm) recording from 6 culture wells, with one electrode for each well, and one additional electrode in two wells (since we used a 16 channel data acquisition system, 8 channels were allocated to each device), and a reference electrode (diameter = 3 mm) in the fluid reservoir (Figure 3.1). For the purpose of drug screening, we simplified the MEA design by excluding the isolation process to make the device cheap and quickly fabricated. PDMS microfluidic

system was bonded to metal patterned MEA chip as an insulator to passivate conductor tracks, and the recording electrodes were left uninsulated in the organotypic culture well.

Glass slides (2 × 2 inch, Fisher Scientific) were cleaned in Piranha solution. The electrodes pattern was defined photolithographically with negative lift-off process using AZ nLOF 2070 (MicroChem). Titanium (50 nm) and gold (200 nm) were deposited with e-beam evaporator to make the electrodes. The photoresist was lifted with photoresist stripper AZ 400T (MicroChem) at 80 °C for 3 hours, leaving the electrode pattern on the glass slide. PDMS compartments were assembled to the MEA chip through oxygen plasma bonding, with electrodes centered in culture wells. MEA integrated device was then autoclaved for sterilization before culturing.

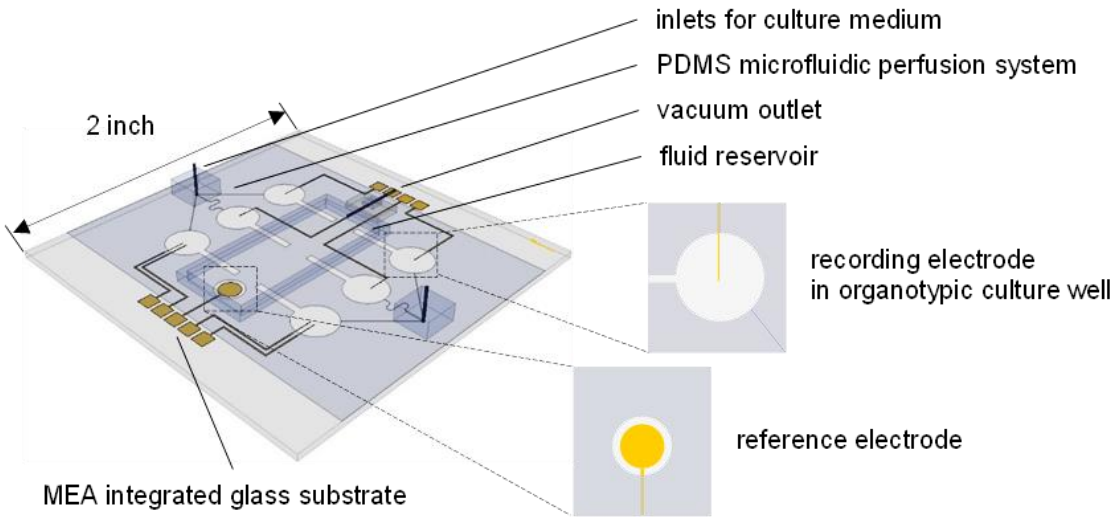

Figure 3.1 Schematic representation of the µflow-MEA chip. This device is the integration of PDMS microfluidic perfusion system [9] and MEA printed glass substrate for long-term parallel recording in 6 organotypic hippocampal cultures.

3.2.2 Field potential simulation

Field potentials were simulated using COMSOL-Multiphysics (COMSOL Inc.). The 3D geometry model included the culture well, current source model of seizure and 2D recoding electrodes. We built a simplified current source model based on the hippocampal slice geomerty to reflect seizure-like activity when the whole hippocampal network is synchronized. Insulating boundary conditions were assigned to the circumference and the floor of the culture well, and the air-medium interface. The conductivity of the medium was set as 1.5 S/m to match reported conductivity of artificial cerebrospinal fluid (aCSF) [27–29].

3.2.3 Preparation of organotypic cultures

For experiments in stage I, slices were maintained in 6-well tissue culture plates. For µflow perfused culture in stage II, slices were placed in the mini culture wells of µflow-MEA device and perfused at the rate of 1 ml/day per culture. Details are described in Chapter 2.

3.2.4 Morphology Analysis

Brightfield images were taken on an upright microscope (Olympus) with 4x objective. Cultures' "health" was evaluated based on three morphological criteria: 1. Blurriness of the culture edge. Blurry edges indicate that the slice has attached well to the polylysine substrate, while distinct edge indicates that the slice has not integrated well with the substrate. Very unhealthy slices become completely detached and float in the culture media. 2. Brightness of the slices. Unhealthy slices appear darker than healthy slices due to accumulation of cellular debris. 3. Integrity and distinctness of neural layers. Healthy slices

have well-preserved cytoarchitecture with distinct CA1, CA3 neural layers and dentate gyrus (DG).

3.2.5 Drug application and assays

Phenytoin was dissolved in dimethylsulfoxide (DMSO), and added to the culture medium at 100 μM concentration. Phenytoin was applied when consistent seizure-like activity was observed. Cultures were perfused by medium with phenytoin for 10 hours, then switched back to normal medium perfusion. Electrical recordings before, during and after drug perfusion were analyzed to evaluate the drug efficacy.

Cultures from the same animal were organized into four experimental groups to test three drugs with a vehicle-treated control (n = 3 cultures each condition). All inhibitors were dissolved in DMSO and applied to cultures starting on 3 DIV. Control cultures were treated with 0.1% DMSO as vehicle. Toxicity pre-screen (0-7 DIV) was conducted by morphology analysis and measurement of LDH on 7 DIV. Cultures showed either unhealthy morphology or significantly higher LDH than control were deemed toxic and a lower concentration of applied drug was retested until the maximum nontoxic concentration was identified. The maximum nontoxic concentration of each drug were then applied in two stage chronic screens. In stage I, culture supernatant was collected on 3, 7, 10, 14, 17 and 21 DIV and seizure-like activity and cell death were measured by lactate and LDH assay, respectively. Lactate and LDH concentrations in the supernatant were determined by using kits (Eton Bioscience and Roche Diagnostics, respectively) according to manufacturers' protocols. Lactate concentrations were calculated relative to known lactate standards, while LDH concentrations were calculated in terms of arbitrary units (a.u.), normalized to the 0

- 3 days in vitro (DIV) average of LDH concentration in control culture supernatant. In stage II, cultures were perfused by culture medium with drugs from 3 DIV to 14 DIV. Chronic electrical recordings were then used to evaluate drug efficacy.

3.2.6 Immunohistochemistry

NeuN staining refers to Chapter 2. Slices were then washed and mounted for confocal microscopy. Z-stack images were collected on confocal microscope (Zeiss LSM 510 META, Germany) with 5x and 40x objectives. Z-stack layers were separated by 1 µm, and slices were imaged over their total depth. Images were then processed in Fiji (ImageJ) [30]. Neurons in CA1 and CA3 pyramidal layers were quantified with a counting algorithm modified from existing "3D watershed technique" for counting cell nuclei (ImageJ macro developed by [31]).

3.2.7 Electrophysiology and data analysis

Electrical recordings were carried out by connecting the electrode contact pads on MEA to a 16-channel extracellular amplifier with high impedance head stage (3600, A-M Systems). Signals were digitized with a multiple-channel digital acquisition board (Measurement Computing). Sampling rate was 200 Hz per channel. Chronic data acquisition will be initiated on 1 DIV, and continued until 14 DIV, with short interruptions for medium supply. Data were recorded with dClamp software (available from authors upon request), and analyzed with Matlab (Mathworks). A data binning algorithm was developed for automated quantification of seizure-like activity in chronic recordings. Color raster plots were created by binning the data at 0.5 s and calculating the number of super-threshold

bins (represent paroxysmal events) per 10 seconds sliding window. Threshold was set at 20 ~ 30 µV, since the system noise was about 10 µV.

3.2.8 Statistical Methods

We used Student's t test for two-variable comparisons, one-way ANOVA with Holm-Sidak post hoc analysis for multiple variable comparisons, and Kolmogorov-Smirnov test for cumulative distribution analysis. Number of samples n refers to the number of cultures.

3.3 Results and discussion

3.1.1 Simulation of field potential in organotypic culture well

In our simplified MEA design, recording electrodes were uninsulated in the organotypic culture well with relatively large active area (30 µm × 3 mm). Increased electrode area can reduce electrical noise, but also moderate detection sensitivity by averaging out field potentials occurring over the length of electrode. Different from normal electrophysiology platform, in which case the brain slice is placed in a large culture or perfusion chamber (~30 mm diameter, containing 1~2 ml conducting culture medium), µflow-MEA records from cultures that are physically confined in PDMS mini well (6 mm diameter, containing 5~10 µl conducting culture medium).We hypothesized that electrical signal attenuation is highly reduced in spatially confined culture well, which offsets the loss of detection sensitivity. Therefore the uninsulated electrodes can still achieve good detection of field

potentials, particularly population electrical fields resulting from seizure-like activity that is characterized by highly synchronous neuronal firing over the entire culture area.

To test this hypothesis, we built a current source model of seizure-like activity in hippocampal slice culture (Figure 3.2A,C). Due to the diversity of neuron geometry and the way neurons assemble in the hippocampus, the anatomy of hippocampal slice is defined by multiple neural layers: stratum oriens (o) is where the basal dendrites of pyramidal neurons (the principal excitatory neurons of the hippocampus) are located; pyramidal layer (p) contains the cell body (soma) of pyramidal neurons; stratum radiatum (r) contains apical dendrites of pyramidal neurons; stratum lacunosum-moleculare (lm) also contains apical dendrites of pyramidal neurons; dentate molecular layer (m) contains dendrites of the dentate granule cells; granule cell layer (g) contains cell body of the dentate granule cells. The cell body assembly can be observed in confocal imaging of NeuN staining (Figure 3.2A). When spontaneous synchronized activity involves the whole hippocampus, at the moment that dendrites are depolarized by excitatory inputs, current sink forms in the layers that contain dendrites (o, r, m). Correspondingly, current source forms in the layers that contain cell body (p, g, CA3p). Reversely, at the moment that dendrites are hyperpolarized by inhibitory inputs, the current sink forms in soma layers, and current source forms in dendrite layers. Therefore, during dynamic activity, the current sink-source pattern will flip over the time [32,33]. The current sink-source pattern of epileptiform activity in hippocampal slice have been observed in previous works [1,34–36]. Based on these data, we created a simplified current source model of seizure-like activity in hippocampus with the whole slice synchronized. Current sink forms in o, r, m layers, and current source forms in p, lm, g, CA3p layers (Figure 3.2C). The current source in lm layer is probably due to

the formation of current quadrupoles in CA1 pyramidal neurons [33]. The current source density was set at 10^5 A/m^3. This value was estimated by multiplying synaptic current amplitude (200 pA, based on reported amplitude of evoked and spontaneous postsynaptic currents in epileptic hippocampal slice [37–40]) by neuron density in hippocampal slice (5×10^5 mm^3, based on our previous cell counting results [41]). We then simulated the field potential in mini culture well (diameter = 6 mm, fluid depth = 100 µm), and field potential in standard petri dish (diameter = 35 mm, fluid depth = 2 mm), which mimics the widely used submerged slice chamber [42,43]. The field potential distribution in the plane 50 µm above the substrate (mini culture well midpoint) is shown in Figure 3.2D. The plot of field potential distribution along the x and y coordinate showed that the electrical field due to synchronized activity is highly amplified in mini well, compared with standard well (Figure 3.2E).

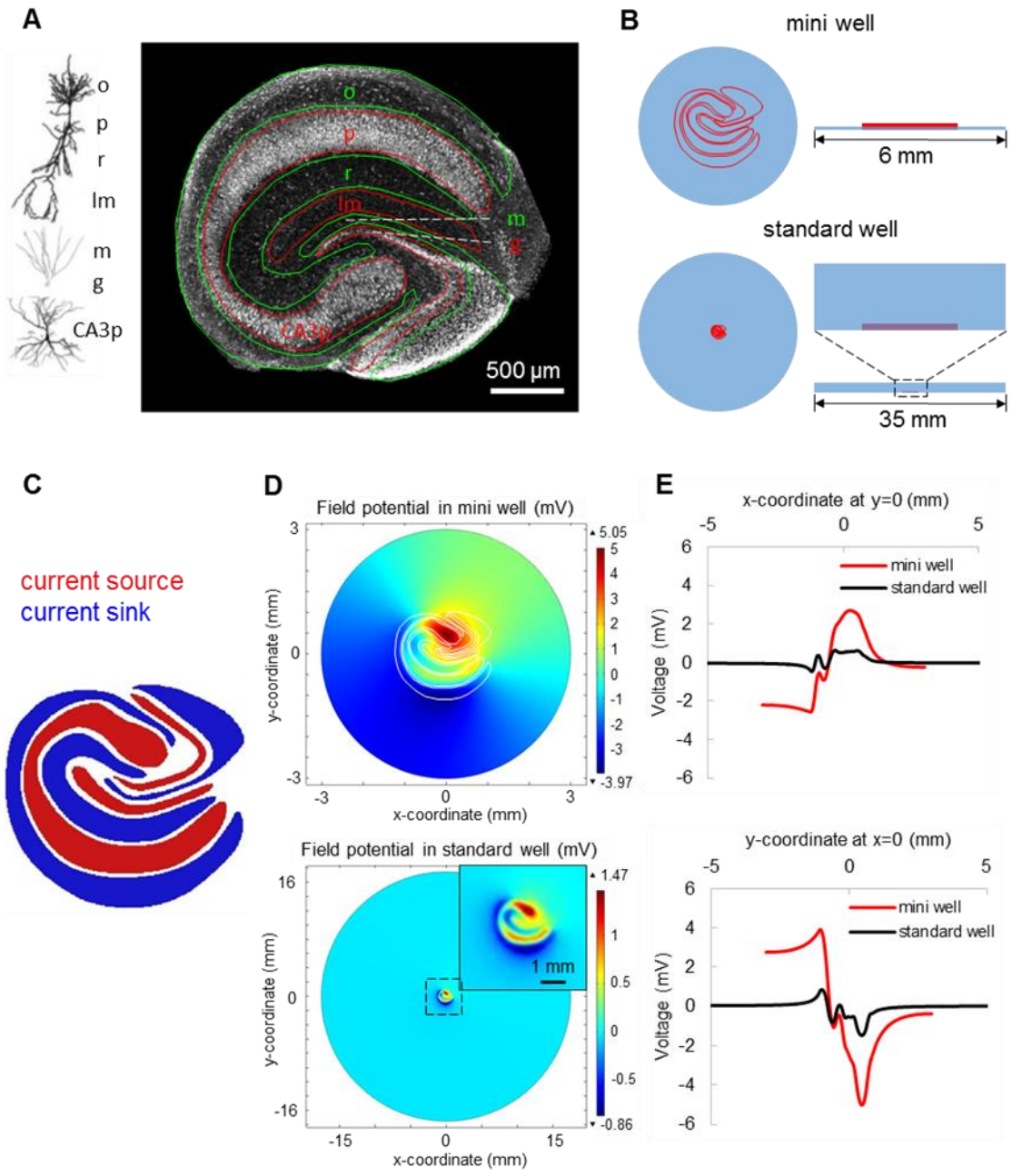

Figure 3.2 Simulation of field potential generated by seizure-like activity. (A) Hippocampal slice anatomy. Red and green lines represent opposite polarity of current source in each neural layer during synchronized synaptic transmission (when dendrite layers are receiving excitatory synaptic inputs: green, sink; red, source). (B) Slice culture maintained in an interface mini well (top; diameter = 6 mm, fluid depth = 100 µm), and in a submerged standard well (bottom; diameter = 35 mm, fluid depth = 2 mm). (C) Current source pattern during seizure-like activity with whole hippocampal circuit synchronized (blue, sink; red, source). (D) Simulated field potential in mini well (top; white lines show the outline of neural layers), and standard well (bottom). The insert zooms in on the hippocampal slice. Scale bar, 1 mm. (E) Field potential distribution along the x (top) and

y (bottom) coordinates at the middle of well (red, mini well; black, standard well). The simulation results refer to the horizontal plane at 50 μm from the well floor. o, stratum oriens; p, pyramidal layer; r, stratum radiatum; lm, stratum lacunosum-moleculare; m, dentate molecular layer; g, granule cell layer; CA3p, hilus, pyramidal layer of CA3c subregion.

We then calculated the potential amplitude that can be detected by uninsulated electrode at different positions in the culture well (Figure 3.3A). Field potential distribution along the length of the electrode is shown in Figure 3.3B, and the corresponding average potential of each electrode position is shown in Figure 3.3B. The electrode can detect field potential ranging from 0.2 mV to 3.5 mV, similar to previous observed potential amplitude of epileptiform activity in brain slice [44–46]. We conclude that field potential is amplified in spatially confined mini culture well, which offsets the loss of sensitivity caused by increased electrode area, and the uninsulated electrode can still achieve good detection of seizure-like activity in hippocampal slice culture.

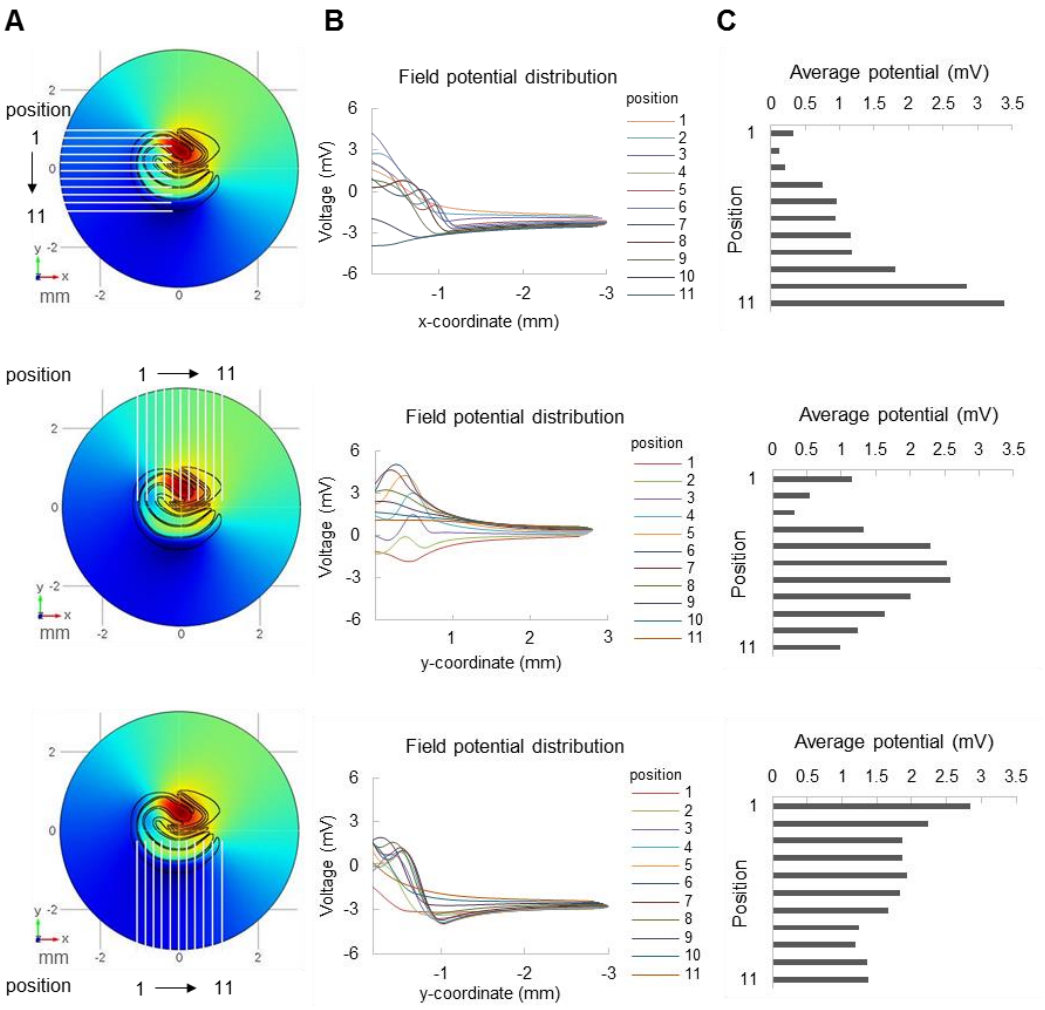

Figure 3.3 Amplitude of potential detected by microelectrodes at different positions. (A) Different positions of recording electrodes. (B) Field potential distribution along each microelectrode. (C) Average potential that is detected by each microelectrode.

3.3.2 Validation of in vitro model of epileptogenesis on μflow-MEA

We developed a system capable of operating two μflow-MEA devices with a 16-channel data acquisition setup (Figure 3.4A). Based on this system, we conducted a series experiments to validate the organotypic hippocampal culture model of epilepsy on μflow-

MEA, through culture viability evaluation, epileptogenesis verification, and drug response test.

We evaluated the culture viability by counting the number of surviving neurons at 14 DIV, and compared perfused μflow-MEA and control (interface method) cultures. Confocal imaging of NeuN staining showed similar well maintained cytoarchitecture and densely packed neurons in perfused and control cultures (Figure 3.4B). Neuron counts showed no difference between control and perfused cultures in CA3c, CA3b and CA1 subregions (Figure 3.4C; $p = 0.366$, 0.491, and 0.289, respectively, student *t* test, $n = 9$ each condition). This result suggested that microfluidic perfusion and chronic electrophysiology do not compromise the viability of organotypic cultures.

Continuous electrical recording was conducted from 3 DIV to 16 DIV. Raster plots were constructed from electrical data with interictal and ictal (seizure) activities pseudocolored based on paroxysmal event frequency (Figure 3.4D). Electrographic seizures were defined as paroxysmal events (with significantly larger amplitudes than unit and multi-unit neural activity) that occurred for at least 10 seconds with event frequency of at least 2 Hz, and colored red in the raster plot. Neural activity was observed in all cultures, including unit and multiunit activity, population spikes, as well as epileptiform ictal and interictal-like activity, with examples shown in Figure 3.4D. The chronic data showed that organotypic cultures go through a latent period with little population activity before developing electrographic seizures (Figure 3.4E, $n = 5$). Seizure-like activity occurred after one week in vitro and continued in the later culture days. These activity patterns and epileptogenesis time course were similar to previous observations in organotypic hippocampal cultures maintained with traditional methods [23,24,47,48].

We tested the effect of phenytoin, a first-line anticonvulsant that is used to treat epilepsy in human patients, on seizure-like activity in hippocampal cultures. In the phenytoin wash-in and wash-out experiment, seizure-like activity was transiently abolished when phenytoin was applied and rebounded after the termination of drug application (Figure 3.4F, G, n = 3). Thus phenytoin exerted acute, reversible anticonvulsive effects on this model, which is consistent with previous findings [23].

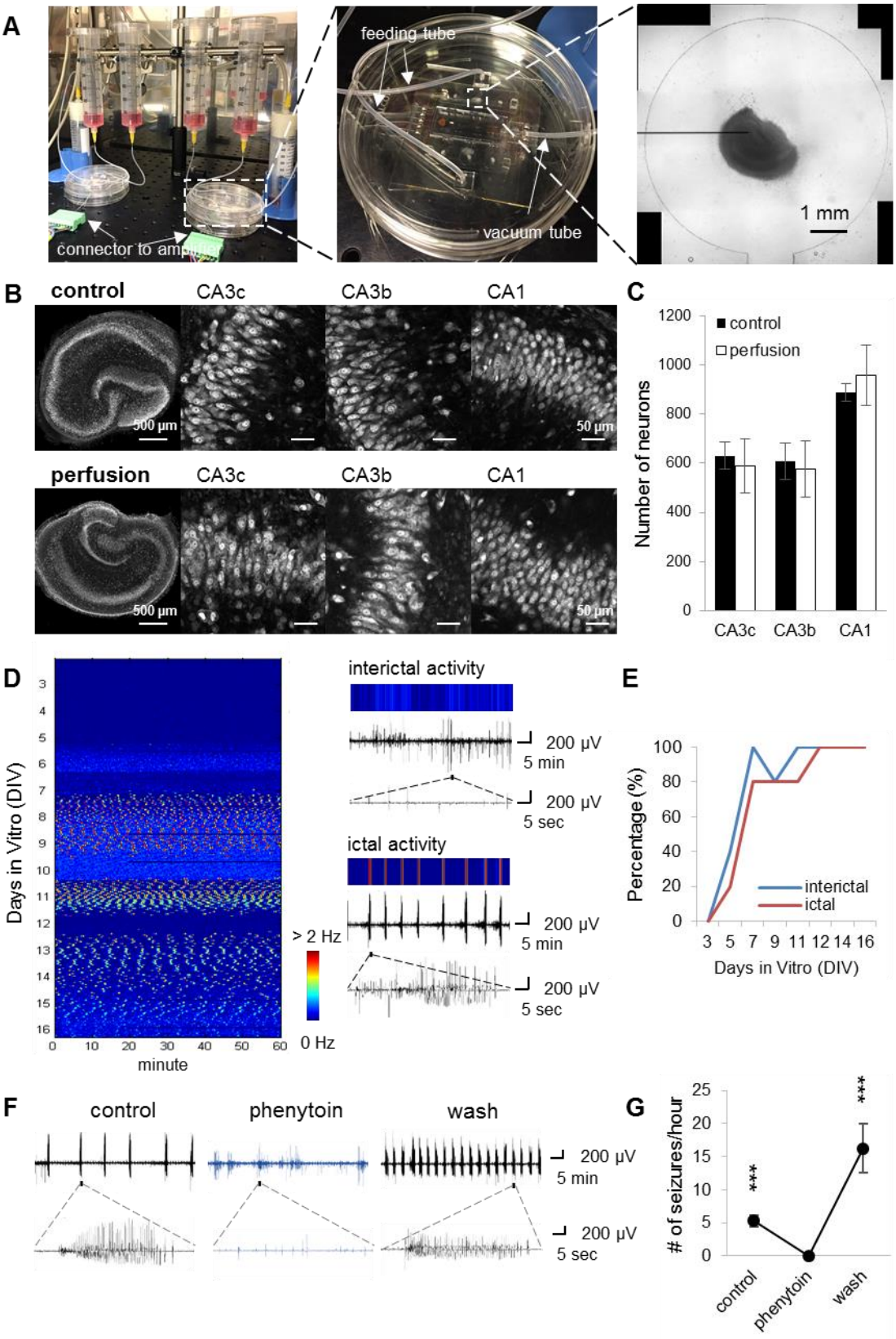

Figure 3.4 Epilepsy-on-a-chip model validation. (A) Photograph of the fully assembled system prototype, with a zoom in photo of the device, and a brightfield image of a

hippocampal culture maintained in the mini well with one substrate-integrated microelectrodes. Scale bar, 1 mm. (B-C) Culture viability validation. (B) Representative confocal imaging of NeurN staining in control cultures (interface methods) and microfluidic perfused cultures on 14 DIV, and higher magnification imaging in CA3c and CA3b, and CA1 regions. Scale bars as indicated in figure. (C) Neuron counts in CA3c, CA3b, and CA1. n = 9 each condition. (D-E) Chronic recordings reveal epileptogenesis. (D) Left: representative raster plot of chronic recording from 3 to 16 DIV. Color corresponds to the frequency of paroxysmal events, with low frequency indicated by blue color, and high frequency of paroxysmal events (seizures) indicated by red. Each horizontal line of the raster plot represents one hour of recording, with 24 lines per DIV. Right: the color map of interictal activity (top trace); seizures-like activity (ictal activity, bottom trace). (E) Incidence of ictal and interictal activity as a percentage of cultures recorded on MEA, with age of culture. n = 5 cultures. (F-G) Phenytoin showed anticonvulsive effect on this model. (F), representative recordings for each time period (control, phenytoin treatment, wash). (G) Seizure frequency during each period. n = 3, Error bars indicate SD. Statistical significance is indicated as ***, representing $p < 0.001$.

3.3.3 Receptor tyrosine kinase (RTK) inhibitors screen results

Before chronic screening, a short-term neurotoxicity pre-screen (0-7 DIV) was conducted to determine the non-toxic maximum concentrations of each inhibitors. The pre-screen results is shown in Table 3.1. Those concentrations were then applied to cultures for chronic screen in stage I (lactate and LDH assay), and stage II (chronic electrical assay).

Inhibitor name	Concentration
VEGF RTK Inhibitor II	5 µM
PDGF RTK Inhibitor III	2 µM
AG 1295 (PDGFR inhibitor)	5 µM
GTP-14564 (c-fms, c-kit, Flt3 inhibitor)	5 µM
EGFR/ErbB-2 Inhibitor	2 µM
Flt-3 Inhibitor III	1 µM
EGFR/ErbB-2/ErbB-4 Inhibitor	2 µM
Met Kinase Inhibitor	0.5 µM
Flt-3 Inhibitor	2 µM
VEGFR2 Kinase Inhibitor II	0.5 µM
cFMS RTK Inhibitor	2 µM
VEGF RTK Inhibitor IV	0.3 µM

Table 3.1 Pre-screen results.

In stage I, we screened 12 hippocampal RTK inhibitors listed in Table 3.1, and found that several inhibitors showed strong reducing effect in lactate and LDH levels (Figure 3.5A). Lactate and LDH production reached their peaks between 14-17 DIV, as the consequence of established epilepsy and seizure-induced cell death [23]. We therefore used the period of 7-14 DIV, the time between spontaneous seizure onset and significant neuron death caused by chronic epilepsy, to evaluate the drug efficacy on epileptogenesis. We integrated the lactate and LDH production of inhibitor-treated cultures between 7-14 DIV, and normalized it to vehicle-treated control from the same animal (n = 3). A scatter plot of lactate versus LDH is shown in Figure 3.5B for individual cultures. Some lactate and LDH values were lower than the mean of controls by more than 3 times the mean standard derivation (data points that are outside the dashed circle), suggesting antiepileptogenic effect. Significantly lower LDH was observed for VEGF, PDGF, and cFMS inhibitors, and significantly lower lactate for GTP-14564, a multi-target inhibitor for c-fms, c-kit and Flt-3, and EGFR/ErbB-2 inhibitor (one-way ANOVA with Holm-Sidak post hoc analysis, n = 3 cultures each condition). However, a different EGFR/ErbB-2/ErbB-4 inhibitor did not show significant results, suggesting that inhibitor non-specificity may be responsible.

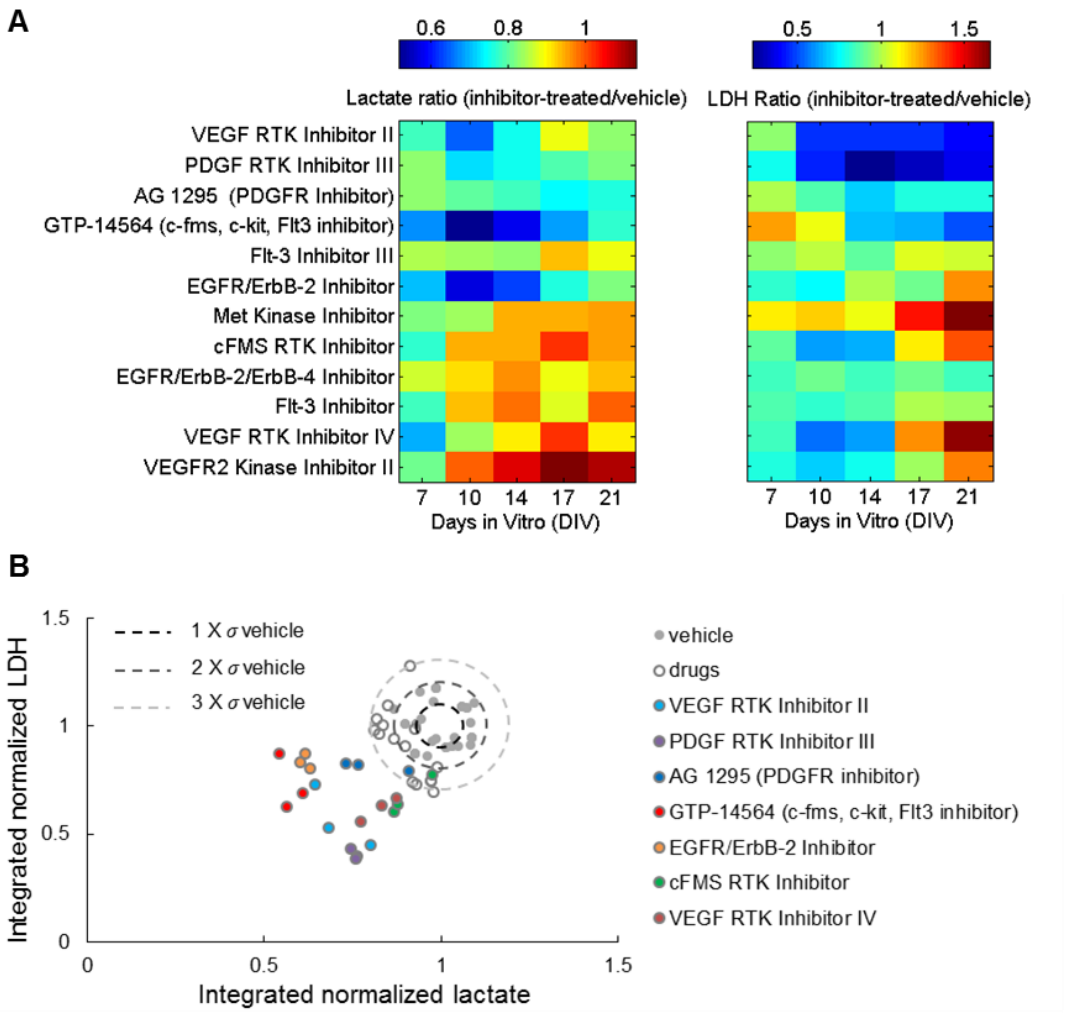

Figure 3.5 Screen of inhibitors by lactate and LDH. (A) Lactate and LDH data are shown as ratios of levels found in inhibitor-treated cultures and levels found in vehicle-treated controls. n = 3 each condition. (B) Integrated lactate production (DIV7–14) versus integrated LDH production (DIV7-14), and data was normalized to controls from the same animal. σ = standard deviation of integrated lactate (horizontal axis) and LDH (vertical axis) of controls. Data are plotted for 12 RTK inhibitors. Drugs that showed strong reducing effect are highlighted.

In stage II, a chronic electrical assay was conducted to verify the results we obtained in stage I. As is shown in Figure 3.4A, each screen was run by two µflow-MEA chips to test 3 drug-treated conditions with one vehicle-treated control (n = 3 each condition, cultures were from the same animal). Chronic recording was initiated on 1 DIV and continued until

14 DIV. Drugs and vehicle were applied since 3 DIV. A representative 1 hour recording in 12 cultures from one screen is presented in Figure 3.6A. In our preliminary data, a potential reducing effect in cumulative time seizing was observed in cFMS and EGFR/ErbB-2 (Figure 3.6B). The cumulative number of seizures was also analyzed and showed similar results. Significant antiepileptogenic effect was revealed in cFMS inhibitor (Figure 3.6C-G). Compared with the control, cumulative time seizing (Figure 3.6D) and cumulative number of seizures (Figure 3.6E) were significantly reduced in cultures treated by cFMS inhibitor. Cumulative distribution of normalized time seizing per day and normalized number of seizure per day showed significant decrease in cFMS inhibitor-treated cultures ($p = 0.005$, and 0.009, respectively, Kolmogorov-Smirnov test; $n = 5$, from 2 animals).

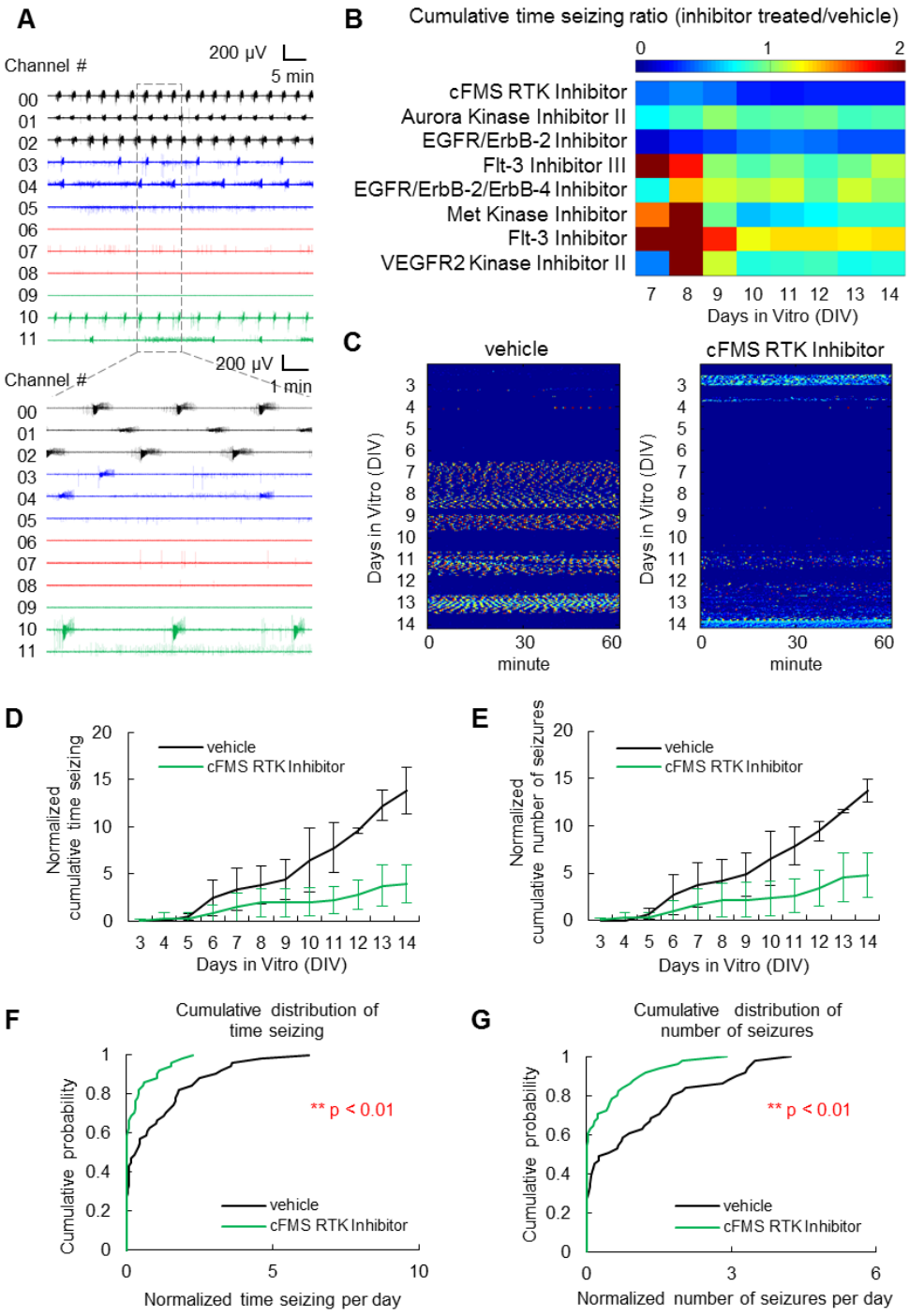

Figure 3.6 Screen of inhibitors by chronic electrical assay. (A) Representative plot of 1 hour recording, showing parallel monitoring of epileptogenesis in 12 organotypic hippocampal cultures (black, vehicle; blue, red and green represents different inhibitors treated conditions). n = 3 each condition, cultures are from the same animal. (B) Ratios of cumulative time seizing in inhibitor-treated cultures and in vehicle-treated controls. n = 3 each condition. (C) Representative chronic recordings of vehicle-treated control and cFMS RTK Inhibitor-treated cultures. (D-G) Antiepileptogenic effect of cFMS RTK Inhibitor.

(D, E) Normalized cumulative time seizing and normalized cumulative number of seizures. (F, G) Cumulative distribution of normalized time seizing per day and normalized number of seizures per day. Data was normalized to controls from the same animal. n = 5, from 2 screens. Error bars indicate SD. ** $p < 0.01$, Kolmogorov-Smirnov test.

In the simulation of field potential, we present a simplified current source model of seizure-like activity in a hippocampal slice in an instant where the whole slice is synchronized. In this moment, the layers occupied by dendrites are activated by excitatory inputs, resulting in current sink formation in these layers and current source formation in soma occupied layers (Figure 3.2C). However, neural activity is dynamic, and at most points in time, seizure-like activity is propagating or synchronized in a specific neural layer [49,35]. We calculated the current source density using constant neuron density and synaptic current amplitude. However, neuron density is not homogenous throughout the hippocampal slice, and the amplitude of synaptic current varies depending on the strength of synaptic input. To build a more sophisticated model, all these factors need to be taken into account.

To validate the in vitro model of epilepsy on our μflow-MEA device, we conducted drug response test of phenytoin. Interestingly, the cultures showed even higher seizure frequency after the phenytoin treatment termination. This might due to the long time scale (20 hours) of this microfluidic perfusion based wash-in and wash-out experiment. Seizure frequency progressively increased during epileptogenesis, even though phenytoin was applied for a period during this time. In our microfluidic culture platform, cultures are maintained at an liquid-air interface, so that the surface of the culture is not perfused. Therefore the applied drug can only reach the cells in the culture by diffusion, which could possibly explain the length of time it took to show drug effect. Our results suggest that

phenytoin cannot prevent epilepsy progression in this model, which agrees with previous observations [23].

In our preliminary data of the µflow-MEA based chronic electrical assay, cFMS and EGFR/ErbB-2 inhibitors showed potential reducing effects in cumulative time seizing (Figure 3.6B), confirming the LDH and lactate data. The most consistent and significant result was seen in cFMS inhibitor (Figure 3.6D-G), suggesting its antiepileptogenic effects. GW-2580, the compound's name of the cFMS inhibitor we used in this work, has been reported to also inhibit Trk receptors [50]. It is important to note that conditional deletion or inhibition of TrkB kinase can attenuate or eliminate seizures in animal models of epilepsy [51–55]. Therefore, there is likelihood that the antiepileptogenic effect we observed in cFMS inhibitor is due to its non-specific inhibition of Trk kinases. To verify the antiepileptogenic properties of cFMS inhibitor, its inhibition selectivity and potential off target effects will be further investigated. In EGFR/ErbB-2 treated cultures, the data was more variable, and a larger sample size is needed to confirm the drug efficacy. The system described in this work represents a single unit of the scalable epileptogenesis assay platform: 12 cultures on 2 µflow-MEA chip, recorded by 12 channel electrophysiology station to test 3 drug-treated conditions and a vehicle-treated control. This system can be easily scaled up through additions of more units for high-throughput drug discovery.

3.4 Conclusion

We developed a hybrid µflow-MEA technology for scalable chronic electrical assay of epileptogenesis in organotypic hippocampal culture model. The simplified MEA electrode

design rendered cost-effective device without compromising the sensitive detection of seizure-like activity. As a proof of concept, μflow-MEA based chronic electrical screening of inhibitors of hippocampal RTKs confirmed the results of biochemistry assay and identified inhibitors with antiepileptogenic effects. This epilepsy-on-a-chip screening platform provides a rapid dissection of complex signaling pathways associated with epileptogenesis, paving the way for high-throughput antiepileptogenic drug discovery.

3.5 Acknowledgements

This work was supported by NIH/NINDS grant R21NS088358.

3.6 References

1. Egert U, Schlosshauer B, Fennrich S, Nisch W, Fejtl M, Knott T, et al. A novel organotypic long-term culture of the rat hippocampus on substrate-integrated multielectrode arrays. Brain Res Protoc. 1998;2: 229–242.

2. Corner M, Van Pelt J, Wolters P, Baker R, Nuytinck R. Physiological effects of sustained blockade of excitatory synaptic transmission on spontaneously active developing neuronal networks—an inquiry into the reciprocal linkage between intrinsic biorhythms and neuroplasticity in early ontogeny. Neurosci Biobehav Rev. 2002;26: 127–185.

3. Beggs JM. Neuronal Avalanches Are Diverse and Precise Activity Patterns That Are Stable for Many Hours in Cortical Slice Cultures. J Neurosci. 2004;24: 5216–5229. doi:10.1523/jneurosci.0540-04.2004

4. Johnson HA, Buonomano DV. Development and Plasticity of Spontaneous Activity and Up States in Cortical Organotypic Slices. J Neurosci. 2007;27: 5915–5925. doi:10.1523/jneurosci.0447-07.2007

5. Hofmann F, Guenther E, Hämmerle H, Leibrock C, Berezin V, Bock E, et al. Functional re-establishment of the perforant pathway in organotypic co-cultures on microelectrode arrays. Brain Res. 8;1017: 184–196. doi:10.1016/j.brainres.2004.05.044

6. Hofmann F, Bading H. Long term recordings with microelectrode arrays: Studies of transcription-dependent neuronal plasticity and axonal regeneration. J Physiol-Paris. 3;99: 125–132. doi:10.1016/j.jphysparis.2005.12.005

7. Gong W, Sencar J, D J, x00E, ckel, J M, et al. Long-term, high-spatiotemporal resolution recording from cultured organotypic slices with high-density microelectrode arrays. 2015. pp. 1037–1040. doi:10.1109/TRANSDUCERS.2015.7181103

8. Killian NJ, Vernekar VN, Potter SM, Vukasinovic J. A Device for Long-Term Perfusion, Imaging, and Electrical Interfacing of Brain Tissue In vitro. Front Neurosci. 2016;10: 135. doi:10.3389/fnins.2016.00135

9. Liu J, Pan L, Cheng X, Berdichevsky Y. Perfused drop microfluidic device for brain slice culture-based drug discovery. Biomed Microdevices. 2016;18: 46. doi:10.1007/s10544-016-0073-z

10. Bonnauron M, Saada S, Rousseau L, Lissorgues G, Mer C, Bergonzo P. High aspect ratio diamond microelectrode array for neuronal activity measurements. Diam Relat Mater. 2008;17: 1399–1404. doi:10.1016/j.diamond.2007.12.065

11. Berdondini L, Chiappalone M, van der Wal PD, Imfeld K, de Rooij NF, Koudelka-Hep M, et al. A microelectrode array (MEA) integrated with clustering structures for investigating in vitro neurodynamics in confined interconnected sub-populations of neurons. Sens Actuators B Chem. 2006;114: 530–541. doi:10.1016/j.snb.2005.04.042

12. Heuschkel MO, Fejtl M, Raggenbass M, Bertrand D, Renaud P. A three-dimensional multi-electrode array for multi-site stimulation and recording in acute brain slices. J Neurosci Methods. 2002;114: 135–148.

13. Seker E, Berdichevsky Y, Begley MR, Reed ML, Staley KJ, Yarmush ML. The fabrication of low-impedance nanoporous gold multiple-electrode arrays for neural electrophysiology studies. Nanotechnology. 2010;21: 125504. doi:10.1088/0957-4484/21/12/125504

14. Liu B, Chen H, Johns TG, Neufeld AH. Epidermal Growth Factor Receptor Activation: An Upstream Signal for Transition of Quiescent Astrocytes into Reactive Astrocytes after Neural Injury. J Neurosci. 2006;26: 7532–7540. doi:10.1523/JNEUROSCI.1004-06.2006

15. Leadbeater WE, Gonzalez A-M, Logaras N, Berry M, Turnbull JE, Logan A. Intracellular trafficking in neurones and glia of fibroblast growth factor-2, fibroblast growth factor receptor 1 and heparan sulphate proteoglycans in the injured adult rat cerebral cortex. J Neurochem. 2006;96: 1189–1200. doi:10.1111/j.1471-4159.2005.03632.x

16. Nagayama T, Nagayama M, Kohara S, Kamiguchi H, Shibuya M, Katoh Y, et al. Post-ischemic delayed expression of hepatocyte growth factor and c-Met in mouse brain following focal cerebral ischemia. Brain Res. 2004;999: 155–166. doi:10.1016/j.brainres.2003.11.052

17. Schäbitz W-R, Krüger C, Pitzer C, Weber D, Laage R, Gassler N, et al. A Neuroprotective Function for the Hematopoietic Protein Granulocyte-Macrophage Colony Stimulating Factor (GM-CSF). J Cereb Blood Flow Metab. 2008;28: 29–43. doi:10.1038/sj.jcbfm.9600496

18. Tokita Y, Keino H, Matsui F, Aono S, Ishiguro H, Higashiyama S, et al. Regulation of Neuregulin Expression in the Injured Rat Brain and Cultured Astrocytes. J Neurosci. 2001;21: 1257–1264.

19. Sköld MK, Gertten CV, Sandbergnordqvist A-C, Mathiesen T, Holmin S. VEGF and VEGF Receptor Expression after Experimental Brain Contusion in Rat. J Neurotrauma. 2005;22: 353–367. doi:10.1089/neu.2005.22.353

20. Helmy A, Carpenter KL, Menon DK, Pickard JD, Hutchinson PJ. The Cytokine Response to Human Traumatic Brain Injury: Temporal Profiles and Evidence for

Cerebral Parenchymal Production. J Cereb Blood Flow Metab. 2011;31: 658–670. doi:10.1038/jcbfm.2010.142

21. Pitkänen A, Lukasiuk K. Mechanisms of epileptogenesis and potential treatment targets. Lancet Neurol. 2011;10: 173–186. doi:10.1016/s1474-4422(10)70310-0

22. Loscher W, Brandt C. Prevention or Modification of Epileptogenesis after Brain Insults: Experimental Approaches and Translational Research. Pharmacol Rev. 2010;62: 668–700. doi:10.1124/pr.110.003046

23. Berdichevsky Y, Dzhala V, Mail M, Staley KJ. Interictal spikes, seizures and ictal cell death are not necessary for post-traumatic epileptogenesis in vitro. Neurobiol Dis. 2012;45: 774–785.

24. Berdichevsky Y, Dryer AM, Saponjian Y, Mahoney MM, Pimentel CA, Lucini CA, et al. PI3K-Akt signaling activates mTOR-mediated epileptogenesis in organotypic hippocampal culture model of post-traumatic epilepsy. J Neurosci. 2013;33: 9056–9067.

25. Berdichevsky Y, Saponjian Y, Park K-I, Roach B, Pouliot W, Lu K, et al. Staged anticonvulsant screening for chronic epilepsy. Ann Clin Transl Neurol. 2016;3: 908–923. doi:10.1002/acn3.364

26. Bonfoco E, Krainc D, Ankarcrona M, Nicotera P, Lipton SA. Apoptosis and necrosis: two distinct events induced, respectively, by mild and intense insults with N-methyl-D-aspartate or nitric oxide/superoxide in cortical cell cultures. Proc Natl Acad Sci U S A. 1995;92: 7162–7166.

27. Nunez PL, Srinivasan R. Electric fields of the brain: the neurophysics of EEG. Oxford University Press, USA; 2006.

28. Logothetis NK, Kayser C, Oeltermann A. In Vivo Measurement of Cortical Impedance Spectrum in Monkeys: Implications for Signal Propagation. Neuron. 2007;55: 809–823. doi:10.1016/j.neuron.2007.07.027

29. Miceli S, Ness TV, Einevoll GT, Schubert D. Impedance Spectrum in Cortical Tissue: Implications for Propagation of LFP Signals on the Microscopic Level. eNeuro. 2017;4. doi:10.1523/ENEURO.0291-16.2016

30. Schindelin J, Arganda-Carreras I, Frise E, Kaynig V, Longair M, Pietzsch T, et al. Fiji: an open-source platform for biological-image analysis. Nat Methods. 2012;9: 676–682.

31. Bindokas V. 17 Sep 2014. Available: https://digital.bsd.uchicago.edu/%5Cimagej_macros.html

32. Buzsáki G, Anastassiou CA, Koch C. The origin of extracellular fields and currents—EEG, ECoG, LFP and spikes. Nat Rev Neurosci. 2012;13: 407–420.

33. Buzsáki G. Hippocampal sharp wave-ripple: A cognitive biomarker for episodic memory and planning. Hippocampus. 2015;25: 1073–1188. doi:10.1002/hipo.22488

34. Wheeler BC, Novak JL. Current Source Density Estimation Using Microelectrode Array Data from the Hippocampal Slice Preparation. IEEE Trans Biomed Eng. 1986;BME-33: 1204–1212. doi:10.1109/TBME.1986.325701

35. Gonzalez-Sulser A, Wang J, Motamedi GK, Avoli M, Vicini S, Dzakpasu R. The 4-aminopyridine in vitro epilepsy model analyzed with a perforated multi-electrode array. Neuropharmacology. 2011;60: 1142–1153. doi:10.1016/j.neuropharm.2010.10.007

36. Tsintsadze V, Minlebaev M, Suchkov D, Cunningham MO, Khazipov R. Ontogeny of kainate-induced gamma oscillations in the rat CA3 hippocampus in vitro. Front Cell Neurosci. 2015;9. doi:10.3389/fncel.2015.00195

37. Simmons ML, Terman GW, Chavkin C. Spontaneous Excitatory Currents and κ-Opioid Receptor Inhibition in Dentate Gyrus Are Increased in the Rat Pilocarpine Model of Temporal Lobe Epilepsy. J Neurophysiol. 1997;78: 1860–1868.

38. Okazaki MM, Molnár P, Nadler JV. Recurrent Mossy Fiber Pathway in Rat Dentate Gyrus: Synaptic Currents Evoked in Presence and Absence of Seizure-Induced Growth. J Neurophysiol. 1999;81: 1645–1660.

39. Prince DA, Parada I, Scalise K, Graber K, Jin X, Shen F. Epilepsy following cortical injury: Cellular and molecular mechanisms as targets for potential prophylaxis. Epilepsia. 2009;50: 30–40. doi:10.1111/j.1528-1167.2008.02008.x

40. Kovács R, Rabanus A, Otáhal J, Patzak A, Kardos J, Albus K, et al. Endogenous Nitric Oxide Is a Key Promoting Factor for Initiation of Seizure-Like Events in Hippocampal and Entorhinal Cortex Slices. J Neurosci. 2009;29: 8565–8577. doi:10.1523/JNEUROSCI.5698-08.2009

41. Liu J, Saponjian Y, Mahoney MM, Staley KJ, Berdichevsky Y. Epileptogenesis in organotypic hippocampal cultures has limited dependence on culture medium composition. PLOS ONE. 2017;12: e0172677. doi:10.1371/journal.pone.0172677

42. Hájos N, Ellender TJ, Zemankovics R, Mann EO, Exley R, Cragg SJ, et al. Maintaining network activity in submerged hippocampal slices: importance of oxygen supply. Eur J Neurosci. 2009;29: 319–327. doi:10.1111/j.1460-9568.2008.06577.x

43. Hájos N, Mody I. Establishing a physiological environment for visualized in vitro brain slice recordings by increasing oxygen supply and modifying aCSF content. J Neurosci Methods. 2009;183: 107–113.

44. Hill AJ, Jones NA, Williams CM, Stephens GJ, Whalley BJ. Development of multi-electrode array screening for anticonvulsants in acute rat brain slices. J Neurosci Methods. 1;185: 246–256. doi:10.1016/j.jneumeth.2009.10.007

45. Berdichevsky Y, Sabolek H, Levine JB, Staley KJ, Yarmush ML. Microfluidics and multielectrode array-compatible organotypic slice culture method. J Neurosci Methods. 2009;178: 59–64. doi:10.1016/j.jneumeth.2008.11.016

46. Ferrea E, Maccione A, Medrihan L, Nieus T, Ghezzi D, Baldelli P, et al. Large-scale, high-resolution electrophysiological imaging of field potentials in brain slices with microelectronic multielectrode arrays. Front Neural Circuits. 2012;6. doi:10.3389/fncir.2012.00080

47. Dyhrfjeld-Johnsen J, Berdichevsky Y, Swiercz W, Sabolek H, Staley K. Interictal spikes precede ictal discharges in an organotypic hippocampal slice culture model of epileptogenesis. J Clin Neurophysiol. 2010;27: 418–424.

48. Lillis KP, Wang Z, Mail M, Zhao GQ, Berdichevsky Y, Bacskai B, et al. Evolution of network synchronization during early epileptogenesis parallels synaptic circuit alterations. J Neurosci. 2015;35: 9920–9934.

49. Chang PY, Taylor PE, Jackson MB. Voltage Imaging Reveals the CA1 Region at the CA2 Border as a Focus for Epileptiform Discharges and Long-Term Potentiation in Hippocampal Slices. J Neurophysiol. 2007;98: 1309–1322. doi:10.1152/jn.00532.2007

50. Davis MI, Hunt JP, Herrgard S, Ciceri P, Wodicka LM, Pallares G, et al. Comprehensive analysis of kinase inhibitor selectivity. Nat Biotechnol. 2011;29: 1046–1051. doi:10.1038/nbt.1990

51. He X-P, Kotloski R, Nef S, Luikart BW, Parada LF, McNamara JO. Conditional deletion of TrkB but not BDNF prevents epileptogenesis in the kindling model. Neuron. 2004;43: 31–42. doi:10.1016/j.neuron.2004.06.019

52. Kotloski R, McNamara JO. Reduction of TrkB expression de novo in the adult mouse impairs epileptogenesis in the kindling model. Hippocampus. 2010;20: 713–723. doi:10.1002/hipo.20673

53. Liu G, Gu B, He X-P, Joshi RB, Wackerle HD, Rodriguiz RM, et al. Transient inhibition of TrkB kinase after status epilepticus prevents development of temporal lobe epilepsy. Neuron. 2013;79: 31–38.

54. Liu G, Kotloski RJ, McNamara JO. Antiseizure effects of TrkB kinase inhibition. Epilepsia. 2014;55: 1264–1273. doi:10.1111/epi.12671

55. Gu B, Huang YZ, He X-P, Joshi RB, Jang W, McNamara JO. A Peptide Uncoupling BDNF Receptor TrkB from Phospholipase Cγ1 Prevents Epilepsy Induced by Status Epilepticus. Neuron. 2015;88: 484–491. doi:10.1016/j.neuron.2015.09.032

Chapter 4

Disease model validation: Culture medium study

The work described in this chapter has been published in "Epileptogenesis in organotypic hippocampal cultures has limited dependence on culture medium composition" by Liu J, Saponjian Y, Mahoney MM, Staley KJ, and Berdichevsky Y, PLoS ONE. 2017;12: e0172677.

4.1 Motivation

Brain insults, including traumatic brain injury, trigger a series of changes at molecular, cellular, and network levels, that can cause epilepsy [1,2]. It has been hypothesized that the triggering event of epileptogenesis in organotypic cultures is the trauma of brain slice preparation [3]. In cultures, this trauma results in axonal and dendritic reorganization [4–8] and glial activation [9,10] that are associated with epileptogenesis. In this view, organotypic cultures are an in vitro analogue of animal models of traumatic brain injury-induced epileptogenesis [11–13]. However, unlike brain tissue in vivo, organotypic slices are maintained in an artificially controlled environment. It may be possible that epileptogenesis in organotypic cultures is driven by artificial environmental factors. Here, we test this hypothesis by focusing on the most artificial aspect of organotypic culture environment: the culture medium.

Mammalian tissues must be bathed in a mixture of metabolic substrates, hormones and growth factors (culture medium) to maintain them in vitro longer than 24 hours. Early versions of culture media were often supplemented by actual blood-derived serum [14,15]. Since concentrations of hormones and metabolites can sometimes vary significantly in samples of animal serum, fully chemically-defined media were developed to enhance reproducibility [16,17]. We have previously used both serum-supplemented and chemically defined media to maintain organotypic hippocampal cultures, and found that epileptogenesis occurs in both types of media [18,19]. One concern is that chemically defined culture medium is based on the composition of blood plasma rather than cerebrospinal fluid (CSF). Epileptogenesis in vivo may be enhanced by the opening of the blood-brain barrier (BBB) after brain injury [20,21]. This enhancement is thought to arise from direct exposure of brain tissue to components of blood that normally do not cross BBB, or to compounds that are present in blood at different concentration than in CSF [22,23]. Therefore, it may be possible that epileptogenesis in organotypic cultures is not triggered by the trauma of dissection, but by exposure of hippocampal tissue to a cocktail of compounds that are present at much lower concentration or not present at all in normal CSF.

Organotypic slices are prepared from perinatal (postnatal day 7) rodent brain, so the culture media is typically that used for the culture of postnatal neurons (Neurobasal-A, the NeurA column in Table 4.1) with B27 supplement (Table 4.2). It can be readily seen that concentrations of glucose, potassium, and magnesium in Neurobasal-A are substantially different than those found in CSF [24–26]. Some of these differences, such as increased potassium and decreased calcium and magnesium concentrations, may contribute to in

vitro hyperexcitability [22,27]. In addition, many amino acids are contained in Neurobasal-A at significantly higher concentrations than in CSF [28–31]. Altered concentrations of amino acids such as glycine, serine, leucine, isoleucine, valine, phenylalanine and others are found in metabolic epilepsies [32,33], and might also play a role in development of spontaneous epileptiform activity in organotypic cultures. Neurobasal-A medium is usually supplemented with B27, which contains Bovine Serum Albumin (BSA), insulin, transferrin, progesterone, putrescine, and selenium along with others for a total of 20 components (Table 4.2). These components may also play a role in epileptogenesis [34].

Components	Concentration (mM)				Components	Concentration (mM)			
	NeurA	CST	CBM			NeurA	CST	CBM	
Essential Amino Acids					**Vitamins**				
L-Arginine hydrochloride	0.40	0.40	0.40	a	Biotin	0.016	0.016	0.016	b
L-Asparagine·H_2O	0.0055	-	-		Choline chloride	0.029	0.029	0.029	b
L-Cysteine	0.26	0.25	0.25	a	D-Calcium pantothenate	0.0084	0.0084	0.0084	b
L-Histidine hydrochloride·H_2O	0.20	0.20	0.20	a	Folic Acid	0.0091	0.0091	0.0091	b
L-Isoleucine	0.80	0.79	0.79	a	Niacinamide	0.033	0.033	0.033	b
L-Leucine	0.80	0.79	0.79	a	Pyridoxine hydrochloride	0.020	-	-	
L-Lysine hydrochloride	0.80	0.81	0.81	a	Riboflavin	0.0011	0.0011	0.0011	b
L-Methionine	0.20	0.20	0.20	a	Thiamine hydrochloride	0.012	0.012	0.012	b
L-Phenylalanine	0.40	0.40	0.40	a	Vitamin B12	0.000005	-	-	
L-Threonine	0.80	0.81	0.81	a	i-Inositol	0.040	-	-	
L-Tryptophan	0.08	0.08	0.08	a	**Inorganic Salts**				
L-Tyrosine	0.40	0.40	0.40	a	Calcium Chloride ($CaCl_2$)	1.80	1.80	2.00	*
L-Valine	0.80	0.80	0.80	a	Magnesium Chloride ($MgCl_2$)	0.81	0.81	1.30	*
Non-essential Amino Acids					Potassium Chloride (KCl)	5.33	5.33	3.50	*
Glycine	0.40	0.40	0.40		Sodium Bicarbonate ($NaHCO_3$)	26.19	26.19	25.00	*
L-Alanine	0.023	-	-		Sodium Chloride (NaCl)	68.97	68.97	88.70	c
L-Proline	0.068	-	-		Sodium Phosphate monobasic ($NaH_2PO_4.H_2O$)	0.91	0.91	1.20	*
L-Serine	0.40	0.40	0.40		Zinc sulfate ($ZnSO_4 \cdot 7H_2O$)	0.00067	-	-	
Other Components					Ferric Nitrate ($Fe(NO_3)_3 \cdot 9H_2O$)	0.00025	-	-	
D-Glucose (Dextrose)	25.00	25.00	11.00	*					
HEPES	10.92	10.92	10.92						
Phenol Red	0.07	0.07	0.07						
Sodium Pyruvate	0.23	-	-						

a = from Basal Medium Eagle (BME) amino acids solution B6766 (Sigma)
b = from BME vitamins solution B6891 (Sigma)
c = concentration was adjusted to match osmolarity
- = excluded from medium
* = concentration was according to/approximated CSF composition

Table 4.1 Composition of Neurobasal-A, customized medium (CST) and CSF based medium (CBM).

Components	Concentration (mg/L)†	Components	Concentration (mg/L)†
Vitamins		**Other components**	
Biotin		D-Galactose	
DL Alpha Tocopherol Acetate		Ethanolamine HCl	
DL Alpha-Tocopherol		Glutathione (reduced)	
Vitamin A (acetate)		L-Carnitine HCl	
Proteins		Linoleic Acid	
BSA, fatty acid free Fraction V	250	Linolenic Acid	
Catalase		Putrescine 2HCl	16.1
Human Recombinant Insulin	3.5	Sodium Selenite	0.014
Human Transferrin	5	T3 (triodo-I-thyronine)	
Superoxide Dismutase		Progesterone	0.0063
		Corticosterone	

†Concentrations of B27 components are not published. The concentrations listed here were used in our media component replacement experiments. Numbers represent final concentrations in culture medium.

Table 4.2 Composition of B27 medium supplement.

In this work, we tested the hypothesis that the composition of culture medium influences epileptogenesis in organotypic hippocampal cultures. To do this, we altered the concentration of individual components of the media and measured the effects on epileptogenesis in this model.

4.2 Experimental methods

4.2.1 Culture media preparation

Customized culture media were prepared with different compositions and concentrations of electrolytes, amino acids, and glucose (all from Sigma) as described in the text. The osmolarity of all custom media was matched to Neurobasal-A (240 – 260 mOsm/kg) by adjusting the NaCl concentration. Unless otherwise indicated, all culture media were supplemented with bovine serum albumin (BSA) (250 mg/L: physiological range of

albumin in healthy CSF is 70 – 266 mg/L [35–38]), insulin (3.5 mg/L), selenium (14 µg/L), from Sigma, and glutaMAX (0.5 mM) and gentamicin (30 mg/L), from Life Technologies. In experiments addressing role of B27 components, concentrations of BSA, insulin and

4.2.2 Morphology Analysis

Morphology analysis is described in detail in Chapter 3. Here, slice brightness was quantified by calculating mean greyscale value of the slice area minus the background in bright field images (Fiji/ImageJ).

4.2.3 Electrophysiological recordings and data analysis

Cover slips with cultures were transferred to a 35 mm petri dish and placed in an interface chamber perfused with culture medium at 37 °C. Extracellular field potential recordings were performed using tungsten microelectrodes (0.1 MOhm) connected to an amplifier (RZ2, Tucker Davis Technologies) fitted with high-impedance multiple-channel pre-amplifier stage (PZ2-64, Tucker Davis Technologies) (band-pass 1 Hz-3 kHz, gain ×1000). Sampling rate was 6 kHz per channel. To record the population activity and multiple unit activity, microelectrodes were placed in CA3 pyramidal cell layer. OpenEx (Tucker Davis Technologies) and Matlab (MathWorks) were used for signal processing and data analysis. Ictal events (electrographic seizures) were defined as paroxysmal events of much larger amplitude than background multiple unit activity and lasting longer than 10 s, including discrete shorter paroxysmal events that occurred with event frequency of at least 2 Hz for at least 10 s.

4.2.4 Nissl and NeuN staining and image analysis

For Nissl staining, cultures were fixed in 4% paraformaldehyde, permeabilized for 1 h in 0.3% Triton-X on a shaking platform, and stained with propidium iodide (Invitrogen; 1 mg/ml stock) diluted 1:250 in phosphate-buffered saline (PBS) for 5 h. NeuN staining was carried out as described in Chapter 2. Slices were then washed and mounted for confocal microscopy. Z-stack images were collected on a confocal microscope (Zeiss LSM 510 META, Germany) with 40× objective. Z-stack layers were separated by 2 µm, and slices were imaged over their total depth. Images were then processed in Fiji (ImageJ). Neurons in CA1 and CA3 pyramidal layers were quantified with a counting algorithm modified from existing "3D watershed technique" for counting cell nuclei (ImageJ macro developed by [42]).

4.2.5 Statistical Methods

We used Student's t test for two-variable comparisons, one-way ANOVA with Holm-Sidak post hoc analysis for multiple variable comparisons, and z-test for seizure-like event incidence comparison. Number of samples n refers to the number of cultures or the number of cells as indicated.

4.3 Results

The summary of our experiments is provided in chart form in Figure 4.1. We focused on identifying components of B27 and Neurobasal-A that were vital for viability of

organotypic hippocampal cultures. We then simplified the culture medium, and varied concentrations of essential components to determine effects on epileptogenesis.

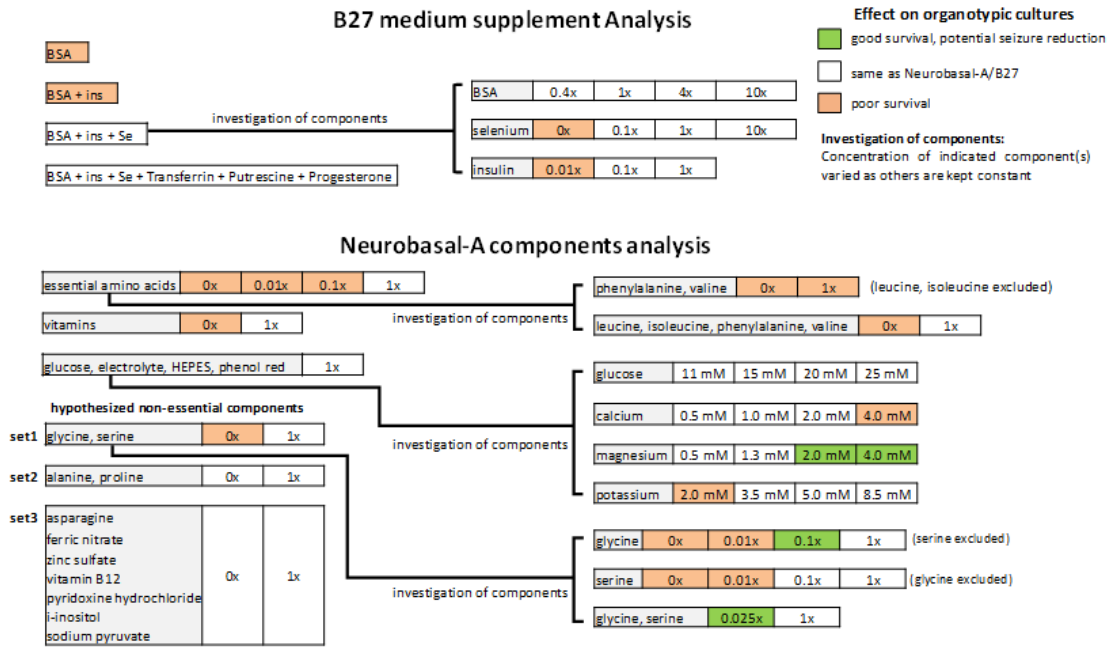

Figure 4.1 Summary of experiments.

4.3.1 Replacement of B27 supplement with BSA, insulin and selenium

We hypothesized that only BSA and a subset of components of B27 with concentrations indicated in Table 4.2 (these components make up the widely used N2 supplement) are essential to maintain viable slice cultures. The following compositions were tested: BSA only; BSA and insulin (BSA + ins); BSA, insulin and selenium (BSA + ins + Se); BSA + insulin + Se + transferrin + putrescine + progesterone; and B27. The concentration of each component is listed in Table 4.2. Supplements were added to Neurobasal-A medium, which was further supplemented with GlutaMAX and gentamycin as described in section 4.2.1. Confocal images taken on 8 DIV showed that cultures kept in medium supplemented with BSA only or with BSA + insulin had missing or fragmented pyramidal layers,

indicating poor neuronal survival (Figure 4.2A). Slices maintained in media with 3 other supplements showed intact pyramidal layers and maintained hippocampal morphology. To further compare these 3 supplements, we quantified the neuron numbers in CA3c, CA3b and CA1. Compared with B27 group, BSA+ins+Se+transferrin+putrescine+progesterone group had a significantly lower number of neurons in CA3b (ANOVA with *post hoc* Holm-Sidak analysis in this and subsequent statistical tests, $p = 0.007$, $n = 3$ cultures, each condition) (Figure 4.2B). BSA + insulin + selenium group showed similar neuron numbers to B27 group in CA3c, CA3b and CA1 ($p = 0.222, 0.410, 0.398$, respectively, $n = 3$ cultures, each condition). We conclude that BSA, insulin and selenium were essential and sufficient supplements to Neurobasal-A medium for neuronal survival in organotypic hippocampal cultures until 8 DIV.

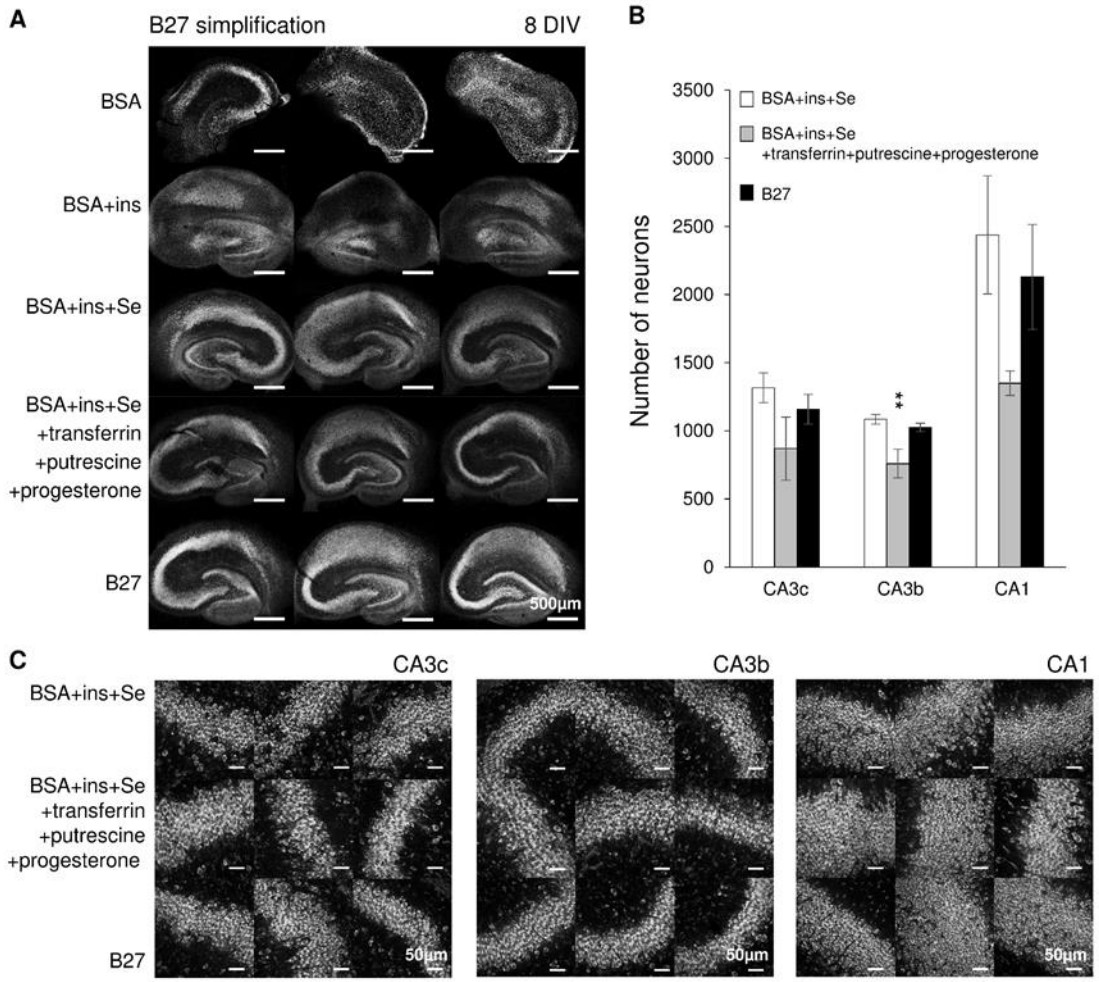

Figure 4.2 Essential components of B27 supplement. (A) Low magnification confocal images of Nissl staining in cultures at 8 DIV, conditions are indicated on the left side of images, scale bars, 500 µm. (B) Corresponding neuron counts in CA3c, CA3b and CA1. Statistical differences are indicated for comparisons between B27 group versus other groups. Error bars indicate SD. Statistical significance is indicated as **, representing $p < 0.01$. (C) Confocal images of Nissl staining in CA3c, CA3b and CA1, scale bars, 50 µm. n = 3 cultures, each condition.

4.3.2 Reduction of selenium and insulin affects cell survival

We modified concentrations of each component of the simplified supplement (BSA + insulin + selenium) to investigate their effect on cultures. Following concentrations were tested: for BSA, 0.4x (BSA concentration equal to 0.4 times that listed in Table 4.2), 1x

(BSA concentration equal to that listed in Table 4.2), 4x (4 times) and 10x (10 times); for selenium, 0x (no selenium), 0.1x (selenium concentration equal to 1/10 of that listed in Table 4.2), 1x (selenium concentration equal to that listed in Table 4.2), 10x (10 times); for insulin, 0.01x (insulin concentration is 1/100 of listed), 0.1x (insulin concentration equal to 1/10 of that listed in Table 4.2), 1x (insulin concentration equal to that listed in Table 4.2), and B27. The concentration of only one component was varied in each experiment while the other components were included at concentrations found in Table 4.2. It was not possible to reduce albumin below 100 mg / L due to reductions in the uniformity of wetting of the hippocampal slice surface by the media. Brightfield microscope images were taken at 21 DIV. We measured LDH and lactate concentrations in spent culture media. Data were from medium collected on 3, 7, 10, 14, 17 and 21 DIV. There were no significant differences in gross culture morphology or LDH and lactate concentrations in medium containing different concentrations of BSA (Figure 4.3A). Cultures in medium with 0x selenium had undistinguishable neural layers, indicating poor survival (Figure 4.3B). Compared with 1x selenium group, 0x selenium group had significantly higher LDH at 7 DIV, 10 DIV, 14 DIV and 17 DIV ($p < 0.001$ for 7, 10, 14 DIV, $p = 0.01$ for 17 DIV, $n = 3$ cultures, each condition) and significantly lower lactate at 10 DIV, 14 DIV, 17 DIV, 21 DIV ($p < 0.001$ for all these days, $n = 3$ cultures, each condition), confirming morphology results and indicating that selenium is essential for culture survival. No differences in morphology or lactate and LDH concentrations were observed between cultures supplemented with 0.1x, 1x, or 10x selenium. Cultures in medium with 0.01x insulin were brighter and smaller than cultures with 0.1x or 1x insulin or B27 (Figure 4. 3C; inverted greyscale values of cultures were 123.41 ± 8.35, 142.13 ± 8.31, 149.47 ± 3.40 and 132.72

± 7.63 for 0.01x, 0.1x, 1x and B27 group respectively, n = 3 cultures, each condition. A significant difference was found in comparison of 0.01x vs. 1x group, $p = 0.007$, n = 3 cultures, each condition). Compared with 1x insulin group, 0.01x insulin group had significantly lower LDH from 10 DIV to 21 DIV ($p < 0.001$ for 10, 14, 17 DIV, $p = 0.005$ for 21 DIV, n = 3 cultures, each condition) and significantly lower lactate from 7 DIV to 21 DIV ($p < 0.001$ for 7, 10, 14 DIV, $p = 0.007$ for 17 DIV, $p = 0.003$ for 21 DIV, n = 3 cultures, each condition). However, LDH concentration for 0.01x group was moderately higher on DIV 3 than for cultures supplemented with higher concentrations of insulin or with B27. This, together with smaller size of the 0.01x insulin cultures, suggested that more cells died by DIV 3 due to lack of sufficient concentration of insulin, leading to lower lactate production in these cultures later on.

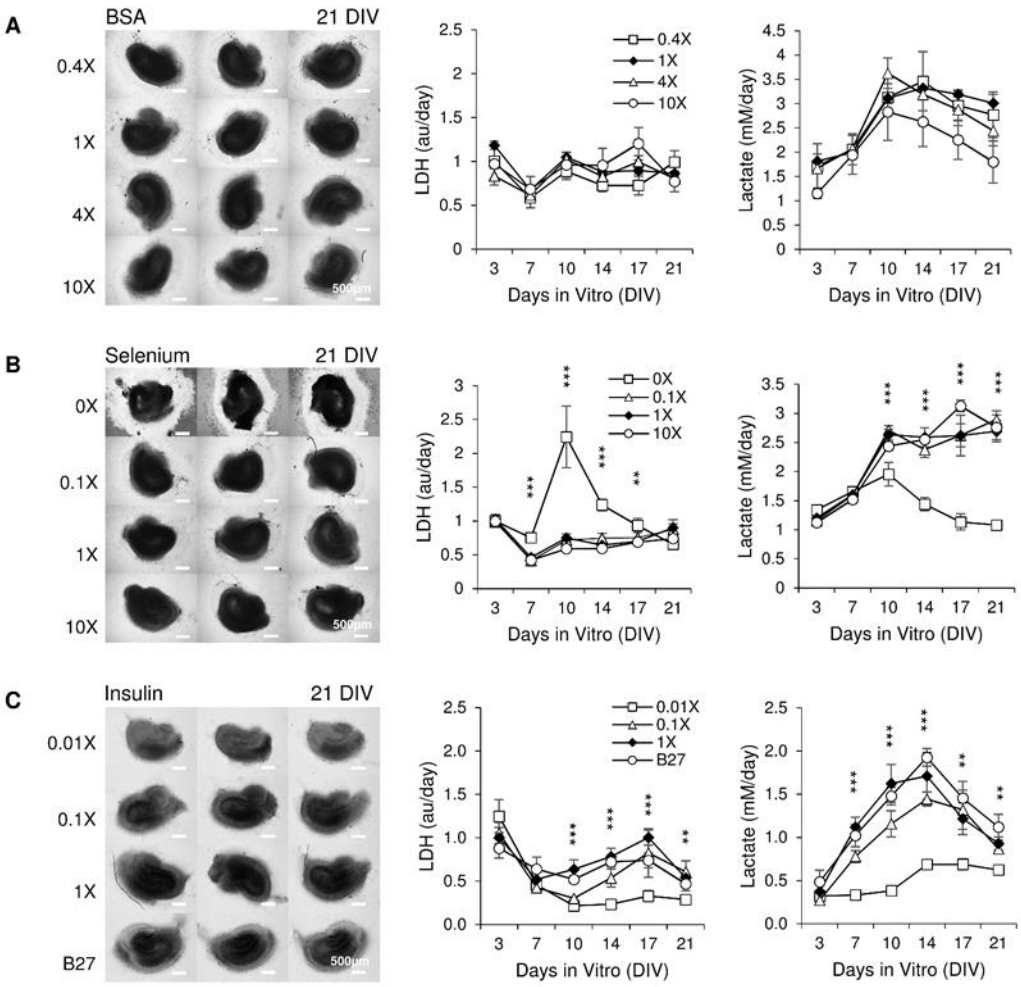

Figure 4.3 Effects of different concentrations of BSA, selenium, and insulin. (A-C) Left: brightfield images of cultures maintained in media with indicated concentrations of BSA, selenium or insulin, scale bars represent a distance of 500 μm; Right: time course of LDH and lactate concentration in culture supernatant of cultures; n = 3 cultures, each condition. Error bars indicate SD. Significant statistical differences are indicated for comparison of 0X selenium versus 1X selenium and 0.01X insulin versus 1X insulin, with ***$p < 0.001$, **$p < 0.01$.

We further investigated the influence of insulin concentration on culture survival. We used the following conditions: 0x (no insulin), 0.01x (insulin concentration is 1/100 of that listed in Table 4.2), and 1x. Confocal images taken on 8 DIV showed that 0x group had smaller slice area compared with other groups (Figure 4.4A). We measured the slice area and a significant difference was seen between the 0x group and 1x group ($p = 0.011$, n = 3

cultures, each condition). We quantified the number of neurons in CA3c, CA3b and CA1 (Figure 4.4B, left chart). However, we found that due to the more compact size of 0x insulin cultures, a larger proportion of the pyramidal cell layer would fit into a single field of view for those cultures compared to 0.01x and 1x cultures. To arrive at a correct relative number of neurons between the cultures, we corrected neuronal counts with normalized total slice area (Figure 4.4B, right chart). Compared to the 1x group, the 0x group and 0.01x group showed significantly lower neuron numbers in CA1 (before slice area correction: $p = 0.002$ for 0x group, $p = 0.011$ for 0.01x group, $n = 3$ cultures, each condition; after slice area correction: $p < 0.001$ for both conditions). We inspected the size of individual neurons and found that 0x group and 0.01x group had smaller neurons compared to the 1x group (Figure 4.4D). A significant difference was seen between the 0x group and 1x group ($p < 0.001$, $n = 30$ cells, each condition). We concluded that insulin affects neuronal size, survival and slice size. However, insulin concentrations that were reduced by a factor of 10 from the standard N2 levels had no significant effects on our measures of the health of the slice cultures. In subsequent experiments, we supplemented all media with BSA, insulin and selenium at concentrations listed in Table 4.2, since these concentrations were optimal for neural survival by DIV 8.

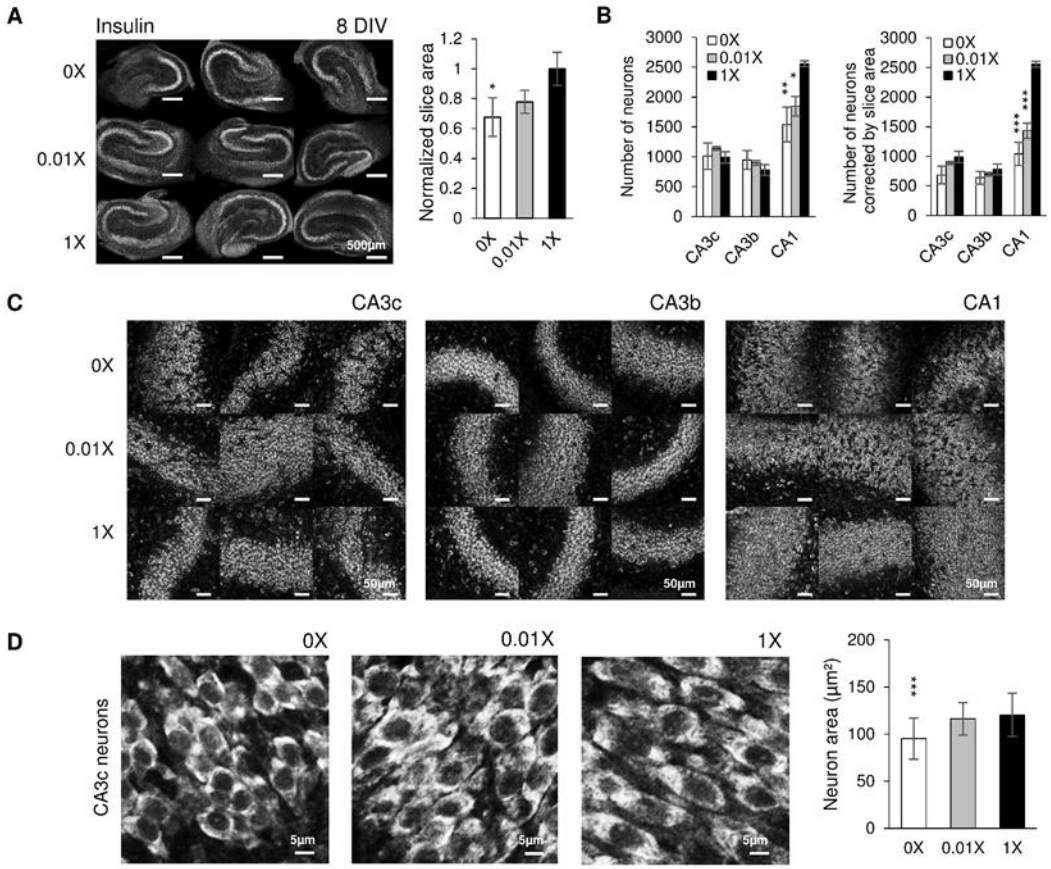

Figure 4.4 Insulin enhances neuronal survival. (A) Low magnification confocal images of Nissl staining in cultures at 8 DIV, conditions are indicated on the left side of images, scale bars, 500 µm. Chart shows effect of insulin on slice area; (B) Left: neuron counts in CA3c, CA3b and CA1; Right: neuron counts corrected by the normalized slice area. n = 3 cultures, each condition. Statistical differences are indicated for comparison between 1X group and other groups. (C) Representative confocal images of Nissl staining in CA3c, CA3b and CA1, scale bars, 50 µm. (D) Left: representative confocal images of neurons in CA3c, scale bars represent a distance of 5 µm; Right: corresponding cell size in CA3c. n = 30 cells, each condition. Significant statistical differences are indicated for comparison of 0X group versus 1X group. Error bars indicate SD. Significant differences are labeled as *$p < 0.05$, **$p < 0.01$ and ***$p < 0.001$.

4.3.3 Identification of essential components of Neurobasal-A

We grouped the hypothesized non-essential components into three sets listed in Figure 4.5A. We then replicated Neurobasal-A by combining BME amino acids solution (B6766,

Sigma, 1:12.5 dilution) and BME vitamins solution (B6891, Sigma, 1:25 dilution) with other components in Neurobasal-A formulation in appropriate concentrations (Table 4.1, NeurA columns). Suspected noncritical components were included in the replicate experimental group, or excluded as indicated. Cultures were maintained in replicated NeurA or replicated NeurA with set 1, set 2, or set 3 excluded (-set1, -set2, -set3 experimental groups). Brightfield microscope images taken on 21 DIV showed that cultures without glycine and L-serine (-set1) were significantly brighter than other groups (Figure 4.5B; inverted greyscale = 152.60 ± 6.74, 110.28 ± 9.29, 148.85 ± 2.98 and 152.65 ± 7.39 for replicate, -set1, -set2 and –set3 group respectively; $p < 0.001$ for –set1 vs. replicate, n = 3 cultures, each condition). Slices in –set2 and –set3 had morphologies similar to control (replicated NeurA) slices. Group lacking set1 was found to have lower LDH and lactate concentrations than the other three groups from 14 DIV to 21 DIV. Significant differences in lactate between –set1 group and NeurA replicate group appeared on 14, 17, 21 DIV ($p < 0.001$, $p = 0.004$, $p = 0.007$, respectively, n = 3 cultures, each condition). Based on the altered morphology, LDH, and lactate, we conclude that glycine and L-serine play a role in cell survival and activity. On the other hand, exclusion of set2 or set3 had no noticeable effect on culture morphology or LDH and lactate release. In subsequent experiments, we used NeurA medium with the noncritical sets 2 and 3 excluded, which we termed customized medium (CST, Table 4.1). The role of glycine and L-serine was investigated further in experiments described in the section 4.3.4.

Based on CST, we generated media with different concentrations of essential amino acids: control (essential amino acid concentrations equal to those listed for CST), 0.1x (essential amino acid concentrations equal to 1/10 of those listed for CST), 0.01x (1/100) and 0x (no

essential amino acids). By 7 DIV, cultures in 0x group were significantly darker than control cultures, indicating poor survival (Figure 4.5C; inverted greyscale values were 135.19 ± 3.42, 124.77 ± 3.87, 144.46 ±15.32 and 170.53 ± 10.56 for control, 0.1x, 0.01x and 0x group respectively; $p = 0.001$ for 0x vs. control group, n = 3 cultures, each condition). Neural layers became undistinguishable in 0x cultures by 7 DIV. 0.01x and 0x group had significantly higher LDH than control at 7 DIV ($p < 0.001$, n = 3 cultures, each condition). We conclude that concentrations of essential amino acids lower than 1/100 of what is found in Neurobasal-A are insufficient for culture survival. We then compared 0.1x and control groups (Figure 4.5D). No observable differences in culture morphology were found in microscope images at 14 DIV. However, 0.1x group had significantly higher LDH than control at 10 DIV ($p = 0.03$, n = 3 cultures, each condition) and 14 DIV ($p = 0.006$, n = 3 cultures, each condition). Thus, we conclude that reduction of all essential amino acid concentrations was detrimental to culture survival.

We then examined the possibility that we could reduce seizure activity in organotypic slice cultures by reducing the concentrations of some of the essential amino acids, without increasing cell death. We focused on the amino acids that play a role in metabolic epilepsy: leucine, isoleucine, phenylalanine and valine (Figure 4.5E). Control cultures were maintained in CST with all essential amino acids, -leucine & isoleucine cultures were maintained in CST without leucine and isoleucine, and -4S cultures were maintained in CST without leucine, isoleucine, phenylalanine, and valine. The cultures of the last two groups had a deformed shape with a hole in the slice center, and much thinner neural layers compared with the control group at 10 DIV. The control group showed significantly higher LDH than the other two groups at 7 DIV ($p < 0.001$ for both groups), 10 DIV ($p = 0.009$

for –leucine and isoleucine group, $p = 0.035$ for -4S group), and 14 DIV ($p < 0.001$ for both groups). In this case, early cell death in –leucine & isoleucine and -4S cultures (detected by poor morphology of these cultures) resulted in lower LDH at later time-points, due to fewer surviving cells. We conclude that leucine, isoleucine, phenylalanine, and valine are essential for organotypic hippocampal culture viability.

We also excluded all vitamins (-vitamins mix), and compared it with 1x vitamins concentration medium (control). Microscope images at 10 DIV revealed that the -vitamins mix group slices shrank, with significantly darker neural layers than control cultures, despite no significant difference in LDH (Figure 4.5F; inverted greyscale = 125.77 ± 8.21 and 157.73 ± 0.30 for control and –vitamins mix group respectively, $p = 0.005$, $n = 3$ cultures, each condition). We conclude that exclusion of vitamins increased cell death in cultures.

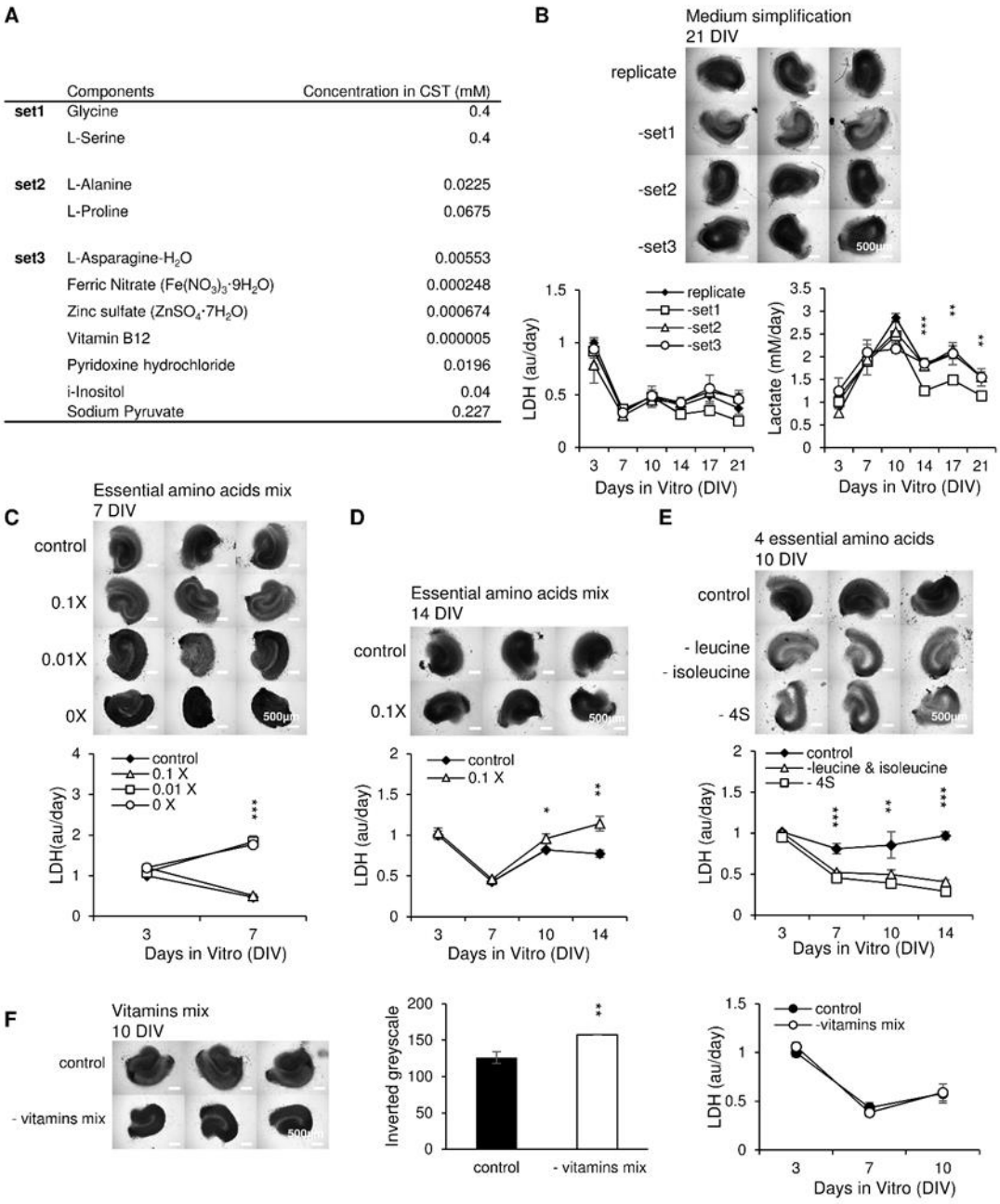

Figure 4.5 Neurobasal-A simplification. (A) List of hypothesized noncritical components. (B) Left: brightfield microscope images at 21 DIV, scale bars represent a distance of 500 µm; Right: time course of LDH and lactate concentration in spent culture media from cultures treated with replicated NeurA, or NeurA without set1, set2 or set3; n = 3 cultures, each condition. Significance is shown for replicate group versus –set1 group. (C) Cultures maintained in the presence of different concentrations of essential amino acids. Top: photomicrographs at 7 DIV. Scale bars, 500 µm; n = 3 cultures, each condition. Statistical significance is indicated for 0x group and 0.01x group versus control. (D) Cultures maintained in the presence of reduced and control concentrations of amino acids. Images are from 14 DIV; n = 3 cultures, each condition. (E) Evaluation of the removal of 4 metabolic epilepsy-related essential amino acids (4S: leucine, isoleucine, phenylalanine

and valine). Images are from 10 DIV; n = 3 cultures, each condition. Statistical differences are shown for experimental groups versus control. (F) Cultures maintained in the presence of 1x (control) and without vitamins (- vitamins mix) and corresponding greyscale and LDH measurements. Images are from 10 DIV; n = 3 cultures, each condition. Error bars indicate SD. Significances are labeled as ***$p < 0.001$, **$p < 0.01$ and *$p < 0.05$.

4.3.4 Reduction of non-essential amino acids affects cell survival

We investigated glycine and L-serine in more detail. We maintained cultures in media containing different concentrations of glycine or L-serine (only one of those amino acids was present in media described in this paragraph and Figure 4.6A and B. Base concentration (1x) of glycine or L-serine was 0.4 mM as in NeurA. 0x medium contained neither glycine nor L-serine. Confocal images of cultures stained with anti-NeuN neuron-specific antibody were taken at 21 DIV (Figure 4.6A). Cultures maintained in 0x and 0.01x glycine had very few neurons remaining by 21 DIV. NeuN staining in 0.1x glycine group revealed distinct neuron layers similar to 1x group. Neuronal counts in area CA1 revealed that compared with 1x group, significantly less neurons remained in 0x ($p < 0.001$, n = 3 cultures, each condition) and 0.01x ($p = 0.009$, n = 3 cultures, each condition) glycine groups, while more neurons remained in 0.1x ($p = 0.041$, n = 3 cultures, each condition) group. Cultures maintained in 0x serine group cultures shrank and lost hippocampal morphology, while cultures maintained in 0.01x serine had distinct CA1 and CA3 neuronal layers but few neurons in DG (Figure 4.6B). In 0.1x and 1x L-serine groups, cultures had well preserved and distinct pyramidal and granule neuron layers (bright NeuN staining). The number of neurons in CA1 was significantly lower in 0x L-serine group ($p < 0.001$, n = 3 cultures, each condition) compared with 1x group. There were no significant differences between numbers of CA1 neurons in 0.01x, 0.1x and 1x L-serine groups. Based

on CA1 neuron counts and preservation of DG, we conclude that concentrations of glycine and L-serine less than 0.1x (0.04mM) were insufficient to support culture survival.

We then examined whether combined glycine and L-serine could support neurons in organotypic cultures at lower concentration than glycine or L-serine alone. We compared lactate and LDH release in media containing 0.01 mM glycine and L-serine and in medium containing 0.4 mM glycine and L-serine (CST medium) (Figure 4.6C). Slightly less lactate and LDH was released in medium with 0.01 mM glycine and serine compared to medium with 0.4 mM glycine and serine, although results were not statistically significant except for LDH on 17 DIV ($p = 0.036$, $n = 3$ cultures, each condition). We conclude that when both L-serine and glycine are included in culture media, concentrations can be reduced to 0.01 mM without adversely affecting cell survival. Slightly higher LDH and lactate release in medium with higher glycine and serine concentrations pointed to a potential pro-epileptic effect of these amino acids.

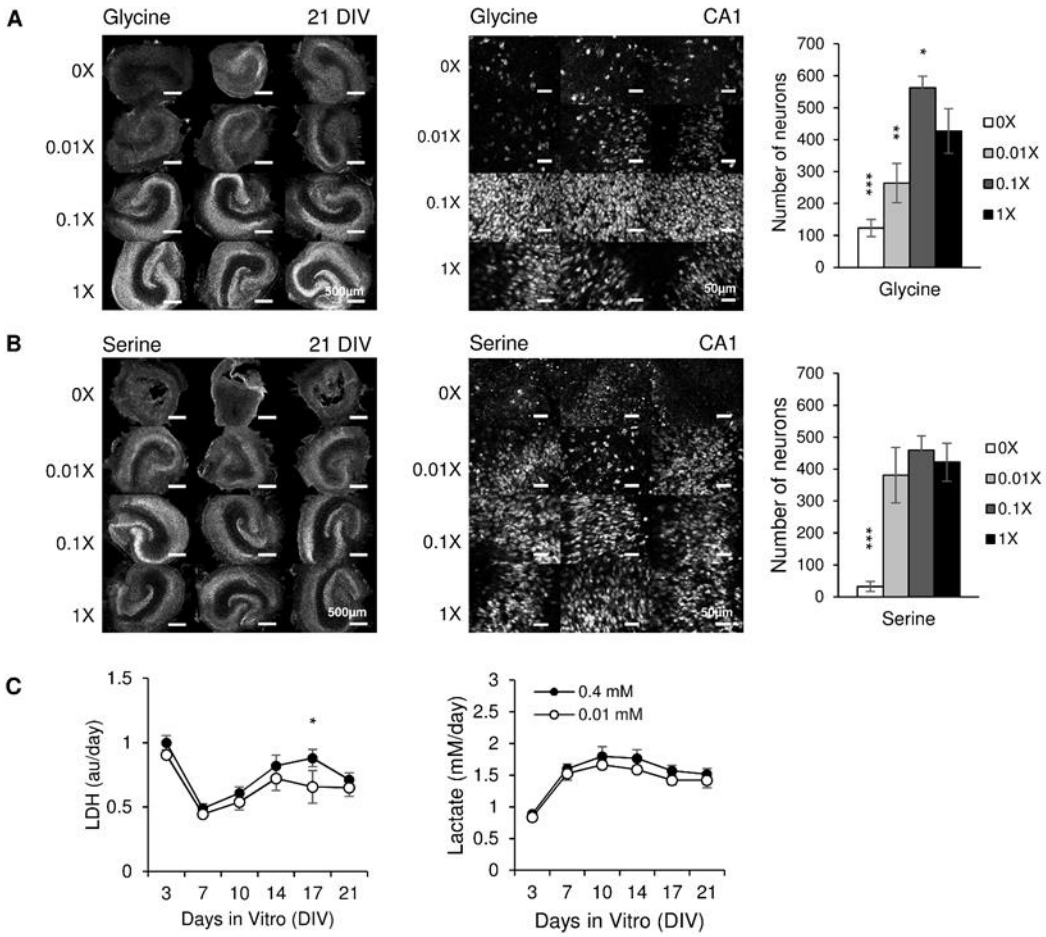

Figure 4.6 Cultures in media with different glycine and serine concentrations. (A) Left: low magnification confocal images of NeuN staining in cultures at 21 DIV, glycine concentrations are indicated on left side of images, scale bars, 500 µm; Middle: representative confocal images of NeuN staining in CA1, scale bars, 50µm; Right: corresponding CA1 neuron counts; n = 3 cultures, each condition. Statistical differences are indicated for comparisons between 1x group versus other groups. (B) Cultures maintained in different concentrations of serine. Significances are indicated for 0x group versus 1x group; n = 3 cultures, each condition. (C) Lactate and LDH results for cultures treated with combined glycine and serine, n = 3 cultures, each condition. Error bars represent SD. Significant differences are labeled as *p < 0.05, **p < 0.01 and ***p < 0.001.

4.3.5 Modification of electrolyte and glucose concentrations affects cell survival and ictal activity

Concentrations of glucose, calcium, magnesium and potassium in CST are different from those found in rat CSF. We modified the concentrations of these components to investigate their effect on cultures. The following concentrations were tested: for glucose, 11 mM (glucose concentration used in typical artificial CSF (aCSF) for acute slice experiments [19]), 15 mM, 20 mM, and 25 mM; for calcium, 0.5 mM, 1 mM, 2 mM ($[Ca^{2+}]$ used in typical aCSF), 4 mM; for magnesium, 0.5 mM, 1.3 mM ($[Mg^{2+}]$ used in typical aCSF), 2 mM, and 4 mM; for potassium, 2 mM, 3.5 mM ($[K^{+}]$ used in typical aCSF), 5 mM, and 8.5 mM. Concentration of only one medium component was varied in each experiment; other components were included at concentrations found in CST (Table 4.1). Brightfield microscope images were taken at 14 DIV. There were no differences in culture morphology or LDH and lactate in media containing different concentrations of glucose (Figure 4.7A). Cultures in medium with $[Ca^{2+}] = 4$ mM had dark edges around neuron layers, indicating that cell death occurred (Figure 4.7B). Compared with $[Ca^{2+}] = 2$ mM group, $[Ca^{2+}] = 4$ mM group had significantly higher LDH ($p = 0.004$, $n = 3$ cultures, each condition) and significantly lower lactate ($p < 0.001$, $n = 3$ cultures, each condition) at 7 DIV, confirming morphology results and indicating that high Ca^{2+} concentration is toxic for organotypic hippocampal cultures. Cultures in medium with $[Mg^{2+}] = 4$ mM had significantly brighter neural layers than cultures in media with lower $[Mg^{2+}]$, which is potentially due to lower dead cell accumulation (Figure 4.7C; inverted greyscale = 144.94 ± 1.19, 146.73 ± 3.43, 141.21 ± 3.60 and 130.20 ± 2.08 for 0.5 mM, 1.3 mM, 2.0 mM and 4.0 mM group respectively; $p < 0.001$ for 4.0 mM vs. 1.3 mM, and 4.0 mM vs. 0.5 mM, $p = 0.04$ for 4.0

mM vs. 2.0 mM, n = 3 cultures, each condition). Interestingly, cultures in $[Mg^{2+}]$ = 2 mM and $[Mg^{2+}]$ = 4 mM groups had significantly lower LDH and lactate release compared with $[Mg^{2+}]$ = 1.3 mM group at 10 DIV (p = 0.001, LDH, n = 3 cultures, each condition, and p = 0.006, lactate, n = 3 cultures, each condition). Cultures in media containing $[K^+]$ = 5 mM and $[K^+]$ = 8.5 mM group had better morphology (lighter, clearer neuronal layers) than cultures in $[K^+]$ = 3.5mM, while cultures in $[K^+]$ = 2 mM group had the worst morphology (dark, neuronal layers not visible) (Figure 4.7D). $[K^+]$ = 8.5 mM group released significantly less LDH than $[K^+]$ = 3.5 mM group at 10 and 14 DIV (p = 0.007 and p = 0.008, respectively, n = 3 cultures, each condition). There were no significant differences found in lactate release by cultures in media with different $[K^+]$. Brighter neural layers and lower LDH in $[K^+]$ = 8.5 mM group indicated that high concentration of K^+ was neuroprotective (inverted greyscale = 169.73 ± 4.27, 168.07 ± 6.20, 152.08 ± 0.45 and 143.69 ± 4.17 for 2.0 mM, 3.5 mM, 5.0 mM and 8.5 mM group respectively; $p < 0.001$ for 8.5 mM vs. 2.0 mM, and 8.5 mM vs. 3.5 mM, p = 0.003 for 5.0 mM vs. 2.0 mM, p = 0.006 for 5.0 mM vs. 3.5 mM, n = 3 cultures, each condition). This finding was surprising, since acute application of high $[K^+]$ was previously found to increase ictal activity in acute hippocampal slice preparations [43]. The potential anticonvulsant effect of elevated $[Mg^{2+}]$ in organotypic cultures, evidenced by lower lactate production, is consistent with data from other models [44,45].

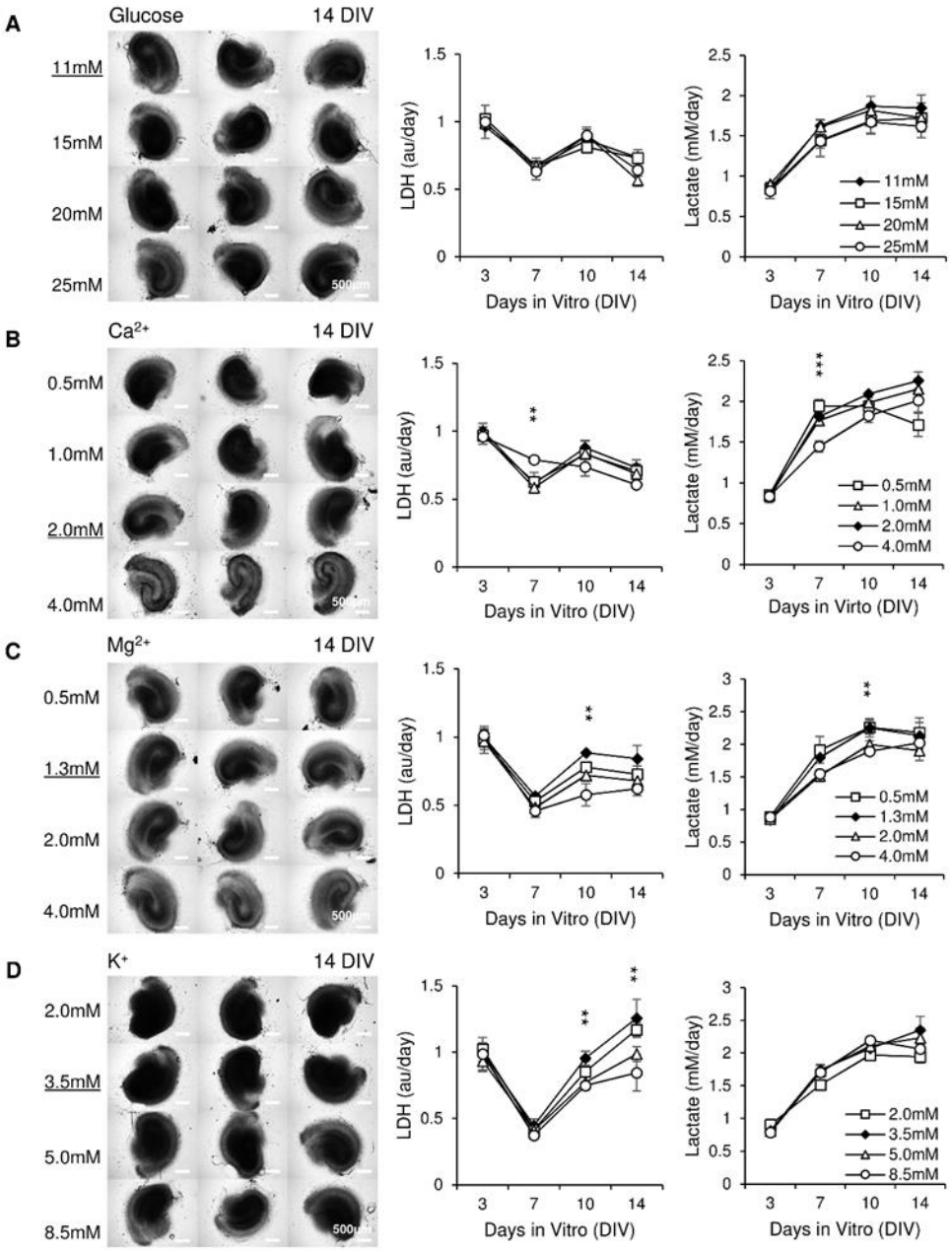

Figure 4.7 Modification of glucose and electrolyte concentrations affects cell survival and ictal activity. (A-D) Left: brightfield images of cultures maintained in media with indicated concentrations of glucose, Ca^{2+}, Mg^{2+}, or K^{+} at 14 DIV, scale bars, 500 µm; Right: time course of LDH and lactate release into culture medium. n = 3 cultures, each condition. Error bars indicate SD. Concentrations of ions that correspond to rat CSF are underlined and indicated by solid symbols. Significant statistical differences are indicated for comparison of 4 mM Ca^{2+}, 4 mM Mg^{2+} and 8.5 mM K^{+} versus CSF concentrations of corresponding ions. , with $^{**}p < 0.01$ and $^{***}p < 0.001$.

4.3.6 CSF-based medium can support organotypic hippocampal cultures

We hypothesized that changing concentrations of glucose, Ca^{2+}, Mg^{2+}, and K^{+} simultaneously may produce different effects than changing their concentrations individually. We made another medium, defined as CSF-based medium (CBM). CBM has the same components as CST, but concentrations of electrolytes were changed to reflect concentrations in rat CSF, while glucose concentration was changed to match typical concentration used in aCSF for acute slice experiments [46] (Table 4.1). Cultures maintained in CST or CBM were compared to cultures maintained in NeurA (Figure 4.8A). Compared with NeurA slices, CST and CBM cultures showed similar well-preserved hippocampal morphology with clear neuronal layers. No significant differences in LDH release were found between the three experimental groups, confirming morphology results (n = 3 cultures, each condition). On the other hand, significantly lower lactate release in CST and CBM groups were found in comparison to the NeurA group starting from 7 DIV to 21 DIV (at 7 DIV, 10 DIV, 14 DIV, 17 DIV and 21 DIV, for CST versus NeurA, p = 0.003, 0.015, 0.023, 0.012, 0.002, respectively; for CBM versus NeurA, p = 0.002, 0.001, 0.001, 0.002, 0.006, respectively, n = 3 cultures, each condition). Significant differences were also found between CST and CBM groups at 10 DIV and 14 DIV (p = 0.038, and 0.036, respectively, n = 3 cultures, each condition).

Confocal images of NeuN-stained cultures showed that pyramidal neuronal layers were well organized and densely packed in both NeurA and CBM cultures at 10 DIV (Figure 4.8B). The numbers of surviving neurons were not different between NeurA and CBM cultures in either CA1 (p = 0.663, student *t* test, n = 3 cultures, each condition) or CA3 (p = 0.317, student *t* test, n = 3 cultures, each condition).

To further investigate the reduced lactate production in CBM and CST vs. NeurA culture media, we quantified electrographic seizures (ictal events) in NeurA and CBM cultures from 0 to 14 DIV. To compare effects of NeurA and CBM, data were grouped into four time periods: 0-3 DIV, 4-7 DIV, 8-10 DIV, and 11-14 DIV (at each time point, for NeurA: n = 17 from 6 animals, 9 from 6 animals, 8 from 4 animals, 10 from 4 animals, respectively; for CBM: n = 15 from 6 animals, n = 8 from 6 animals, n =10 from 3 animals, n = 10 from 4 animals, respectively; 10 animals were used in total, n represents the number of cultures). Seizure incidence was slightly, but not significantly lower in cultures maintained in CBM compared to cultures maintained in NeurA during all time periods (Figure 4.8C, D; p = 0.141, 0.742, 0.769, 0.348 for 0-3, 4-7, 8-10, 11-14 DIV, respectively, z-test). We then examined seizure frequency, duration, and total time seizing per hour only in cultures with seizures. The only significant reduction in average seizure duration was found in CBM vs. NeurA during the 4 - 7 DIV time period (p = 0.039, n = 6 for NeurA, n = 5 for CBM). Thus, CBM cultures were somewhat less epileptic than NeurA cultures, which matches well with the differences in lactate between cultures maintained in CBM and NeurA media. However, electrical recordings also revealed that number of seizures per hour (p = 0.094 on 8-10 DIV, n = 6 for NeurA, n = 7 for CBM; p = 0.344 on 11-14 DIV, n = 8 for NeurA, n = 5 for CBM, n represents the number of cultures), and time seizing per hour (p = 0.201 on 8-10 DIV, n = 6 for NeurA, n = 7 for CBM; p = 0.713 on 11-14 DIV, n = 8 for NeurA, n = 5 for CBM) were slightly but not significantly lower in CBM compared to NeurA after 8 DIV. In cultures that had electrographic seizures, average seizure duration was actually slightly, but not significantly higher in CBM compared to NeurA at 11 – 14 DIV (p = 0.057, n = 8 for NeurA, n = 5 for CBM).

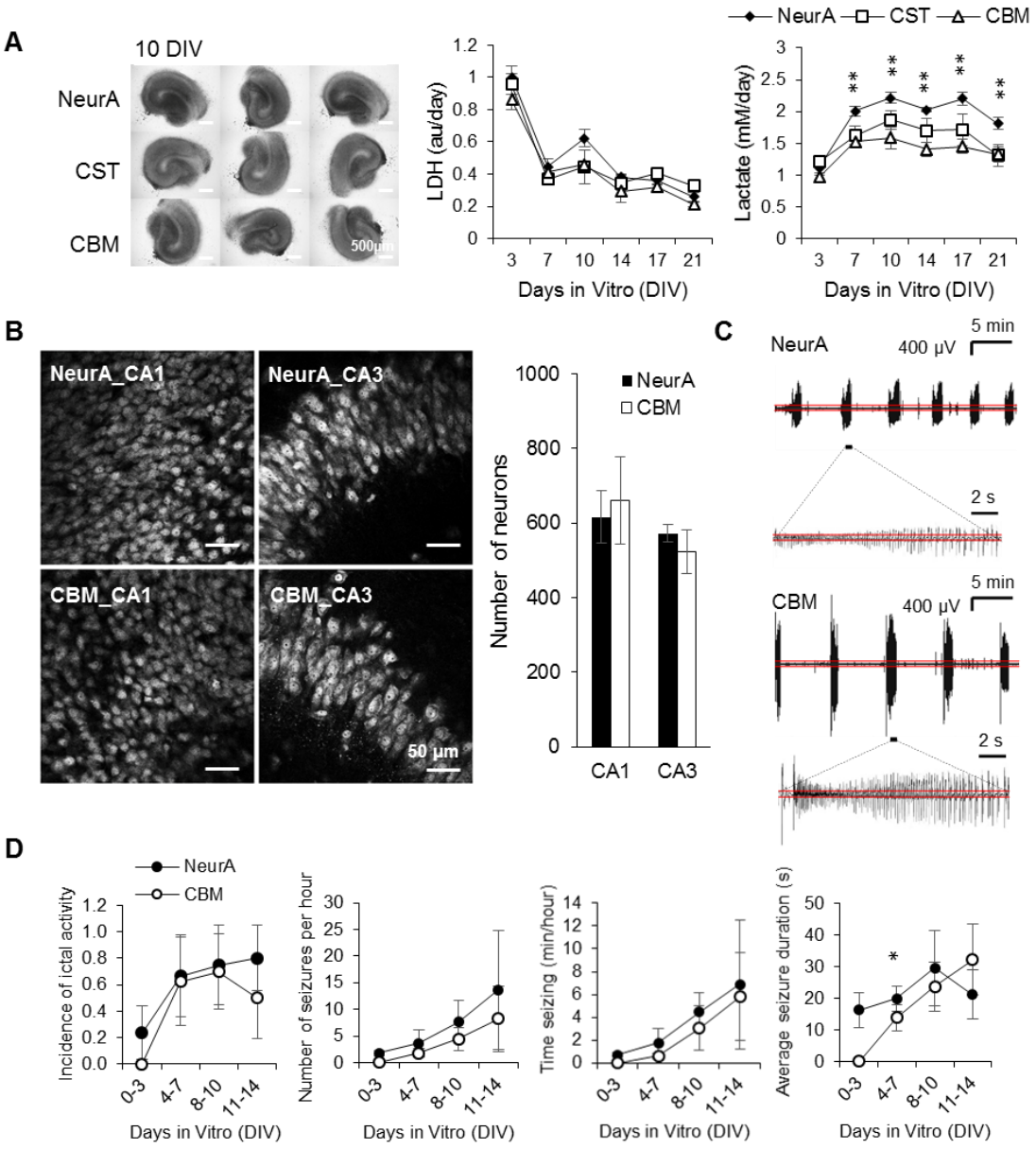

Figure 4.8 Comparison between NeurA, CST and CBM media. (A) Brightfield images at 10 DIV. Scale bars, 500 µm. Time course of LDH and lactate concentration in culture supernatant; n = 3 each condition per time point. Error bars indicate SD. Statistical significant differences are indicated for CBM and CST versus NeurA, with **p < 0.01. (B) Representative confocal images of CA1 and CA3 area of NeuN-stained organotypic hippocampal cultures at 10 DIV. Scale bars, 50 µm. Neuron counts in CA1 and CA3 are shown on the right; n = 3 each condition. (C) Representative recordings of electrographic seizure-like events in organotypic cultures on 10 DIV. Seizure detail is shown in lower traces. Red lines indicate the threshold for paroxysmal event detection. (D) Electrographic seizures (ictal events) in NeurA and CBM in electrographic recordings of seizing slices. For 0-3 DIV, 4-7 DIV, 8-10 DIV, 11-14 DIV,n = 17, 9, 8, 10 for NeurA, n = 15, 8, 10, 10 for CBM, respectively. n represents the number of cultures. *p < 0.05. Error bars represent 95% confidence intervals for incidence of ictal activity and SD for other graphs.

4.3.7 Epileptogenesis occurs independently of medium composition

Previous experiments revealed that reduction of glycine and L-serine concentrations to 0.01 mM and increase of [Mg^{2+}] to 2 mM significantly decreased cell death and reduced lactate production (Figure 4.6C and 4.7C). We integrated these two modifications into a modified medium, and compared it with CBM. Microscope images at 14 DIV revealed that cultures in modified media had significantly brighter neural layers than cultures in CBM (Figure 4.9A; inverted greyscale = 155.22 ± 8.37 and 134.15 ± 5.06 for CBM and modified medium group respectively, $p = 0.038$, n = 3 cultures, each condition). Cultures maintained in modified medium released significantly less LDH than slices in CBM at 14 DIV ($p = 0.048$, n = 3 cultures, each condition). No significant differences were observed in lactate release between two groups. We recorded electrographic activity in CBM and modified media cultures from 10 DIV to 14 DIV (Figure 4.9B, C; for CBM, n = 13 cultures from 3 animals; for modified medium, n = 14 cultures from 3 animals). No significant differences were observed in ictal activity incidence ($p = 0.853$, z-test). In cultures with seizures (n = 7 cultures for CBM and modified medium), no significant differences were observed in the number of seizure per hour, average seizure duration or time seizing ($p = 0.642$, $p = 0.937$, $p = 0.506$ respectively, *t* test). It therefore appears that this modified medium was moderately neuroprotective (better morphology, lower LDH), but did not affect epileptogenesis.

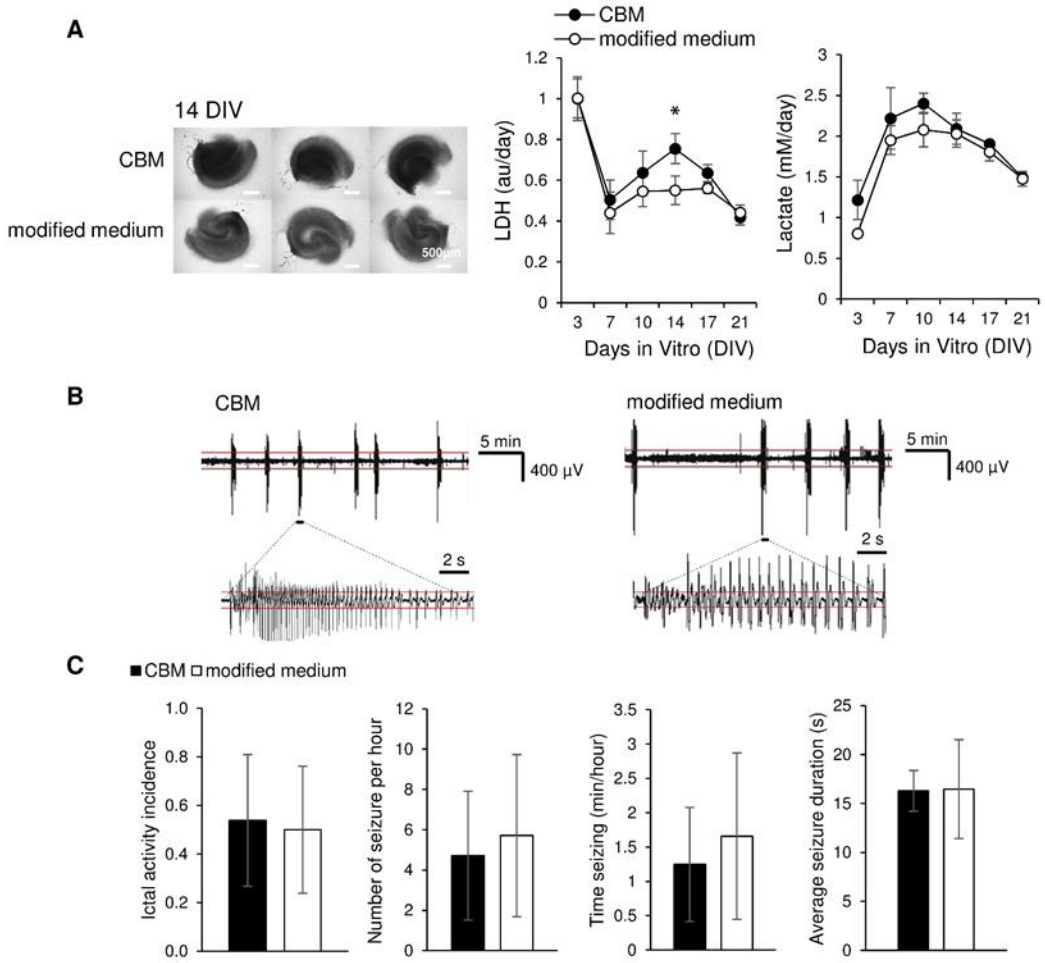

Figure 4.9 Epileptogenesis occurs independently of medium composition. (A) Left: brightfield images at 14 DIV. Modified medium refers to the medium with lower concentrations of glycine and serine (0.01 mM) and higher concentration of magnesium (2.0 mM) compared to CBM. Scale bars, 500 µm; Right: time course of LDH and lactate concentration; n = 3 cultures, each condition. Error bars indicate SD. *p < 0.05. (B) Representative recordings of electrographic seizure-like events in organotypic cultures maintained in CBM and modified medium on 11 DIV. Seizure detail is shown in lower traces. Red lines indicate the threshold for paroxysmal event detection. (C) Comparison of electrographic seizures in cultures maintained in CBM or modified medium during 10-14 DIV. n = 13 cultures for CBM; n = 14 cultures for modified medium; only cultures with seizures used for quantification of seizure frequency, duration, and time seizing. Error bars represent 95% confidence intervals for incidence of ictal activity and SD for other graphs.

4.4 Discussion

4.4.1 Interpretation of morphology, lactate, and LDH data

Slice dissection results in substantial cell death at the surface layers of hippocampal slices. Cell death in organotypic hippocampal cultures continues until 3 DIV, and then almost completely disappears by 7 DIV as dead cells are cleared from organotypic cultures maintained in serum-based or Neurobasal-A/B27 media [19]. Brightfield microscope images taken at 3 DIV show relatively dark but clearly distinguishable neural layers, while images taken at 7 DIV show much brighter neural layers. Measurement of LDH in the culture medium at 3 DIV (capturing LDH release between 0 and 3 DIV) reveals much higher LDH concentration (corresponding to higher cell death [40]) than at 7 DIV (LDH release between 3 and 7 DIV) [19]. From 7 to 14 DIV, the incidence of spontaneous electrographic seizures increases in organotypic hippocampal cultures maintained in serum-based or Neurobasal-A media [18,19]. Spontaneous seizures are accompanied by activity-dependent neuron death, which results in darker, less distinguishable neural layers by 10 – 14 DIV. The glutamate receptor antagonist kynurenic acid and anticonvulsant phenytoin reduce occurrence of spontaneous seizures and accompanying cell death. Cultures maintained in the presence of kynurenic acid or phenytoin have clearer neural layers and release less LDH into spent culture media between 10 – 14 DIV than vehicle-treated cultures [19,47]. Thus, in cultures maintained in serum-based or Neurobasal-A media, morphology and LDH release are closely linked, and follow a predictable pattern: darker cultures and high LDH release signifying high cell death between 0 and 3 DIV, brighter, clearer cultures, low LDH release, and low cell death, between 3 and 7 DIV, and darker cultures and increasing LDH release accompanying seizure-induced cell death after

7 DIV. Lactate release into culture medium is correlated to the amount of time spent cultures seizing per hour [4]. Thus, little lactate is released into culture medium until 7 DIV, while after 7 DIV, increasing incidence of seizures causes increasing lactate release.

We found that changes in medium composition can negatively affect culture survival, and reduce the correlation between morphology and LDH release. For example, exclusion of vitamins in culture medium did not affect LDH release, but caused significant changes in morphology (Figure 4.5F). This may occur because LDH release from dead cells is affected by the mode of cell death: loss of membrane integrity in necrotic cells results in release of LDH into culture supernatant, while most of LDH in apoptotic cells may be degraded without release into extracellular space [39]. Therefore, we used culture morphology as first determinant of culture survival in different media, while LDH release was used to gauge culture survival when no differences were detected morphologically. When a change in medium composition resulted in decreased culture survival, lactate release was also decreased (effects of 0.01x insulin in Figure 4.3C or 4 mM Ca^{2+} in Figure 4.7B). This decrease occurred due to fewer surviving cells present in the culture to release lactate, and not necessarily due to lower seizure load. Thus, lactate, LDH, and morphology data needed to be analyzed together to determine effects of a medium composition on culture survival and development of epilepsy.

4.4.2 Effect of medium composition on epileptogenesis

We investigated the influence of BSA, selenium and insulin on culture survival. Albumin may play a role in epileptogenesis by triggering TGF-β pathway activation after blood-brain barrier is compromised [34,48]. However, we did not observe any significant differences in morphology, LDH or lactate in cultures maintained in various concentrations

of BSA. Selenium is an antioxidant trace element that is protective against oxidative damage and can prevent the development of epilepsy induced by peroxidative injury [49–51]. Our experiments confirmed that selenium is essential to culture survival, but increasing the concentration of selenium had no beneficial or harmful effects. Insulin is frequently used in serum-free media formulations to stimulate cell growth [52], and has been reported to prevent apoptosis of external granular layer neurons in rat cerebellar slice cultures [53]. Our experiments confirmed that insulin affects neuronal size and is essential for neuronal survival (Figure 4.4). We therefore supplemented all media used in subsequent experiments with insulin and selenium to promote neuronal survival, and with BSA concentration that was in the range of albumin concentration in normal CSF.

We attempted to change concentrations of essential and non-essential amino acids, vitamins, electrolytes, and glucose to bring culture medium composition closer to CSF composition. We found that changing concentrations of essential amino acids, or removing some essential amino acids, negatively affected culture survival. Similarly, we found that organotypic cultures could not survive without vitamins. On the other hand, we found that cultures were more tolerant of changes in concentrations of non-essential amino acids, electrolytes, and glucose. Alanine and proline could be removed from culture medium, while concentrations of glycine and serine could be varied from 10 to 400 µM without affecting culture viability. We also found that concentration of glucose in the range of 11 – 25 mM, [Ca^{2+}] between 1 - 2 mM, [Mg^{2+}] between 0.5 - 4 mM, and [K^{+}] between 3.5 - 8.5 mM supported culture survival.

In healthy CSF, the concentration of K^{+} is 2.7 - 3.9 mM, the concentration of Mg^{2+} is 1 - 2 mM and the concentration of Ca^{2+} is 1.5 – 2.5 mM [22,25,27]. Changes in the

concentrations of these ions can alter neuronal excitability and lead to spontaneous epileptiform activity [22,27,43,54–57]. Glucose concentration in CSF is approximately 1.5 - 5 mM, although 10 – 11 mM concentrations are used in acute slice preparations to compensate for the altered glucose delivery pathway: rather than active transport from capillaries, glucose is provided via the diffusion gradient between the bathing medium and the extracellular fluid of actively metabolizing cells [27,46]. CSF contains 25 – 300 µM of serine and 5 – 40 µM of glycine depending on age [28,29,58]. Glycine affects excitatory neurotransmission by modulating N-methyl-d-aspartate (NMDA) receptor activation and desensitization [59–61], activates glycine receptors, and alters induced epileptiform activity [62]. L-serine (contained in culture medium) serves as a precursor for the synthesis of neuromodulators glycine and D-serine [63], which is also a co-agonist for the majority of NMDA receptor subtypes [61,64]. Finally, L-serine and glycine can act as trophic factors for survival and dendritogenesis of neurons [65].

We created two CSF-based media, CBM and modified CBM, to examine whether epileptogenesis in organotypic cultures is caused by medium composition. Comparison between CBM and Neurobasal-A revealed that both media supported culture survival equally well, with a trend toward lower excitability in CBM cultures relative to Neurobasal-A cultures. This may be due to lower $[K^+]$ and glucose in CBM. However, the incidence of electrographic seizures was the same in both media, leading us to conclude that effect on epileptogenesis was minor. In modified CBM, we increased $[Mg^{2+}]$ to 2 mM , and reduced glycine and serine concentrations to 10 µM in an effort to minimize excitability but keep medium components within physiological ranges (note that Mg^{2+} was more protective at 4 mM, but this concentration is higher than what is found in CSF).

Reducing glycine concentrations from 400 µM to 10 µM, which is slightly below the point of saturation for NMDA receptors [66], and increasing [Mg^{2+}] from 1.3 mM to 2 mM may reduce Ca^{2+} entry through the NMDA receptors during seizures, thus lowering excitotoxicity [67]. However, electrophysiological recordings revealed that there were no changes in seizure incidence or the total time seizing; in other words, epileptogenesis was not altered in cultures maintained in medium that was formulated for low excitability. On the other hand, culture survival was slightly improved.

4.5 Conclusion

Changes to culture medium composition moderately reduced electrographic seizure load and decreased cell death in organotypic hippocampal cultures. However, epilepsy developed in all media compositions that supported neuronal survival. Thus, medium composition is unlikely to be the cause of epileptogenesis in the organotypic hippocampal culture model of epilepsy.

4.6 References

1. Loscher W, Brandt C. Prevention or Modification of Epileptogenesis after Brain Insults: Experimental Approaches and Translational Research. Pharmacol Rev. 2010;62: 668–700. doi:10.1124/pr.110.003046
2. Pitkänen A, Lukasiuk K. Mechanisms of epileptogenesis and potential treatment targets. Lancet Neurol. 2011;10: 173–186. doi:10.1016/s1474-4422(10)70310-0

3. Heinemann U, Staley KJ. What is the clinical relevance of in vitro epileptiform activity? Issues in Clinical Epileptology: A View from the Bench. Springer; 2014. pp. 25–41.
4. Berdichevsky Y, Dryer AM, Saponjian Y, Mahoney MM, Pimentel CA, Lucini CA, et al. PI3K-Akt signaling activates mTOR-mediated epileptogenesis in organotypic hippocampal culture model of post-traumatic epilepsy. J Neurosci. 2013;33: 9056–9067.
5. Lillis KP, Wang Z, Mail M, Zhao GQ, Berdichevsky Y, Bacskai B, et al. Evolution of network synchronization during early epileptogenesis parallels synaptic circuit alterations. J Neurosci. 2015;35: 9920–9934.
6. Gutiérrez R, Heinemann U. Synaptic reorganization in explanted cultures of rat hippocampus. Brain Res. 1999;815: 304–316.
7. De Simoni A, Griesinger CB, Edwards FA. Development of rat CA1 neurones in acute Versus organotypic slices: role of experience in synaptic morphology and activity. J Physiol. 2003;550: 135–147. doi:10.1113/jphysiol.2003.039099
8. Coltman BW, Earley EM, Shahar A, Dudek FE, Ide CF. Factors influencing mossy fiber collateral sprouting in organotypic slice cultures of neonatal mouse hippocampus. J Comp Neurol. 1995;362: 209–222. doi:10.1002/cne.903620205
9. Hailer NP, Järhult JD, Nitsch R. Resting microglial cells in vitro: Analysis of morphology and adhesion molecule expression in organotypic hippocampal slice cultures. Glia. 1996;18: 319–331. doi:10.1002/(SICI)1098-1136(199612)18:4<319::AID-GLIA6>3.0.CO;2-S
10. del Rio JA, Heimrich B, Soriano E, Schwegler H, Frotscher M. Proliferation and differentiation of glial fibrillary acidic protein-immunoreactive glial cells in

organotypic slice cultures of rat hippocampus. Neuroscience. 1991;43: 335–347. doi:10.1016/0306-4522(91)90298-3

11. Coulter D, Rafiq A, Shumate M, Gong Q, DeLorenzo R, Lyeth B. Brain injury-induced enhanced limbic epileptogenesis: anatomical and physiological parallels to an animal model of temporal lobe epilepsy. Epilepsy Res. 1996;26: 81–91.
12. Santhakumar V, Ratzliff AD, Jeng J, Toth Z, Soltesz I. Long-term hyperexcitability in the hippocampus after experimental head trauma. Ann Neurol. 2001;50: 708–717.
13. Kharatishvili I, Nissinen J, McIntosh T, Pitkänen A. A model of posttraumatic epilepsy induced by lateral fluid-percussion brain injury in rats. Neuroscience. 2006;140: 685–697.
14. Stoppini L, Buchs P-A, Muller D. A simple method for organotypic cultures of nervous tissue. J Neurosci Methods. 1991;37: 173–182.
15. Gahwiler B TS McKinney A, Debanne D, Robertson R. Organotypic Slice Cultures of Neural Tissue. In: Culturing Nerve Cells. 2nd ed. Massachusetts Institute of Technology; 1998.
16. Hayashi I, Sato GH. Replacement of serum by hormones permits growth of cells in a defined medium. Nature. 1976;
17. Brewer G, Torricelli J, Evege E, Price P. Optimized survival of hippocampal neurons in B27-supplemented neurobasal^{TM}, a new serum-free medium combination. J Neurosci Res. 1993;35: 567–576.
18. Dyhrfjeld-Johnsen J, Berdichevsky Y, Swiercz W, Sabolek H, Staley K. Interictal spikes precede ictal discharges in an organotypic hippocampal slice culture model of epileptogenesis. J Clin Neurophysiol. 2010;27: 418–424.

19. Berdichevsky Y, Dzhala V, Mail M, Staley KJ. Interictal spikes, seizures and ictal cell death are not necessary for post-traumatic epileptogenesis in vitro. Neurobiol Dis. 2012;45: 774–785.
20. Heinemann U, Kaufer D, Friedman A. Blood-brain barrier dysfunction, TGFβ signaling, and astrocyte dysfunction in epilepsy. Glia. 2012;60: 1251–1257.
21. van Vliet E, Aronica E, Gorter J. Role of blood–brain barrier in temporal lobe epilepsy and pharmacoresistance. Neuroscience. 2014;277: 455–473.
22. Somjen GG. Ion regulation in the brain: implications for pathophysiology. The Neuroscientist. 2002;8: 254–267.
23. Van Vliet E, da Costa Araujo S, Redeker S, Van Schaik R, Aronica E, Gorter J. Blood–brain barrier leakage may lead to progression of temporal lobe epilepsy. Brain. 2007;130: 521–534.
24. Manthei R, Wright D, Kenny A. Altered CSF constituents and retrograde amnesia in rats: a biochemical approach. Physiol Behav. 1973;10: 517–521.
25. Amtorp O, Sørensen S. The ontogenetic development of concentration differences for protein and ions between plasma and cerebrospinal fluid in rabbits and rats. J Physiol. 1974;243: 387–400.
26. McNay EC, Sherwin RS. From artificial cerebro-spinal fluid (aCSF) to artificial extracellular fluid (aECF): microdialysis perfusate composition effects on in vivo brain ECF glucose measurements. J Neurosci Methods. 2004;132: 35–43.
27. Reid KH, Edmonds Jr HL, Schurr A, Tseng MT, West CA. Pitfalls in the use of brain slices. Prog Neurobiol. 1988;31: 1–18.

28. Korobkin RK, Cutler RWP. Maturational changes of amino acid concentration in cerebrospinal fluid of the rat. Brain Res. January 1;119: 181–187. doi:10.1016/0006-8993(77)90098-1

29. Heiblim DI, Evans HE, Glass L, Agbayani MM. Amino acid concentrations in cerebrospinal fluid. Arch Neurol. 1978;35: 765–768.

30. Globus MY, Busto R, Martinez E, Valdés I, Dietrich WD, Ginsberg MD. Comparative Effect of Transient Global Ischemia on Extracellular Levels of Glutamate, Glycine, and γ-Aminobutyric Acid in Vulnerable and Nonvulnerable Brain Regions in the Rat. J Neurochem. 1991;57: 470–478.

31. Hashimoto A, Oka T, Nishikawa T. Extracellular concentration of endogenous free D-serine in the rat brain as revealed by in vivo microdialysis. Neuroscience. 1995;66: 635–643.

32. Yu JY, Pearl PL. Metabolic causes of epileptic encephalopathy. Epilepsy Res Treat. 2013;2013.

33. Papetti L, Parisi P, Leuzzi V, Nardecchia F, Nicita F, Ursitti F, et al. Metabolic epilepsy: an update. Brain Dev. 2013;35: 827–841.

34. Ivens S, Kaufer D, Flores LP, Bechmann I, Zumsteg D, Tomkins O, et al. TGF-β receptor-mediated albumin uptake into astrocytes is involved in neocortical epileptogenesis. Brain. 2007;130: 535–547.

35. Westergren I, Nystrom B, Hamberger A, Nordborg C, Johansson BB. Concentrations of Amino Acids in Extracellular Fluid After Opening of the Blood-Brain Barrier by Intracarotid Infusion of Protamine Sulfate. J Neurochem. 1994;62: 159–165.

36. Reiber H. Dynamics of brain-derived proteins in cerebrospinal fluid. Clin Chim Acta. 2001;310: 173–186.
37. Seyfert S, Faulstich A, Marx P. What determines the CSF concentrations of albumin and plasma-derived IgG? J Neurol Sci. 2004;219: 31–33.
38. Cassar SC, Tovcimak AE, Rustay NR, Ellis TA, Hooker BA, Witte DG, et al. Comparing levels of biochemical markers in CSF from cannulated and non-cannulated rats. J Neurosci Methods. 2010;192: 249–253.
39. Bonfoco E, Krainc D, Ankarcrona M, Nicotera P, Lipton SA. Apoptosis and necrosis: two distinct events induced, respectively, by mild and intense insults with N-methyl-D-aspartate or nitric oxide/superoxide in cortical cell cultures. Proc Natl Acad Sci U S A. 1995;92: 7162–7166.
40. Decker T, Lohmann-Matthes ML. A quick and simple method for the quantitation of lactate dehydrogenase release in measurements of cellular cytotoxicity and tumor necrosis factor (TNF) activity. J Immunol Methods. 1988;115: 61–9.
41. Korzeniewski C, Callewaert DM. An enzyme-release assay for natural cytotoxicity. J Immunol Methods. 1983;64: 313–320.
42. Bindokas V. 17 Sep 2014. Available: https://digital.bsd.uchicago.edu/%5Cimagej_macros.html
43. Rutecki PA, Lebeda FJ, Johnston D. Epileptiform activity induced by changes in extracellular potassium in hippocampus. J Neurophysiol. 1985;54: 1363–1374.
44. Cotton DB, Janusz CA, Berman RF. Anticonvulsant effects of magnesium sulfate on hippocampal seizures: Therapeutic implications in preeclampsia-eclampsia. Am J Obstet Gynecol. 1992;166: 1127–1136. doi:10.1016/S0002-9378(11)90599-7

45. Safar MM, Abdallah DM, Arafa NM, Abdel-Aziz MT. Magnesium supplementation enhances the anticonvulsant potential of valproate in pentylenetetrazol-treated rats. Brain Res. 2010;1334: 58–64.
46. Hájos N, Mody I. Establishing a physiological environment for visualized in vitro brain slice recordings by increasing oxygen supply and modifying aCSF content. J Neurosci Methods. 2009;183: 107–113.
47. Miller LP, Mahanty N, Connor J, Landis D. Spontaneous pyramidal cell death in organotypic slice cultures from rat hippocampus is prevented by glutamate receptor antagonists. Neuroscience. 1994;63: 471–487.
48. Cacheaux LP, Ivens S, David Y, Lakhter AJ, Bar-Klein G, Shapira M, et al. Transcriptome profiling reveals TGF-β signaling involvement in epileptogenesis. J Neurosci. 2009;29: 8927–8935.
49. Ashrafi MR, Shabanian R, Abbaskhanian A, Nasirian A, Ghofrani M, Mohammadi M, et al. Selenium and Intractable Epilepsy: Is There Any Correlation? Pediatr Neurol. 1;36: 25–29. doi:10.1016/j.pediatrneurol.2006.09.001
50. Nazıroğlu M, Kutluhan S, Yılmaz M. Selenium and Topiramate Modulates Brain Microsomal Oxidative Stress Values, Ca2+-ATPase Activity, and EEG Records in Pentylentetrazol-Induced Seizures in Rats. J Membr Biol. 2008;225: 39–49. doi:10.1007/s00232-008-9132-6
51. Rubin JJ, Willmore LJ. Prevention of iron-induced epileptiform discharges in rats by treatment with antiperoxidants. Exp Neurol. 1980;67: 472–480. doi:10.1016/0014-4886(80)90119-3

52. Barnes D, Sato G. Methods for growth of cultured cells in serum-free medium. Anal Biochem. 1980;102: 255–270. doi:10.1016/0003-2697(80)90151-7

53. Tanaka M, Sawada M, Yoshida S, Hanaoka F, Marunouchi T. Insulin prevents apoptosis of external granular layer neurons in rat cerebellar slice cultures. Neurosci Lett. 10;199: 37–40. doi:10.1016/0304-3940(95)12009-S

54. Zuckermann EC, Glaser GH. Hippocampal epileptic activity induced by localized ventricular perfusion with high-potassium cerebrospinal fluid. Exp Neurol. 1968;20: 87–110.

55. Mody I, Lambert J, Heinemann U. Low extracellular magnesium induces epileptiform activity and spreading depression in rat hippocampal slices. J Neurophysiol. 1987;57: 869–888.

56. Traub RD, Jefferys JG, Whittington MA. Enhanced NMDA conductance can account for epileptiform activity induced by low Mg2+ in the rat hippocampal slice. J Physiol. 1994;478: 379–393. doi:10.1113/jphysiol.1994.sp020259

57. Staley KJ, Bains JS, Yee A, Hellier J, Longacher JM. Statistical model relating CA3 burst probability to recovery from burst-induced depression at recurrent collateral synapses. J Neurophysiol. 2001;86: 2736–2747.

58. Kawai N, Bannai M, Seki S, Koizumi T, Shinkai K, Nagao K, et al. Pharmacokinetics and cerebral distribution of glycine administered to rats. Amino Acids. 2012;42: 2129–2137.

59. Johnson JW, Ascher P. Glycine potentiates the NMDA response in cultured mouse brain neurons. Nature. 1987;325: 529–531. doi:10.1038/325529a0

60. Vyklický L, Benveniste M, Mayer ML. Modulation of N-methyl-D-aspartic acid receptor desensitization by glycine in mouse cultured hippocampal neurones. J Physiol. 1990;428: 313–331. doi:10.1113/jphysiol.1990.sp018214
61. Mothet J, Le Bail M, Billard J. Time and space profiling of NMDA receptor co-agonist functions. J Neurochem. 2015;135: 210–225.
62. Kirchner A, Breustedt J, Rosche B, Heinemann UF, Schmieden V. Effects of Taurine and Glycine on Epileptiform Activity Induced by Removal of Mg2+ in Combined Rat Entorhinal Cortex–Hippocampal Slices. Epilepsia. 2003;44: 1145–1152. doi:10.1046/j.1528-1157.2003.01603.x
63. Tabatabaie L, Klomp LW, Berger R, de Koning TJ. l-Serine synthesis in the central nervous system: A review on serine deficiency disorders. Mol Genet Metab. 3;99: 256–262. doi:10.1016/j.ymgme.2009.10.012
64. Mothet J-P, Parent AT, Wolosker H, Brady RO, Linden DJ, Ferris CD, et al. d-Serine is an endogenous ligand for the glycine site of the N-methyl-d-aspartate receptor. Proc Natl Acad Sci. 2000;97: 4926–4931.
65. Furuya S, Tabata T, Mitoma J, Yamada K, Yamasaki M, Makino A, et al. l-Serine and glycine serve as major astroglia-derived trophic factors for cerebellar Purkinje neurons. Proc Natl Acad Sci. 2000;97: 11528–11533. doi:10.1073/pnas.200364497
66. Kew JN, Richards JG, Mutel V, Kemp JA. Developmental changes in NMDA receptor glycine affinity and ifenprodil sensitivity reveal three distinct populations of NMDA receptors in individual rat cortical neurons. J Neurosci. 1998;18: 1935–1943.
67. Fujikawa DG. Prolonged seizures and cellular injury: understanding the connection. Epilepsy Behav. 2005;7: 3–11.

Chapter 5

Conclusion and future perspectives

5.1 Conclusion

The work presented in this thesis delivers solutions to the throughput limitation in in vitro antiepileptogenic drug discovery (Chapter 2, 3), and provides further validation of the organotypic culture based in vitro model of epilepsy (Chapter 4).

In Chapter 2, we described a microfluidic perfused drop culture method to maintain organotypic cultures for over two weeks. This technique reduced the footprint required by brain slice cultures, and thus enabled the placement of a culture array on a single device, which dramatically improved the scalability.

In Chapter 3, we presented a μflow-MEA technology for antiepileptogenic drug discovery. The integration of the microfluidic perfusion system with customized MEA allowed the maintenance of 6 cultures on a single 2 × 2 inch device for scalable chronic electrical assay of epileptogenesis. Field potential simulation confirmed that a simplified MEA design (with uninsulated electrodes) was able to achieve good detection of seizure-like activity. The in vitro model of epilepsy was validated on the μflow-MEA by neuron viability evaluation, epileptogenesis verification, and anticonvulsant test. A two-stage screening platform was developed to carry out a pilot screen of receptor tyrosine kinases (RTKs)

inhibitors. In stage I, several RTK inhibitors showed significant reducing effect in lactate dehydrogenase (LDH) and lactate levels. In stage II, our preliminary data of μflow-MEA based chronic electrophysiology confirmed the results of the stage I screen and identified the antiepileptogenic properties of cFMS RTK inhibitor. This work demonstrated the capability of μflow-MEA technology to facilitate high-throughput antiepileptogenic drug discovery.

In Chapter 4, we further validated the organotypic hippocampal culture model of epilepsy by studying the influence of culture medium composition on epileptogenesis. We systematically studied the composition of the Neurobasal-A/B27 culture medium system and identified the essential components for culture survival. By excluding the non-essential components, we made a simplified medium for further study. We then altered the concentration of individual components and measured the effects on epileptogenesis and found that the modification of glycine, serine and Mg can moderately reduce ictal activity and that epileptogenesis occurred in all culture medium that supports neuronal survival. This study proved that epileptogenesis is independent of medium composition.

It is hoped that the techniques presented in this thesis will accelerate antiepileptogenic drug discovery and contribute to the development of new therapeutics to treat individuals at risk of epileptogenesis.

5.2 Future perspectives

5.2.1 Microwire based sequential recording platform for broad drug screening

Our μflow-MEA technology provides continuous recording and enables the evaluation of drug efficacy at high-resolution. However, at this point, the throughput of this platform is limited by the number of channels in the data acquisition system we have in the lab, since a 16-channel workstation can support only 1 screen of 3 drugs per 2 weeks. To increase the experimental throughput, an upgraded multichannel workstation is required to support higher degree of parallelism. Besides the μflow-MEA system, we developed a new sequential recording platform based on the microwire electrode technique, so that multiple screen experiments can be performed at the same time with one 16-channel workstation.

The microwire electrode array technique has been developed for decades and is a well-established neural implant for in vivo study [1,2]. To our knowledge, this technique has not been utilized for chronic recordings in organotypic cultures. We cultured a hippocampal slice on a PFA-coated tungsten wire (bare diameter = 50.8 μm, coated diameter = 101.6 μm, A-M systems Inc.) that was affixed to the substrate of 6-well culture plate by PDMS, and we found that the existence of the microwire did not influence the culture survival (Figure 5.1A). We then built a microwire integrated culture plate for neural recording (Figure 5.1B). In each culture well, a recording electrode was fixed to the substrate with the microwire tip placed in the center, where the slice culture would be inserted, and a reference electrode (same type of microwire with 1.5 cm insulation layer removed at the tip) was placed on the side. Then organotypic cultures were maintained in

microwire plates for two weeks. Plates were transferred to a mini incubator (37 ℃ and 5% CO_2) for one hour electrical recordings every other day (Figure 5.1C).

To demonstrate the capability of microwire recording platform to screen drugs, we retested cFMS RTK inhibitor, which was previously identified as having a significant antiepileptogenic effect in the μflow-MEA based screen (Chapter 4), and Flt-3 RTK inhibitor, which did not show an obvious antiepileptogenic effect, as a negative control. We used four parameters to evaluate the drug efficacy: time seizing, tonic time (processing methods are described in section 5.2.2), average event rate, and electrographic load. Average event rate referred to the average paroxysmal event number (in 10 s time window) in one hour recording. Electrographic load was the integration of the power of voltage with time. The screen results agreed with our previous observation (Figure 5.1D-H) that cFMS inhibitor treated cultures showed significantly decreased time seizing and average event rate ($p = 0.0214$, $p < 0.001$, respectively, Kolmogorov–Smirnov test, $n = 4$ each condition, cultures from the same animal), and moderately decreased electrographic load ($p = 0.056$, Kolmogorov–Smirnov test). No significant drug effect was seen in the cultures treated with Flt-3 inhibitor. Representative recordings are shown in Figure 5.1H.

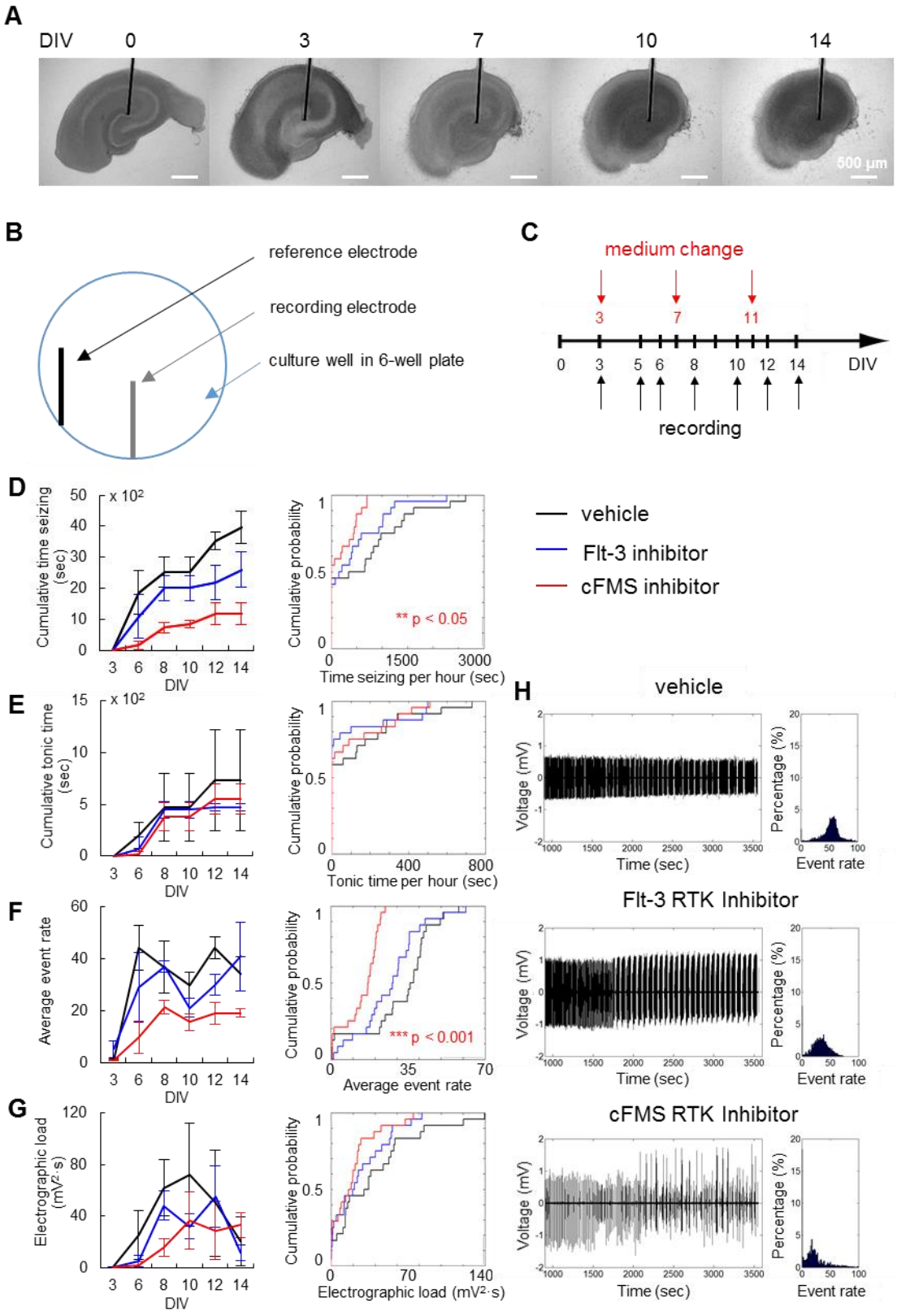

Figure 5.1 Microwire based sequential recording platform for drug screening. (A) Microwire electrode is compatible with organotypic culture. Scale bars, 500 µm. (B) The

electrode layout in a 6-well plate culture well. (C) Recording schedule for two weeks culturing. (D-H) Screen results of cFMS inhibitor and Flt-3 inhibitor. Drug efficacy was evaluated by time seizing per hour (D), tonic time per hour (E), average event rate (F), and electrographic load (G). (H) Representative recordings on 12 DIV. Histogram on the right shows the distribution of event rate in one hour recording. Kolmogorov–Smirnov test, n = 4 each condition, cultures from the same animal. Error bars indicate SD.

In this microwire recording setup, each screen experiment can test 2 drugs and 1 control with n = 4, and at most 6 screens can be conducted every 2 weeks, rendering a throughput of 24 drugs per month. Therefore, microwire recording platform provides higher experimental throughput, allowing for fast and broad screen of compound libraries. However, due to compromised recording resolution, it is important to subject the findings obtained in this platform to subsequent continuous monitoring. We expect the future applications of microwire based screen platform in rapid dissection of complex cell signaling pathways in epilepsy.

5.2.2 Seizure type classification and transition study

We developed an automated algorithm for seizure quantification and seizure type (refers to different tonic and clonic phase composition) classification. Two sets of analysis were performed: (1) bin duration was set as 0.5 s, aiming to identify event rates of up to 2 Hz (tonic-clonic phase of electrographic seizures); (2) bin duration was set as 0.1 s, intending to identify event rates of up to 10 Hz (tonic phase of electrographic seizures) [3–6] (Figure 5.2A).

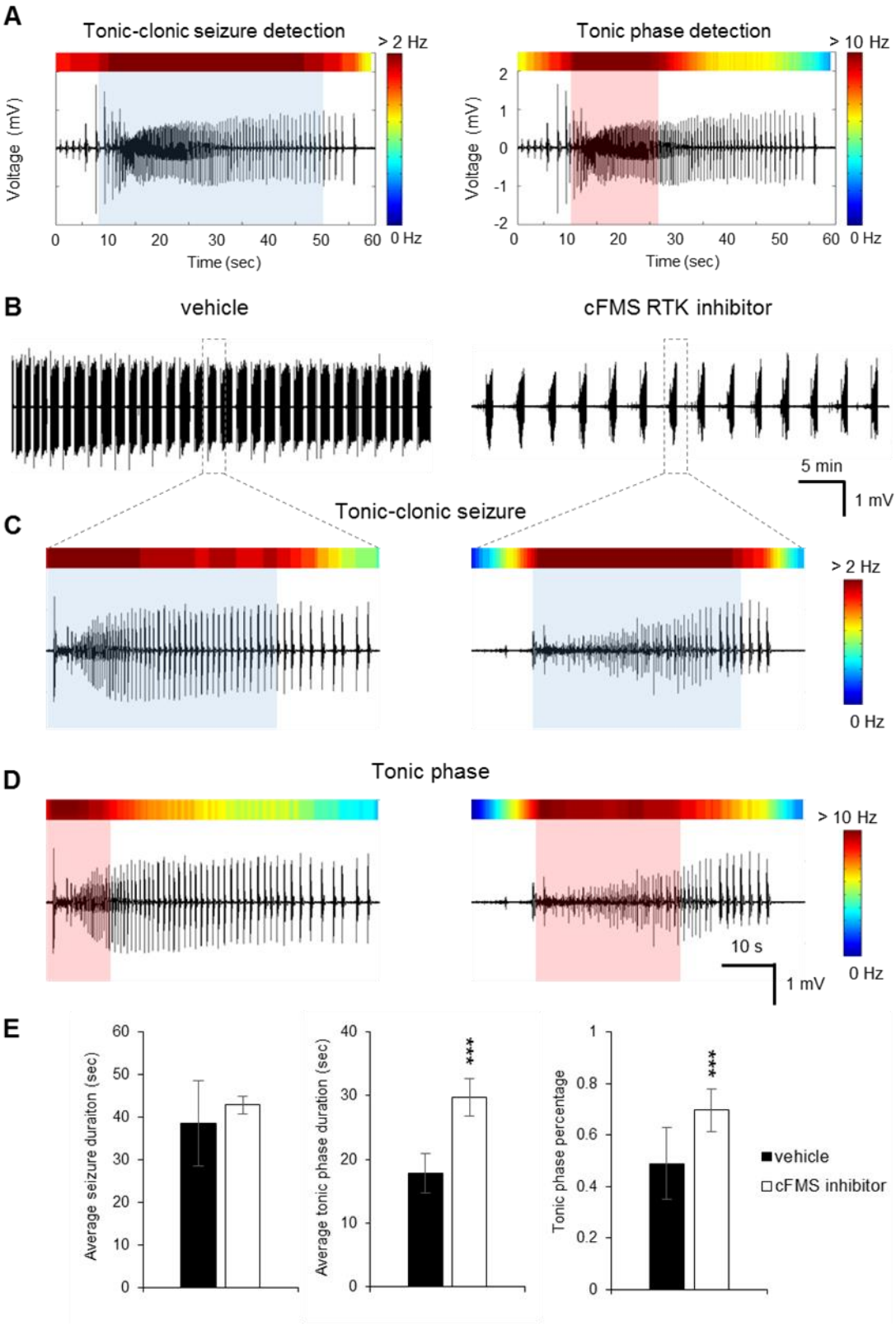

Figure 5.2 Drug effects on seizure type. (A) Tonic-clonic seizures and its tonic phase were quantified separately for seizure type study. (B-E) The influence of cFMS inhibitor

on seizure type. (B) one hour recordings with consistent seizure activity were selected for analysis. (C-D) Representative seizure type and its tonic composition in each condition. (E) Quantification of average seizure duration (left), average tonic phase duration (middle), and tonic phase percentage (right). *** $p < 0.001$, t-test, n = 32 seizures for control, and n = 14 seizures for cFMS-treated culture. Error bars indicate SD.

Interestingly, we found that cFMS inhibitor significantly reduced the duration of tonic-clonic seizures (Figure 5.1D), but it did not show obvious effects on the tonic phase of seizures (Figure 5.1E). Similar results were also observed in our chronic data. It might suggest that cFMS inhibitor modifies the seizure type by increasing the tonic phase duration in tonic-clonic seizures. To test this hypothesis, we quantified the duration of tonic-clonic seizures and the tonic phase duration in one hour recordings. We selected the recordings with consistently occurring seizure activity of a vehicle-treated control and a cFMS-treated culture for this analysis (Figure 5.2B). Treatment with the cFMS inhibitor did not change the duration of individual tonic-clonic seizure, but it significantly increased the tonic phase duration in each seizure, thus increasing the tonic phase percentage (Figure 5.2E, $p = 0.181$, <0.001, and <0.001, respectively, t-test, n = 32 seizures for control, and n = 14 seizures for cFMS inhibitor-treated culture). Representative plots presenting the seizure type modifications are shown in Figure 5.2C, D.

To find the biological explanations of the drug effect on seizure type would be an interesting topic we can explore in future studies. Moreover, seizure type is variable over time. The dynamic of seizure type transition can be studied by analyzing chronic data with sufficient sample size, which might add to our understanding of the mechanism of epilepsy progression.

Finally, we expect that future applications of our antiepileptogenic drug screening platforms will include experiments with libraries of peptides, antibodies, and silencing RNA that would achieve more specific inhibition of a broader range of potential drug targets. We also expect that this platform may have future applications in neurodevelopment research and drug discovery for psychiatric disorders.

5.3 References

1. Williams JC, Rennaker RL, Kipke DR. Long-term neural recording characteristics of wire microelectrode arrays implanted in cerebral cortex. Brain Res Protoc. 1999;4: 303–313. doi:10.1016/S1385-299X(99)00034-3

2. Kralik JD, Dimitrov DF, Krupa DJ, Katz DB, Cohen D, Nicolelis MAL. Techniques for Chronic, Multisite Neuronal Ensemble Recordings in Behaving Animals. Methods. 2001;25: 121–150. doi:10.1006/meth.2001.1231

3. Wuarin J-P, Dudek FE. Electrographic Seizures and New Recurrent Excitatory Circuits in the Dentate Gyrus of Hippocampal Slices from Kainate-Treated Epileptic Rats. J Neurosci. 1996;16: 4438–4448.

4. Khazipov R, Khalilov I, Tyzio R, Morozova E, Ben-Ari Y, Holmes GL. Developmental changes in GABAergic actions and seizure susceptibility in the rat hippocampus. Eur J Neurosci. 2004;19: 590–600. doi:10.1111/j.0953-816X.2003.03152.x

5. Dzhala VI, Talos DM, Sdrulla DA, Brumback AC, Mathews GC, Benke TA, et al. NKCC1 transporter facilitates seizures in the developing brain. Nat Med. 2005;11: 1205–1213. doi:10.1038/nm1301

6. Jirsa VK, Stacey WC, Quilichini PP, Ivanov AI, Bernard C. On the nature of seizure dynamics. Brain. 2014;137: 2210–2230. doi:10.1093/brain/awu133

JING LIU

EDUCATION

Ph.D., Electrical and Computer Engineering
Lehigh University, Bethlehem, PA

B.S., Material Science and Technology
Wuhan University, Wuhan, China

RESEARCH INTEREST

Development of innovative brain-on-chip system and neural interface technologies to facilitate the translational research on neurological diseases.

HONORS AND AWARDS

P.C. Rossin Doctoral Fellowship, Lehigh University
People's Scholarship, Wuhan University

PUBLICATIONS

1. **J. Liu**, L. Pan, X. Cheng, Y. Berdichevsky, "Perfused drop microfluidic device for brain slice culture-based drug discovery", *Biomed. Microdevices*, 18(3), 2016.
2. Y. Song, C. Pimentel, K. Walters, L. Boller, S. Ghiasvand, **J. Liu**, K. J. Staley, Y. Berdichevsky, "Neuroprotective levels of IGF-1 exacerbate epileptogenesis after brain injury", *Scientific Reports*, 6, 2016.
3. **J. Liu**, Y. Saponjian, M. M. Mahoney, K. J. Staley, Y. Berdichevsky, "Epileptogenesis in organotypic hippocampal cultures has limited dependence on culture medium composition", *PLoS ONE*, 12(2), 2017.
4. **J. Liu**, Y. Berdichevsky, "Epilepsy-on-chip system for high-throughput antiepileptic drug discovery", under preparation.